XIN YUAN

COMB-TYPE PILOT-AIDED OFDM CHANNEL ESTIMATION FOR UNDERGROUND WLAN COMMUNICATIONS

Mémoire présenté
à la Faculté des études supérieures de l'Université Laval
dans le cadre du programme de maîtrise en génie électrique
pour l'obtention du grade de Maître ès Sciences (M.Sc.)

FACULTÉ DES SCIENCES ET DE GÉNIE
UNIVERSITÉ LAVAL
QUÉBEC

2007

RÉSUMÉ

La plupart des études d'estimation de signal modulé par multiplexage par répartition orthogonale de la fréquence (OFDM) et parcourant un canal avec évanouissement impliquent un nombre constant de trajets multiples. Cependant, dans un milieu souterrain, le nombre de trajets significatifs varie selon une distribution spécifique.

Nos travaux tentent de résoudre l'estimation d'un canal minier souterrain à large bande, où le nombre de trajets significatifs répond à une distribution de Poisson modifiée et dont les amplitudes sont affectées par des évanouissements de Rayleigh ou de Rice. L'estimation de canal pour un système OFDM s'effectue via un signal comprenant des fréquences pilotes distribuées en peigne. Les fréquences pilotes comprises dans le signal sont tout d'abord estimées par un détecteur de moyenne quadratique logarithmique ou par la méthode des moindres carrés. Par la suite, des méthodes d'interpolation du canal sont étudiées. Les performances de différentes approches, inspirées des modulations spécifiées par la norme IEEE802.11, sont analysées selon le taux d'erreur binaire (BER).

ABSTRACT

Most analytical studies of Orthogonal Frequency Division Multiplexing (OFDM) channel estimation for fading channels assume a constant number of multiple paths. However, in an underground environment, the number of significant multipath components can be variable and follow a specific distribution. This thesis addresses the problem of channel estimation based on a wideband statistical channel model in a mining environment, where the number of arrival paths follows a modified Poisson distribution and their amplitudes undergo Rayleigh or Rician fading. Channel estimations for OFDM systems are based on a comb-type pilot arrangement, which is divided into pilot signal estimation and channel interpolation. The pilot signal estimation based on Least Mean Square (LMS) or Least Square (LS) criteria, together with a variety of interpolation schemes, is studied. Performances for all conditions are presented and compared by measuring the Bit Error rate (BER) with different modulation schemes derived from the IEEE802.11 WLAN standard.

ACKNOWLEDGMENTS

This thesis could not have been completed without the help and support of many people.

First and foremost, I would like to express my sincere gratitude to Professor Paul Fortier, my research director, for providing me many valuable suggestions for my research work. His exciting advice and critical comments on thesis, report, presentations, etc. improved my oral and written communication skills. I would also like to thank Dr. Pierre-Martin Tardif, my co-director, for his guidance, support and encouragement throughout this work. It has truly been an honor to work under their supervision.

I would like to thank all of my colleagues at LRCS and LRTS labs for creating such a helpful and pleasant work environment. Many thanks to them for their friendship, encouragement and all of the unforgettable memories we have shared in the past two years. Special thanks to Salma Ait Fares for her insightful suggestion in the development of this work and help in resolving many questions.

My deepest appreciation goes to my family for their continual love and support throughout my life. I sincerely thank my parents for all their supports during my education. I am forever indebted to them for all that they have provided me. I am most grateful to my husband Hamidreza Bakhshi for his endless love, patience, support and understanding.

I would like to express my appreciation to professors Dominic Grenier and Jean-Yves Chouinard for their judgments and serving on my M.Sc. committee.

I would like to acknowledge the financial supports from the LRCS lab of UQAT.

TABLE OF CONTENTS

LIST OF TABLES

LIST OF FIGURES

LIST OF ACRONYMS

AWGN:	Additive White Gaussian Noise
BER:	Bit Error Rate
BWAN:	Broadband Wireless Access Network
CCK:	Complementary Code Keying
CFR:	Channel Frequency Response
CIR:	Channel Impulse Response
CP:	Cyclic Prefix
CSI:	Cubic Spline Interpolation
DAB:	Digital Audio Broadcasting
DVB:	Digital Video Broadcasting
DFT:	Discrete Fourier Transform
DPSK:	Differential Phase Shift Keying
FEC:	Forward Error Correction
FD:	Frequency Domain
FDM:	Frequency Division Multiplexing
FFT:	Fast Fourier Transform
FPFI:	Frequency Pilot Frequency Interpolation
GI:	Guard Interval
ICI:	Inter-Carrier Interference
IDFT:	Inverse DFT
IFFT:	Inverse FFT
IR:	Impulse Response
ISI:	Inter-Symbol Interference
LI:	Linear Interpolation
LMS:	Least Mean Square
LMMSE:	Linear MMSE
LOS:	Line of Sight
LPI:	Low-Pass Interpolation
LS:	Least Square
MCM:	Multicarrier Modulation
ML:	Maximum Likelihood
MMSE:	Minimum MSE

MSE:	Mean Square Error
NLOS:	Non-Line of Sight
OFDM:	Orthogonal Frequency Division Multiplexing
PBCC:	Packet Binary Convolution Code
PDF:	Probability Density Function
PSA:	Pilot Symbol Assisted
PSK:	Phase Shifting Keying
QAM:	Quadrature Amplitude Modulation
RLS:	Recursive Least Squares
RMS:	Root Mean Squared
SNR:	Signal to Noise Ratio
SOI:	Second-Order Interpolation
TD:	Time Domain
WiMAX:	Worldwide Interoperability for Microwave Access
WLAN:	Wireless Local Area Networks

INTRODUCTION

This thesis is part of a larger project on indoor communication and radiolocation in the underground mining environment, which is undertaken by the "Laboratoire de Recherche en Communications Souterraines" (LRCS). LRCS, which means "Underground Communications Research Laboratory", was founded in 1999 with research facilities in Val-d'Or (Québec), as well as an on-site location at the CANMET (Canadian Centre for Minerals and Energy Technology) experimental mine. Digital wireless communications with good performance in underground mine is very important for improving operational efficiency, worker's safety and remote control of mobile equipments. However, few researches have considered an underground environment, such as a mine or a tunnel, where propagation is different from the conventional indoor environment. LRCS's research projects benefit from the support and participation of the mining industry in order to ultimately develop efficient communication techniques and novel applications in accordance with their needs, such as highly accurate wireless geo-location in underground mines.

At the CANMET experimental mine, there are two experimental galleries, which are located at the 40 m and the 70 m underground levels, respectively. Due to the curvature of the gallery, there exist Non Line Of Sight (NLOS) situations. Moreover, the walls are very rough, the floor is not flat and some pools of water are covering it [1]. The propagation characterization of the radio channel via measurements have been reported for the CANMET experimental mine in [1] and [2]. Based on it, a wideband statistical model for the 70 m underground level was developed by one of LRCS's students, Mathieu Boutin [3]. Boutin has developed the wideband statistical channel model for both LOS and NLOS areas for the 2.4 GHz and 5.8 GHz frequency bands. For the LOS area case, the best arrival-time model has a modified Poisson distribution and its best amplitude model is Rician. For the NLOS area case, the best arrival time model is a modified Poisson distribution as well, but the best amplitude model is Rayleigh. The phase is considered to be uniformly distributed in both cases. However, the parameters of these models depend on the operating frequency.

Since underground mine galleries can be considered as complex transmission channels where multipath, attenuation, reflection, diffraction and scattering effects are dominant, the

transmitted signal is subject to various impairments and distortions caused by the transmission medium. The receiver has to compensate for the distortions introduced by the channel in order to reliably detect the transmitted information bits. With the rapid growth of wireless communication techniques, the need for high-speed data transmission has increased. However, due to multipath, the indirect paths take more time to travel to the receiver and the delayed copies of the signal interfere with the direct signal causing Inter-Symbol Interference (ISI). ISI is a common problem and becomes a limitation of speed in high date rate communications. To support such high data rates with robustness to wireless channel impairments, one must choose the modulation technique carefully.

The OFDM technique is considered to be a highly suitable technique for high-speed wireless transmissions with high bandwidth efficiency that is also robust to multipath delays. It is intrinsically able to handle the most common distortions found in the wireless environment without requiring complex receiver algorithms. OFDM provides a high data rate with long symbol duration, thus helping to eliminate ISI. Compared to traditional single carrier techniques, OFDM has also a low complexity implementation for high-speed systems. Channel estimation is used instead of a complex equalizer to recover the received signal.

OFDM has received considerable attention from the general wireless community and in particular from the Wireless Local Area Network (WLAN) standards groups. Standards group, such as the Institute of Electrical and Electronics Engineers (IEEE) 802.11, has selected OFDM as the best waveform for providing reliable high data rates up to 54Mbps for WLAN systems.

In OFDM systems, the data bits are modulated on the subcarriers by Phase Shift Keying (PSK) or Quadrature Amplitude Modulation (QAM). In the receiver, the reference phase and amplitude of the constellation on each subcarrier is required to estimate the received bits. However, in wireless communication systems, the constellation of each carrier shows a random phase shift and varied amplitude, which is caused by carrier frequency offset, timing offset and frequency selective fading. To cope with these unknown phase and amplitude variations, dynamic estimation of the channel is necessary before the demodulation of OFDM signals.

Generally, there are two main approaches in channel estimation of OFDM systems, which are pilot symbol assisted (PSA) and subspace-based blind channel estimation methods. Blind

estimation methods appear attractive since they avoid the overhead of training sequences which consumes valuable channel bandwidth. There are also semi-blind methods, which combine both the blind method and training symbols to mitigate the computation complexity. But there still exists a large burden of complexity as compared to PSA channel estimation [8].

On the other hand, channel estimation can be avoided by using differential detection, but it experiences a loss of 3 dB in SNR compared to coherent detection. Moreover, coherent demodulation achieves a better performance for higher order constellation than those used with differential detection. In this sense, the coherent detection is preferable in OFDM systems for high data rate applications. It uses the estimation of reference amplitudes and phases to determine the best possible decision boundaries for the constellation of each subcarrier.

The PSA channel estimation method has been proven feasible in OFDM coherent detection [15]-[18]. Because the channel transfer function may have significant changes even within one OFDM symbol, it is better to estimate channel characteristics based on the pilot signals in each individual OFDM data block. PSA channel estimation can be implemented by either inserting pilots into all of the subcarriers of the OFDM symbols with a specific period or inserting them into a subset of the subcarriers at each OFDM symbol [12]. The first approach is called block-type pilot arrangement and is appropriate for slow fading channel and the second one is called comb-type pilot arrangement, and has been introduced for fast changing channels. Several PSA channel estimation schemes for OFDM based on pilot arrangements have been investigated [15], [25], [28], [29]. A low-rank approximation is applied to Linear Minimum Mean-Square Error (LMMSE) estimation by using the frequency correlation of the channel, in which the performance is essentially preserved while the computational complexity of MMSE is mitigated [25]. However, it requires knowledge of the channel frequency correlation and the operating SNR. In [28], a maximum likelihood (ML) estimator is investigated while no information on the channel statistics or the operating SNR is required. [15] compares the above two schemes and accesses their performances. A nonlinear regression channel model based estimation method for Rayleigh fading is discussed in [29]. It needs no channel statistics but does need a satisfactory pilot density in order to achieve performance not far from the theoretical lower bound.

In this thesis, we will deal with channel estimation for OFDM systems based on comb-type pilot arrangements. The pilot signal estimation is based on the LS or LMS estimation schemes, and the channel estimation is implemented by a variety of interpolation techniques including linear interpolation (LI), second-order interpolation (SOI), cubic spline interpolation (CSI) and low-pass interpolation (LPI) [12]. Since all of the channel estimations will be done in the frequency domain, it is also called Frequency Pilot Frequency Interpolation (FPFI).

MATLAB/SIMULINK software has been used for modeling the studied systems. The typical scenario is derived from the IEEE802.11g standard with OFDM mode, where 16-QAM for 24 Mbps links, Quadrature Phase Shift Keying (QPSK) for 12 Mbps links and Binary Phase Shift Keying (BPSK) for 6 Mbps links are used as modulation schemes, which are mandatory for the IEEE802.11 OFDM system. The performances for different modulation schemes and different interpolation algorithms in terms of their error for the estimated channel impulse response (CIR) and transfer functions as well as the resulting Bit Error Rates (BER) are investigated and compared.

This thesis is organized as follows:

In ***CHAPTER 1***, background information on wireless communication channels is provided to aid the understanding of the channel estimation problem. Also, an introduction to OFDM and its development history are given. Finally, OFDM applications in WLAN are presented.

In ***CHAPTER 2***, the important characteristics of OFDM technology is emphasized. The statistical model based on experimental measurements for our underground mine environment is also reviewed. The choice of parameters in OFDM systems is provided at the end of this chapter.

In ***CHAPTER 3***, first a review of the PSA-OFDM channel estimation technique is presented. A literature survey of previous works on PSA channel estimation for OFDM is provided. Different channel estimation algorithms with their mathematical descriptions are studied.

In ***CHAPTER 4***, the computer simulation model design is provided and detailed informations on implementation are presented.

In ***CHAPTER 5***, the channel estimation techniques for different channel models with different modulations are studied by simulations. The system performance through simulation results are compared and analyzed by measuring the BER.

In ***CHAPTER 6***, a conclusion of the work presented in this thesis is given and some possible future works are suggested to extend this research.

CHAPTER 1
OFDM IN WIRELESS COMMUNICATION SYSTEMS

1.1 Introduction

In an ideal wireless channel, the received signal would consist of only a single direct path signal, which would be a perfect reconstruction of the transmitted signal. However, a real channel, such as an underground mine gallery, can be considered as a complex transmission line where multipath, attenuation, reflection, diffraction and scattering effects are present. On top of all this, the channel adds noise to the signal and can cause a shift in the carrier frequency if the transmitter or receiver is moving (Doppler effect). For wideband wireless communication systems, the channel is characterized as frequency-selective and time-varying, thus conventional modulation methods suffer from multipath in both the frequency and time domains. Also there is intersymbol interference (ISI), delay spread, and interference, which make the link quality vary. Understanding of these effects on the received signal is important because the performance of a wireless system is dependent on the wireless channel characteristics. Wireless transmission systems based on OFDM is considered as the best choice to combat the multipath effects because of its high receiving performance and robustness under multipath fading environment. It has already been adopted by the IEEE 802.11a/g standards for WLAN.

In this chapter, basic wireless propagation theory is provided with emphasis on the impact of the small-scale fading effects on the wireless channel. IEEE 802.11-based WLAN system, OFDM history and basic principle of OFDM are also presented.

1.2 Propagation characteristics of wireless channel

1.2.1 Multipath fading effects

The wireless propagation environment places fundamental limitations on the performance of a wireless communication system because the transmitted signal travels through different paths and interacts with objects in the environment. These interactions include reflection, refraction, diffraction, and scattering which cause attenuation and variation in the received signal power and phase of the transmitted signal. This results in a phenomenon known as multipath fading, where the term fading describes the fluctuations of the envelope of the transmitted signal as it travels from the transmitter to the receiver. In addition, the relative movement between the transmitter and receiver generates a Doppler shift which also impacts the fading characteristics of the signal [4].

The multipath effect is a phenomenon that causes multiple versions of the transmitted signal to arrive at the receiver at different time delays, as shown in Figure 1.1. Each of the paths will have different characteristics, such as amplitude, phase, arrival time and angle of arrival. The multiple signals may constructively or destructively add up at the receiver, thus creating the rapid fluctuation in the received signal envelope. Multipath also causes ISI because the transmitted signal arriving at different times will overlap with each other [4].

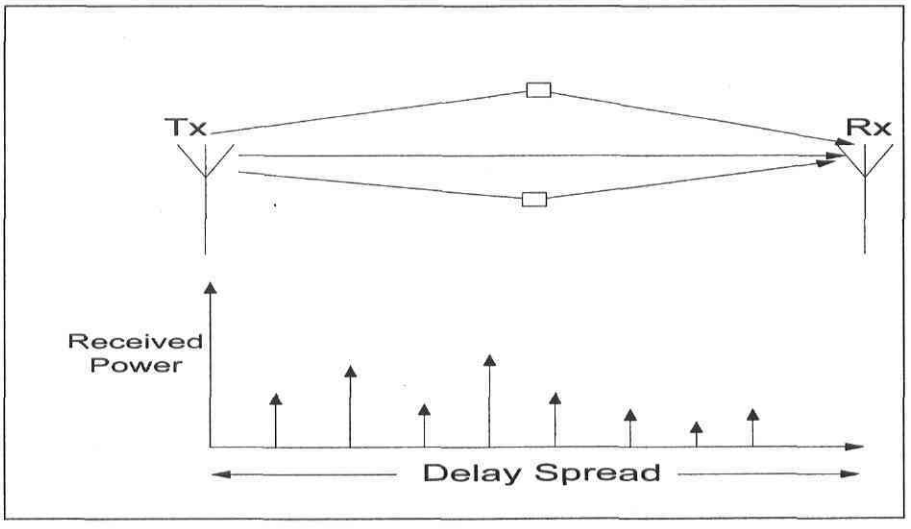

Figure 1. 1: Multipath effect.

1.2.2 Multipath channel model

Although channel fading is unpredictable, stochastic models have been developed to accurately predict the fading characteristics. Multipath fading results in fluctuation of the signal amplitude because of the addition of signals arriving with different phases. Because the phases of the arriving paths are changing rapidly, the received signal amplitude undergoes rapid fluctuations that are often modeled as a random variable with a particular distribution

1.2.2.1 Rayleigh fading channel

The most commonly used distribution for multipath fading is the Raleigh distribution. If there are multiple reflective paths and there is no single dominant path, then the process is zero mean and the envelope of such a received signal is statistically described by a Rayleigh probability density function and the channel is said to be Rayleigh fading. The Rayleigh probability density function is defined as [8]:

$$f(x)=\frac{x}{\sigma^2}\exp\left(-\frac{x^2}{2\sigma^2}\right) \qquad \sigma>0,\quad x\geq 0 \tag{1.1}$$

It is thus characterized by one parameter, σ. The Rayleigh distribution is largely used to describe multipath fading due to its elegant theoretical explanation and occasional empirical justifications [8]. Figure 1.2 shows the level of attenuation that can occur due to Rayleigh fading.

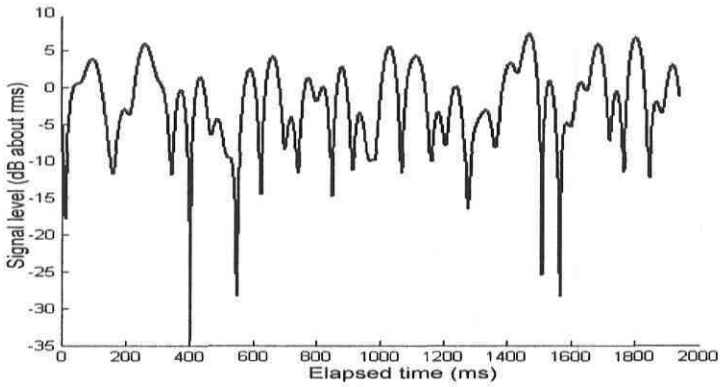

Figure 1. 2: A typical Rayleigh fading envelope.

1.2.2.2 Rician fading channel

This distribution can occur when a strong signal component exists in addition to weaker scattered components. This strong component can be the one occurring on LOS or one having undergone much less attenuation by comparison to other occurring components. The process is nonzero mean and the fading envelope is described by a Rician probability density function. In such a case, the channel is considered to be a Rician fading channel. Its probability density function is defined as [8]:

$$f(x)=\frac{x}{\sigma^2}\exp\left(-\frac{\left(x^2+\sigma^2\right)}{2\sigma^2}\right)I_0\left(\frac{xv}{\sigma^2}\right) \qquad x\geq 0 \tag{1.2}$$

where, I_0 is the modified Bessel function of the zero-th kind and v is the mean due to the fixed scatterers or LOS path.

The Rice distribution can also be characterized by its K-factor which quantifies the power of the dominant signal component, relative to the multipath random components. Let A define the direct wave peak amplitude, and S define the standard deviation of the overall received signal, then the Rician K-factor is given as:

$$K=\frac{A^2}{2S^2} \tag{1.3}$$

For Rician fading, the K-factor is typically between 1 and 10. A K-factor of 0 corresponds to Rayleigh fading [8]. This K-factor will be used in the next section when discussing the statistical modeling of the impulse responses (IR).

1.2.3 Delay spread

Multipath can be described in two domains, namely the frequency response (FR) in the frequency domain (FD) and the impulse response (IR) in the time domain (TD). The IR of a multipath channel generally exhibits a delay spread. For a single transmitted impulse, the time between the

first and the last received components is called the maximum excess delay τ_m, as shown in Figure 1.3.

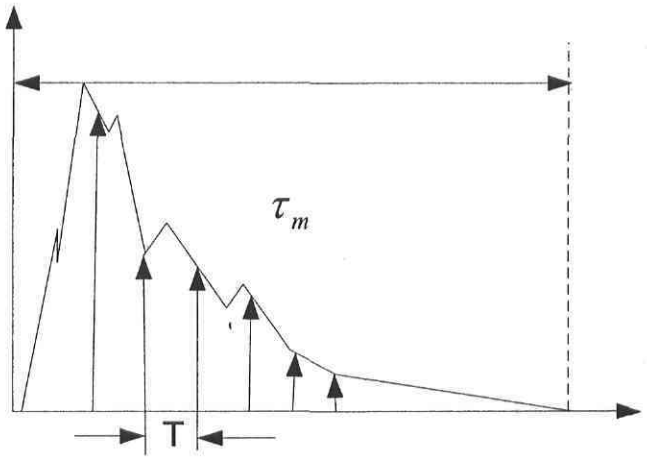

Figure 1. 3: Effective length of channel impulse response.

In a digital system, the delay spread can lead to ISI. It is due to the delayed multipath signal overlapping with the following symbol. This can cause significant errors in high bit rate systems. As the transmitted bit rate is increased, the amount of ISI also increases. The effect starts to become very significant when the delay spread is greater than 50% of the bit duration.

Table 1.1 displays the typical delay spread that can occur in various environments. The maximum delay spread in an outdoor environment is approximately 20 μsec, thus significant ISI can occur at bit rates as low as 25 kbps.

Table 1. 1: Typical delay spread [4].

Environment or cause	Delay Spread	Maximum Path Length Difference
Indoor (room)	40 nsec-200 nsec	12 m-60 m
Outdoor	1 μsec-20 μsec	300 m-6 km

1.2.4 Doppler shift

When a wave source and a receiver are moving relative to one another, the frequency of the received signal will not be the same as the source. For example, when the source and the receiver are moving towards each other, the frequency of the received signal is higher than the source. This is called the Doppler effect. The amount of frequency variation due to the Doppler effect depends on the relative motion between the source and the receiver and the speed of propagation of the wave, and is expressed as:

$$f_D = \pm \frac{f_0 v}{c} \tag{1.4}$$

where, v is the relative velocity of the vehicle, f_0 is the wavelength of the carrier, and c is the speed of light.

The Doppler shift can cause significant problems if the transmission technique is sensitive to carrier frequency offsets or the higher relative speed, such as is the case for OFDM.

1.2.5 Frequency selective fading

A channel is frequency-selective if the frequency response of the channel changes significantly within the band of the transmitted signal, while a constant frequency response is called flat fading. Figure 1.4 (a), (b) exemplifies the frequency-selective channel and flat fading channel. A characteristic of frequency selective fading is that some frequencies are enhanced, whereas others are attenuated.

The modulated signal, as shown in Figure 1.4 (c), going through a frequency-selective fading channel will be distorted, resulting in ISI. To mitigate ISI, the symbol duration must be long enough so that the ISI-affected portion of a symbol can be negligible. From the FD viewpoint, this means transmitting a narrow-band signal within whose bandwidth the channel can be well considered to be flat fading, as shown in Fig 1.4 (d). This brings the idea that we can transmit several low-rate data streams, each at a different carrier frequency through the channel in parallel, each data stream is ISI-free and only a simple one-tap equalizer is needed to compensate the flat

fading. This is illustrated in Figure 1.5 and is in fact the idea of frequency division multiplexing (FDM).

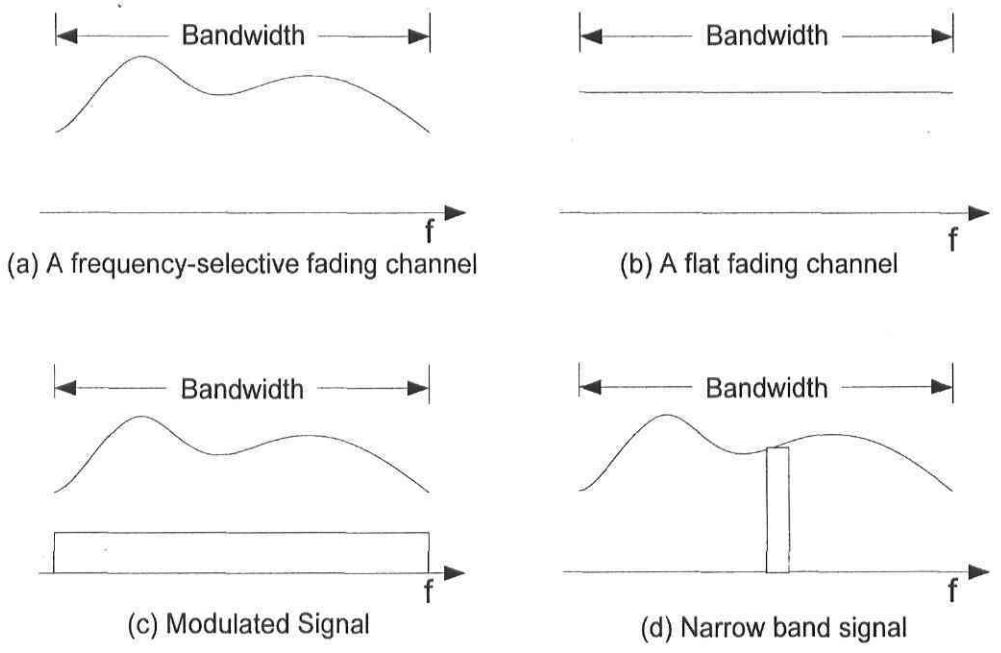

Figure 1. 4: Signals transmitted through frequency-selective channels.

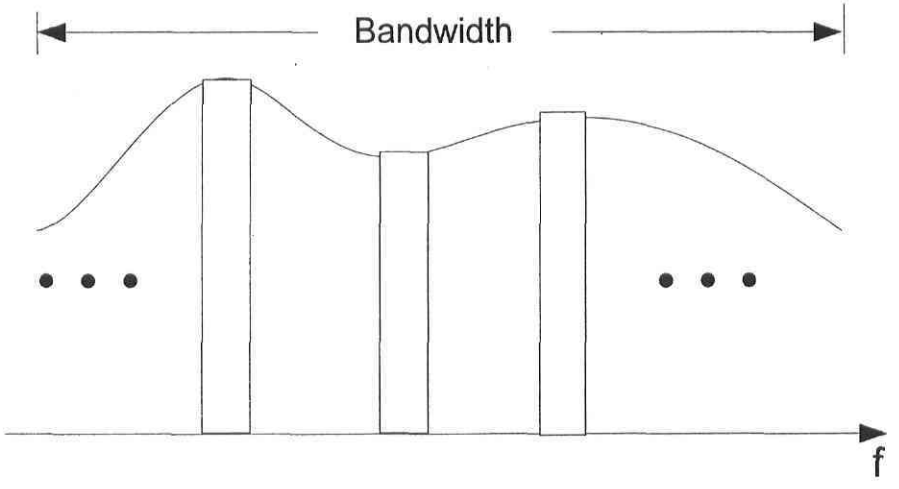

Figure 1. 5: Multicarrier modulation scheme.

However, this multicarrier transmission scheme may suffer inter-carrier interference (ICI), i.e., the signals of neighboring carriers may interfere with each other. To avoid ICI, guard bands are employed in FDM to separate different subcarriers. This results in a waste of the spectrum.

OFDM follows a similar multicarrier modulation strategy. However, it employs the orthogonality among subcarriers to eliminate ICI without the need of the guard bands.

1.3 Introduction to OFDM

OFDM originated from the need of efficient communications through frequency-selective fading channels. OFDM can be simply defined as a form of multicarrier modulation (MCM). MCM is the principle of transmitting a high-rate serial data stream by splitting it into a set of parallel low-rate sub-streams and modulating each of these data streams onto individual subcarriers, where carrier spacing is carefully selected to make each subcarrier orthogonal to the other subcarriers. It is possible to arrange the carriers in an OFDM signal so that the sideband of the individual carriers overlap and the signals can still be received without adjacent carrier interference.

In OFDM signaling, the following orthogonality condition is satisfied,

$$\int_0^T e^{j2\pi f_i t} e^{-j2\pi f_j t} d_t = \int_0^T e^{j2\pi (f_i - f_j) t} d_t = 0, \quad i \neq j \tag{1.5}$$

This means that the space between the frequencies of the subcarriers should be

$$\Delta f = f_i - f_j = \frac{m}{T} \tag{1.6}$$

where m can be any positive integer. The smallest space for orthogonality is equal to the symbol rate $1/T$.

With orthogonality, each subcarrier can be demodulated independently without ICI. It should be noted that the passbands of the subcarriers may overlap in OFDM, as shown in Figure 1.6.

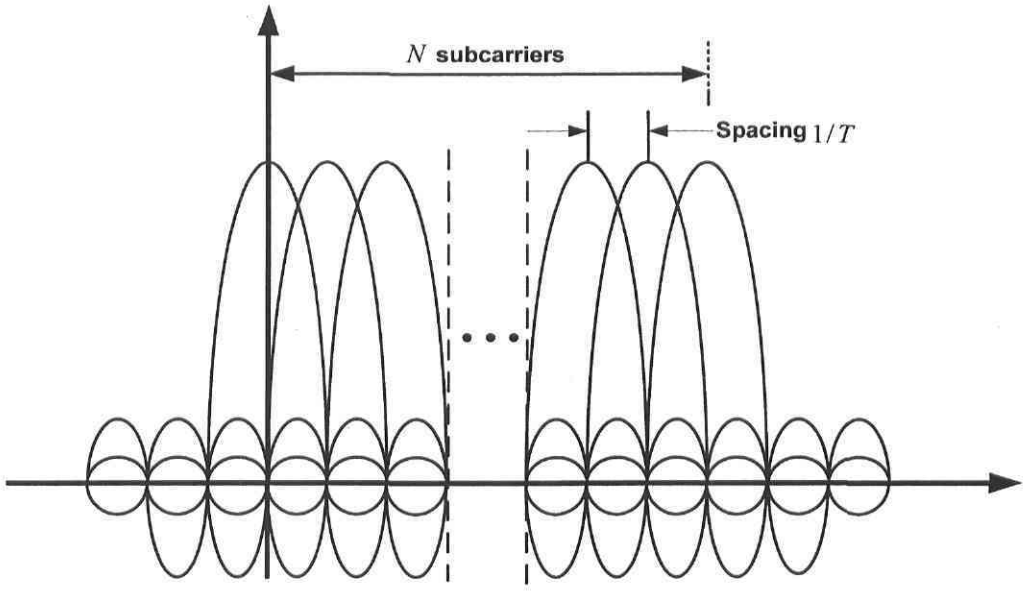

Figure 1. 6 : An OFDM system with N subcarriers over a bandwidth W .

Compared with conventional non-overlapping multicarrier technique, OFDM can save almost 50% of bandwidth by using the overlapping multicarrier modulation technique, as shown in Figure 1.7.

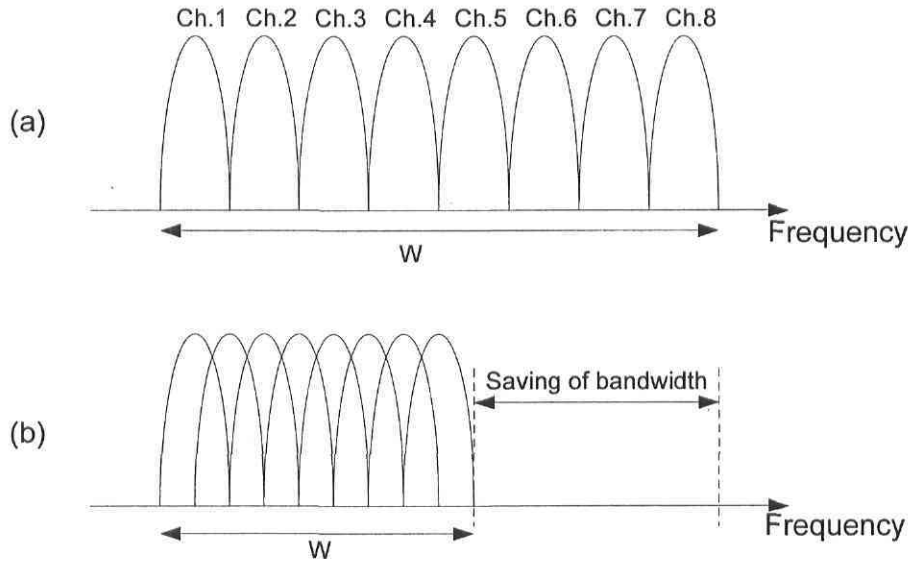

Figure 1. 7: (a) Conventional multicarrier technique and (b) Orthogonal multicarrier modulation technique.

In digital communication systems, the OFDM symbol is a sum of subcarriers that are individually modulated by using PSK or QAM. A detailed description of OFDM can be found in [7] where we can find the expression for one OFDM symbol at $t = t_s$ as follows:

$$s(t) = \mathrm{Re}\left\{ \sum_{i=-\frac{N_s}{2}}^{\frac{N_s}{2}-1} d_{i+N_s/2} \exp\left(j2\pi \left(f_c - \frac{i+0.5}{T} \right)(t - t_s) \right) \right\}, \qquad t_s \le t \le t_s + T \tag{1.7}$$

$$s(t) = 0, \qquad t < t_s, \quad t > t_s + T$$

where, d_i are complex modulation symbols, N_s is the number of subcarriers, T is the symbol duration, and f_c is the carrier frequency .

The equivalent complex baseband notation is given by:

$$s(t) = \sum_{i=-\frac{N_s}{2}}^{\frac{N_s}{2}-1} d_{i+N_s/2} \exp\left(j2\pi \frac{i}{T}(t - t_s) \right), \qquad t_s \le t \le t_s + T \tag{1.8}$$

$$s(t) = 0, \qquad t < t_s, \quad t > t_s + T$$

In this case, the real and imaginary parts correspond to the in-phase and quadrature parts of the OFDM signal. They have to be multiplied by a cosine and sine of the desired frequency to produce the final OFDM signal. Figure 1.8 shows the block diagram for the OFDM modulator.

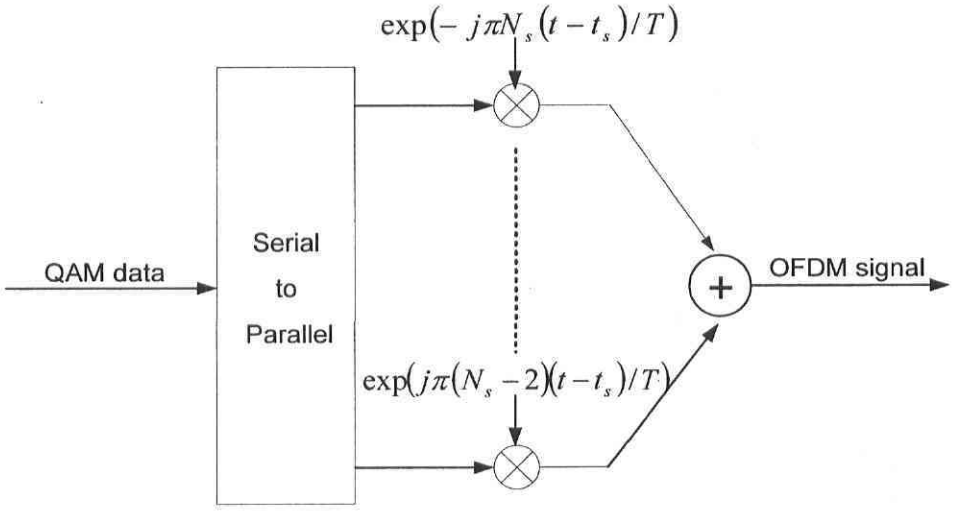

Figure 1. 8: OFDM modulator.

The complex baseband OFDM signal defined by (1.8) is the inverse Fourier transform of N_s QAM input symbols. The time discrete case is the inverse discrete Fourier transform (IDFT). In practice, this transform can be implemented very efficiently by the inverse fast Fourier transform (IFFT). The IFFT drastically reduces the amount of calculations by exploiting the regularity of the operation in the IDFT [7].

OFDM is intrinsically able to handle the most common distortion found in wireless environments without requiring complex receiver algorithms. It also has both advantages and disadvantages, but in many of the modern wireless applications, the disadvantages of OFDM can be overcome with careful design choices. Consequently, OFDM is frequently the best fit when optimizing cost and performance for wireless environments like WLAN systems, where multipath is the primary impairment to reliable communications.

1.4 History of OFDM

OFDM is an old concept. The concept of using parallel data transmission and frequency division multiplexing was published in the mid-1960s. In the late 60's, OFDM was introduced based on the multicarrier modulation technique used in high frequency military radios. However, OFDM did not become popular at that time because it was too expensive and complex for a practical deployment.

In 1971, Weinstein and Ebert [31] proposed the use of the IDFT and Discrete Fourier Transform (DFT) as an efficient way to perform baseband modulation and demodulation in OFDM systems. This new proposal made OFDM technology more practical and it began to attract more and more attention. Currently, OFDM systems apply IFFT and FFT to perform modulating and demodulation of the information data.

The orthogonality of the subcarriers will be destroyed when the signals are transmitted through a frequency-selective fading channel, causing ICI. To combat ICI, Peled and Ruiz [32] introduced the concept of cyclic prefix (CP) in 1980. By using a guard interval (GI) with a cyclic extension of OFDM symbols, the orthogonality will be kept when the CP is longer than the IR of the channel.

OFDM has been particularly successfully in numerous wireless applications, where its superior performance in multipath environments is desirable. OFDM is currently applied in several high rate wireless communications standards such as the European digital audio broadcasting (DAB), digital video terrestrial broadcasting (DVB-T), IEEE802.11a [11], IEEE802.11g [10]. In 2003, the IEEE finalized the Wireless Metropolitan Area Networks (WMAN) standard 802.16 [9], which utilizes OFDM technologies for 2 to 11 GHz broadband wireless access network (BWAN). The HiperMAN working group will utilize the OFDM sections of the IEEE 802.16a standard as the baseline physical layer specification for the European Telecommunications Standards Institute (ETSI) HiperMAN standard. The OFDM Forum also participates in standards work through organization such as the Worldwide Interoperability for Microwave Access (WiMAX) Forum. WiMAX is to 802.16 what the Wi-Fi alliances is to 802.11 LANs. WiMAX will support compliance and interoperability testing of WMAN air interface from 2 to 66 GHz. WiMAX/HiperMAN use 256 OFDM instead of 64 OFDM used in IEEE 802.11a/g on WLAN. IEEE 802.16 technology will likely grow fast in the next few years. It is not seen as a competitor of IEEE802.11, but rather a complement since it handles long distance connections and IEEE802.11 handles local network connections for a single location [9]. A brief list of OFDM history and its applications are shown in Table 1.2.

Table 1. 2: History of OFDM technique and its application.

1957	Kineplex, multicarrier high frequency (HF) modem
1966	R. W. Chang, Bell Labs, OFDM paper + patent
1971	Weinstein & Ebert proposed the use of FFT and guard interval
1985	Cimini described the use of OFDM for mobile communications
1987	Alard & Lasalle proposed OFDM for digital broadcasting
1995	ETSI established the first OFDM based standard, DAB standard
1997	DVB-T standard was adopted
1997	Broadband internet with asymmetrical digital subscriber line (ADSL) was employed
1998	Magic WAND project demonstrated OFDM modems for WLAN
1999	IEEE802.11a and HIPERLAN/2 standards were established for WLAN
2000	Vector OFDM (V-OFDM) for a fixed wireless access
2001	OFDM was considered for the IEEE802.11g and the IEEE802.16 standards

1.5 Applications of OFDM in WLAN systems

WLAN emerged as an extension to the wired LAN. It is the first technology that was examined for wideband local access. Compared with wired LANs, WLAN systems operate in a difficult medium for communication, and they need to support mobility and security. The wireless medium has serious bandwidth limitations and frequency regulations and it suffers from time and location dependent multipath fading [6], [7]. Recently, the need for higher data rates to improve performance of wireless LANs has become crucial due to many reasons.

With higher bandwidth supported by the standards, WLAN systems are deployed for larger numbers of users involving application of email, web browsing and database access. As the first WLAN standard, IEEE802.11 is facing the challenge of organizing a systematic approach for defining a standard for wireless wideband local access. It specifies one medium access control and three different physical layers, which give a data rate of 2 Mbps [11]. Following the initial standards of 1 Mbps and 2 Mbps, IEEE802.11 developed two new physical layer standards, namely IEEE802.11a and IEEE802.11b. The IEEE802.11b specification increased the data rates and maintained compatibility with the original 802.11 DSSS standard and incorporated a more efficient coding scheme known as complementary code keying (CCK) to attain a top-end data rate of 11 Mbps in the 2.4 GHz band. A second coding scheme, packet binary convolution code (PBCC) was included as an option for higher performance at the 5.5 and 11 Mbps rates, as it provided for a 3 dB coding again. The IEEE802.11a ventured into a different frequency band, the 5.2 GHz U-II band, and was specified to achieve data rate up to 54 Mbps using OFDM. IEEE802.11a provides maximum performance with currently available technologies, but more access points are needed because of the weaker range compared to 802.11b [11].

The IEEE 802.11g standard is used presently [10]. It uses the same 2.4 GHz radio spectrum as 802.11b equipments, but with the higher data rates, packet structure, and modulation technology of 802.11a. It can achieve its 54 Mbps data rate by using OFDM. The use of OFDM in standards also allows a better efficiency and enables mixed network operation. The operational mode in the IEEE 802.11g standard is shown in Table 1.3.

Table 1. 3: IEEE 802.11g operational mode.

Mode	Data rate (Mbps)	Modulation technique
802.11b	1, 2, 5.5, 11	DSSS, CCK, PBCC
OFDM	6, 9, 12, 18, 24, 36, 48, 54	OFDM
PBCC-22 and PBCC-33	2, 5.5, 11, 22, 33	DSSS, PBCC
CCK-OFDM	6, 9, 12, 18, 24, 36, 48, 54	DSSS, OFDM

In this thesis, typical scenarios of OFDM are derived from the IEEE802.11a standard based OFDM mode with three different modulation schemes, namely 16-QAM for a 24 Mbps link, QPSK for a 12 Mbps link, and BPSK for 6 Mbps link.

1.6 Summary

As we discussed above, for indoor wireless communications, the channel is generally modeled as frequency selective fading and time-varying, where multipath and fading are the significant characteristics. As a result of multipath fading, the received signal suffers from distortions, such as ISI, delay spread, attenuation, fading etc. Nowadays, OFDM has attracted much interest because of its high-speed data transmission and effectiveness in handling the most common distortions found in the wireless environment without requiring complex receiver algorithms. It has been considered in WLAN standards, such as IEEE 802.11a and IEEE 802.11g, to cope with the problem of multipath reception with high date rate transmissions.

CHAPTER 2
OFDM SYSTEM AND CHANNEL MODELS

2.1 Introduction

In OFDM systems, the high-rate data stream is split into a number of lower rate streams that are transmitted simultaneously over a number of subcarriers. Because the symbol duration increases for the lower rate parallel subcarriers, the relative amount of dispersion in time caused by multipath delay spread is decreased. ISI is almost eliminated completely by introducing a guard interval (GI) in every OFDM symbol. In the guard time, the OFDM symbol is cyclically extended to avoid ICI. This whole process of generating an OFDM signal and the preliminary concepts such as series-to-parallel converter, IFFT and GI will be described in section 2.2.

Channel estimation is the task of estimating the frequency response of the radio channel which the transmitted signal travels before reaching the receiver antenna. In wideband wireless communication systems, especially in the mining environment, the channel is usually frequency selective and time variant and the channel transfer function appears unequal in both frequency and time domains. Therefore, dynamic channel estimation is necessary for the demodulation of OFDM signals. In OFDM system, the coherent demodulation is preferable for high data rate applications, which are of interest in this thesis. The OFDM channel estimation principles will be presented in section 2.3. The statistical channel model and mathematical description will be shown in section 2.4 based on [1], [2], [3]. The choice of OFDM system parameters is described in the last section, with the example of IEEE802.11a OFDM.

2.2 Basic principle of OFDM

At the transmission side, the binary information is first grouped and mapped into complex-valued symbols according to the modulation by different mapping schemes, such as BPSK, QPSK, 16QAM, and 64QAM. Then there is a serial to parallel conversion to prepare different data groups for different OFDM subcarriers. The mapped signals are modulated onto N orthogonal subcarriers by the IFFT. A cyclic prefix (CP) is then added to the multiplexed IFFT output. Finally, the obtained signal is converted to a time continuous analog signal before it is transmitted through the channel. At the receiver side, an inverse operation is carried out and the information data is detected.

2.2.1 Series and parallel concepts

The series and parallel converters are considered to realize the concept of parallel data transmission, as shown in Figure 2.1. In a conventional serial data system, the symbols are transmitted sequentially and the frequency spectrum of each data symbol is allowed to occupy the entire available bandwidth. When the data rate is sufficiently high, several adjacent symbols may be completely distorted over a frequency-selective fading or a multipath delay spread channel.

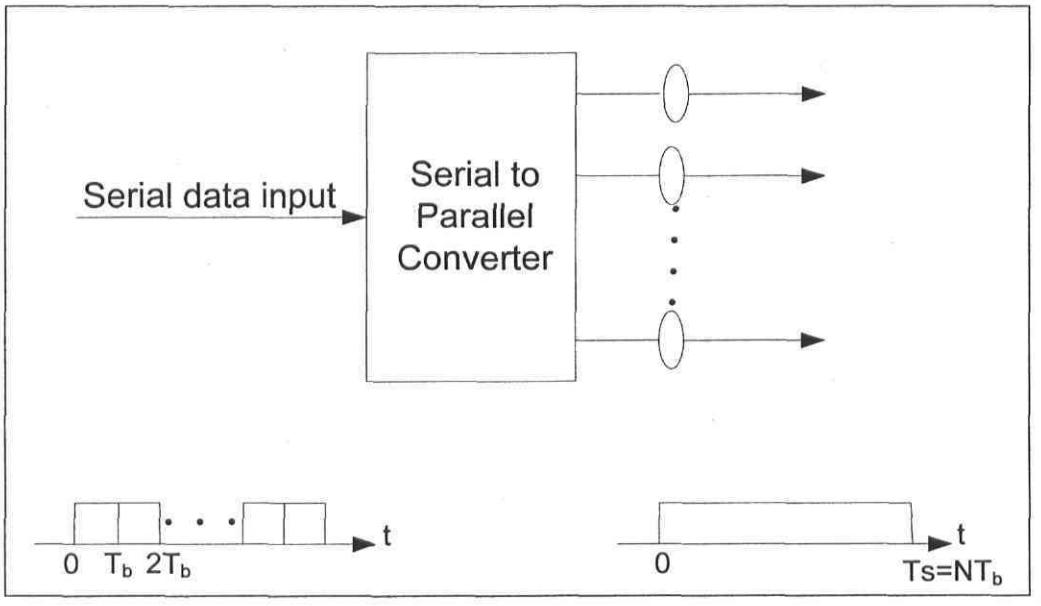

Figure 2. 1: Serial to parallel (S/P) converter.

In an OFDM system, the entire channel bandwidth is divided into many narrow sub-bands and the spectrum of an individual data element occupies only a small part of the available bandwidth, so the frequency response over each individual sub-channel is relatively flat. Hence, the parallel data transmission can resist to frequency selective fading.

2.2.2 FFT and IFFT

The key components of an OFDM system are the IDFT at the transmitter and the DFT at the receiver. These operations perform linear mapping between N complex data symbols and N complex OFDM symbols, resulting in robustness against the multipath fading channel. The complex baseband OFDM signal as defined by (1.7) is in fact nothing more than the inverse Fourier transform of N_s modulated input symbols. The use of DFT and IDFT to replace the sinusoidal generator and the demodulation significantly reduces the implementation complexity of OFDM modulator, as shown in Figure 2.2.

Suppose the data set to be transmitted is

$$X(1),\ X(2),\ \ldots,\ X(N)$$

where, N is the total number of subcarriers.

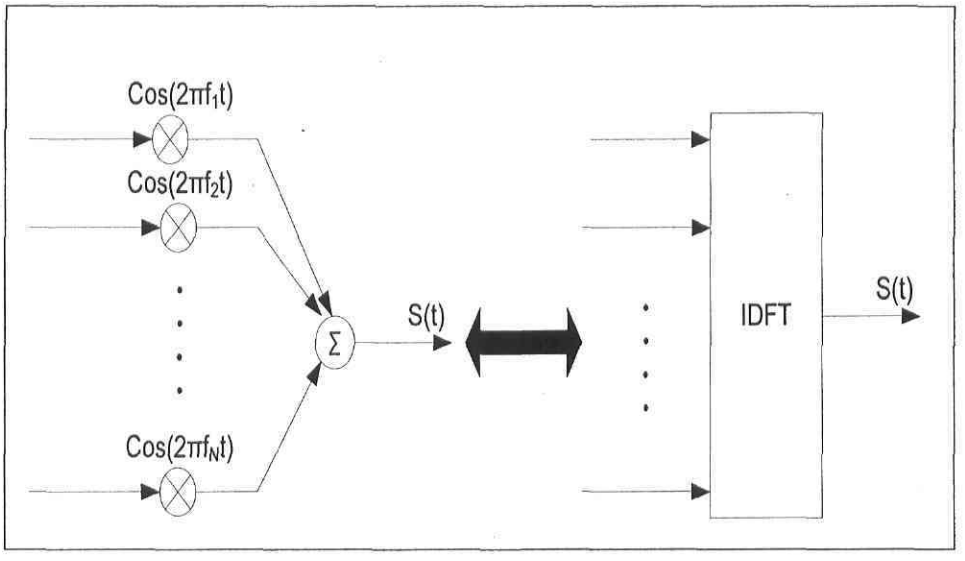

Figure 2. 2: DFT implementation of transmitted waveform.

Then the discrete-time representation of the signal after IDFT is

$$x(n)=\frac{1}{\sqrt{N}}\sum_{k=0}^{N-1}X(k)\exp\left(j2\pi k\frac{n}{N}\right),\qquad n=0,\ 1,\ \ldots,N-1 \tag{2.1}$$

where, $X(k)$ denotes the k^{th} discrete spectral sample of N samples in the FD.

At the receiver side, the data is recovered by performing a DFT on the received signal.

$$X(k)=\frac{1}{\sqrt{N}}\sum_{n=0}^{N-1}x(n)\exp\left(-j2\pi k\frac{n}{N}\right),\qquad k=0,\ 1,\ \ldots,N-1 \tag{2.2}$$

where the sequence $\{x(n)\}$ contains N samples in the TD.

The FFT/IFFT algorithm is well known and widely used in digital signal processing for its efficient evaluation of the DFT/IDFT. An N-point FFT requires only $N\log(N)$ multiplications, which is more computationally efficient than an equivalent single carrier system with an equaliser in the TD.

The IFFT function block is also used to realize the zero forcing equalization to compensate the effective channel in the FD. An efficient OFDM implementation converts a serial symbol stream of modulated data into size M parallel streams. These M streams are then modulated onto M subcarriers via the use of a size N ($N \geq M$) IFFT. The N outputs of the IFFT are then serialized to form a data stream that can then be modulated by a single carrier. The N-point IFFT can modulate up to N subcarriers. When M is less than N, the remaining $N-M$ subcarriers are not in the output stream. Essentially, these subcarriers have been modulated with zero amplitude (zero-padding). For example, the IEEE802.11a standard specifies that 52 ($M = 52$) out of 64 ($N = 64$) possible subcarriers are modulated by the transmitter, as shown in Figure 2.3.

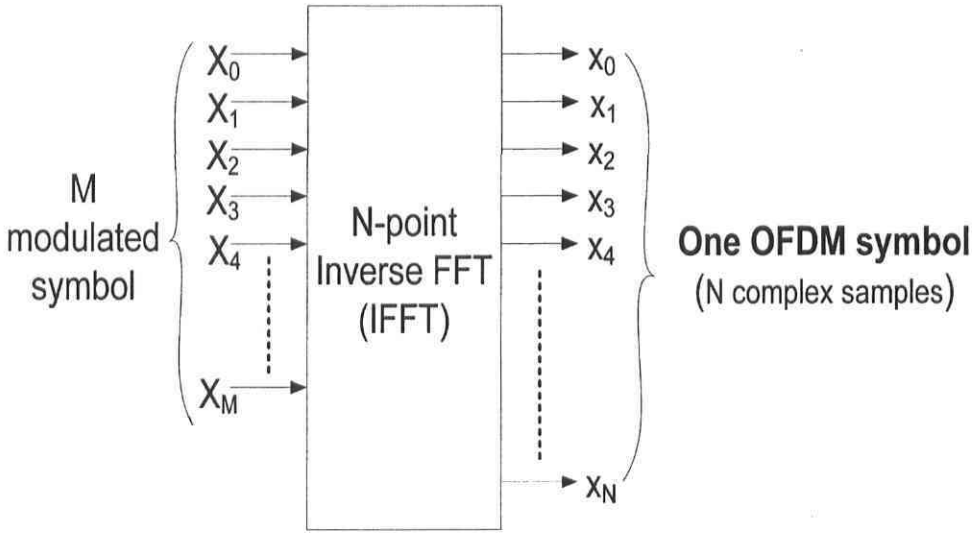

Figure 2. 3: OFDM generation by *N*-point IFFT.

2.2.3 Guard interval and cyclic extension

In the multipath fading channel environment, channel dispersion causes the consecutive blocks to overlap, creating ISI and intercarrier interference (ICI). To eliminate ISI almost completely, a GI is introduced for each OFDM symbol. The GI is chosen larger than the expected delay spread, such that multipath components from one symbol cannot interfere with the next symbol. The GI could consist of no signal at all. However, in this case, the problem of ICI would arise. ICI is crosstalk between different subcarriers, which means they are no longer orthogonal [8].

In order to avoid ICI, a CP is used as GI. This is done by taking symbol period samples from the end of the period and appending them to the front of the period, as shown in Figure 2.4. The CP is equal or greater in length than the channel impulse response (CIR), or the maximum delay spread of the channel. This ensures that delayed replicas of the OFDM symbol always have an integer number of cyclic within the FFT interval.

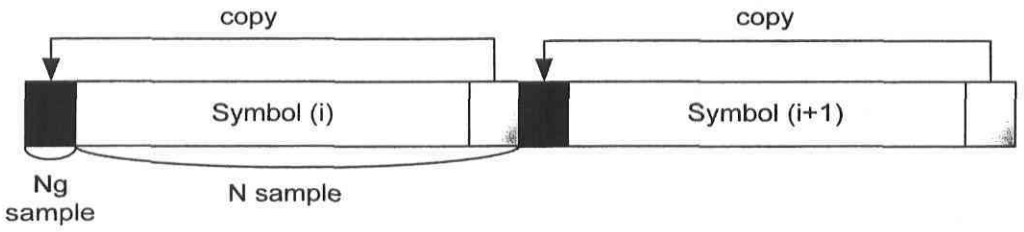

Figure 2. 4 : Guard interval with cyclic extension.

Although the insertion of the CP imposes a penalty on bandwidth efficiency, it is often the best compromise between performance and efficiency in the presence of ISI. Since a complete period is integrated, the orthogonality is maintained. Therefore, both ISI and ICI are eliminated. The counteraction effect of the CP against multipath channel is shown in Figure 2.5.

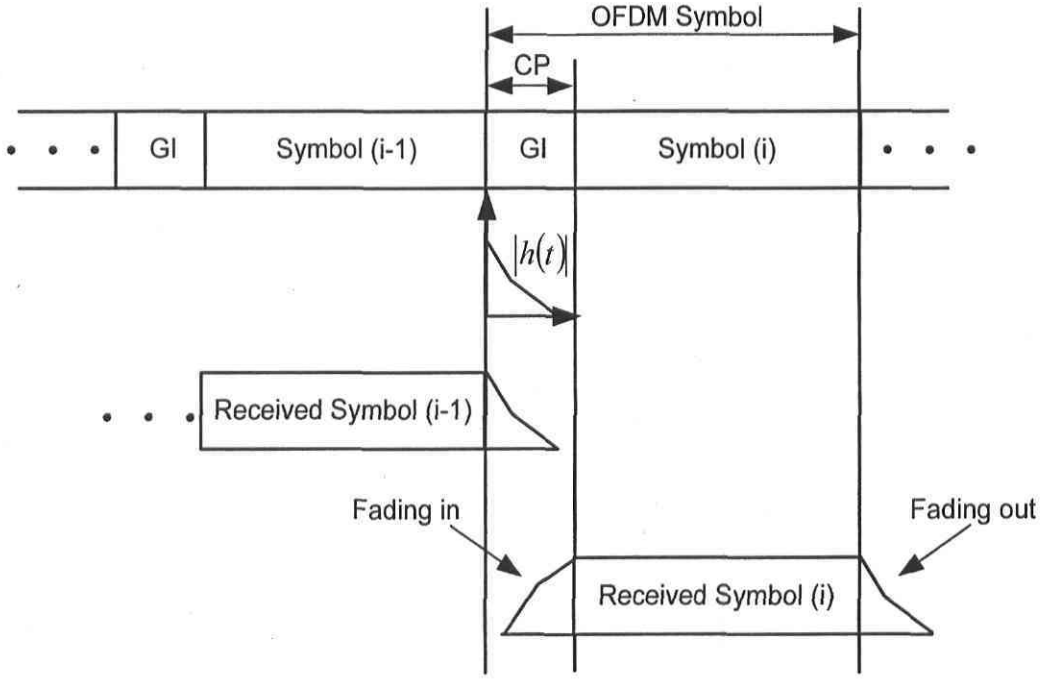

Figure 2. 5: The counteraction effect of CP against ISI and ICI.

2.3 Channel estimation of OFDM systems

Channel estimation is an important component of a communication system. With the information on the CIR or the parameters of a channel, one can perform optimal symbol detection, construct an equalizer or predict the channel.

In OFDM systems, since the channel introduces amplitude and phase shifts due to the frequency-selective and time-varying nature of the wireless channel, modulated bits are distorted during transmission through the channel. In order to acquire the original bits in the receiver, one needs to take into account these unknown changes. The receiver applies either coherent detection or non-coherent detection to recover the original bits. Coherent detection [7] uses reference values that are transmitted along with data bits. The entire channel can then be estimated by using several interpolation techniques. Non-coherent detection [7], [8], on the other hand, does not use any reference values but often uses differential modulation, where the information is transmitted in the difference of two successive symbols. The receiver uses two adjacent symbols in time or two adjacent subcarriers in frequency to compare one with the other to acquire the transmitted symbol. Non-coherent detection has the advantage that the channel estimation is not needed. However, without channel estimation, OFDM systems have to use differential PSK (DPSK), which has a 3 dB signal-to-noise ratio (SNR) loss compared with coherent PSK [16]. DPSK is appropriate for relatively low data rates, such as the European DAB systems [7]. Moreover, the coherent detection achieves a better performance for higher order constellations than those used with non-coherent detection [8], [16]. Therefore, coherent detection is preferable for high data rate applications and is often used in OFDM systems.

Accurate channel estimation algorithms can be applied in OFDM systems to allow coherent detection, thereby improving system performance. Based upon whether the channel estimation algorithms apply training symbols, we can divide them into three categories: training (pilot) based algorithms, blind algorithms, and semi-blind algorithms [7], [8]. Training (pilot) based algorithms assume known symbols (training or pilot symbols) are inserted in the transmitted signals. It is then possible to identify the channel at the receiver by exploiting knowledge of these known symbols. Blind algorithms estimate the channel based on properties of the transmitted signals. Semi-blind algorithms can improve the performance of blind algorithms by exploiting the knowledge of both known symbols and properties of the transmitted signals. The objective of semi-blind channel estimation algorithms is to get better performance than blind algorithms while requiring fewer known symbols than training based channel estimation algorithms.

Most channel estimation methods for OFDM transmission systems have been developed under the assumption of a slow fading channel, where the channel transfer function is assumed

stationary within one OFDM data block. In addition, the channel transfer function for the previous OFDM data block can be used as the transfer function for the present data block. However, in practice, the channel transfer function varies even within one OFDM data block.

Therefore, for coherent detection of OFDM, it is preferable to estimate channel characteristics based on training (pilot) signal in each individual OFDM data block. The pilot symbol assisted (PSA) based channel estimation algorithm is a suitable method for OFDM coherent detection.

2.4 Wideband statistical channel model for the underground environment

2.4.1 Environment description

The CANMET underground environment has two experimental galleries dedicated for LRCS, which are at depths of 40 m and 70 m, respectively, as shown in Figure 2.6. Both of these galleries have very rough surfaces, adjacent smaller galleries and are very humid. The floor is flatter than the ceiling or the walls, but has some water puddles [1], [2].

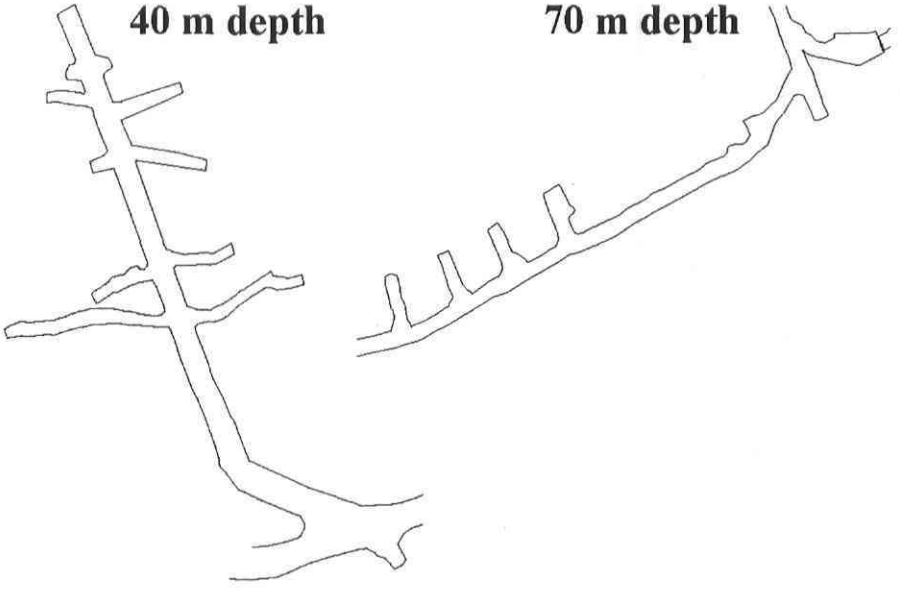

Figure 2. 6: CANMET galleries.

A wideband statistical model was developed based on the gallery at 70 m depth [3]. The picture of this gallery is shown in Figure 2.7. This gallery stretches over a length of 70 meters with a

width of 2.5 to 3 meters and a height of approximately 3 meters [1]. This gallery has greater wall roughness and smaller dimensions than the one at 40 m depth.

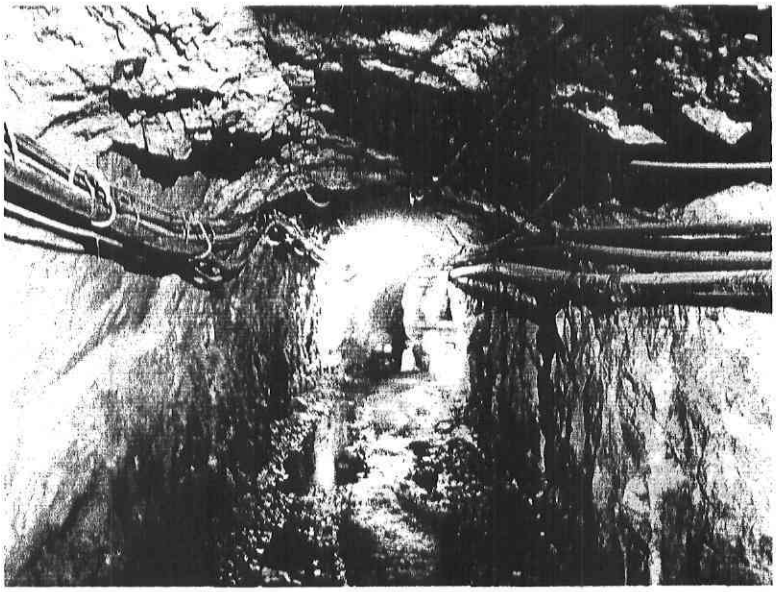

Figure 2. 7: Gallery at 70 m depth.

In this gallery, we consider three separate areas, one LOS and two NLOS (NLOS1 and NLOS2) which are about 24 meters in length each, depicted in Figure 2.8.

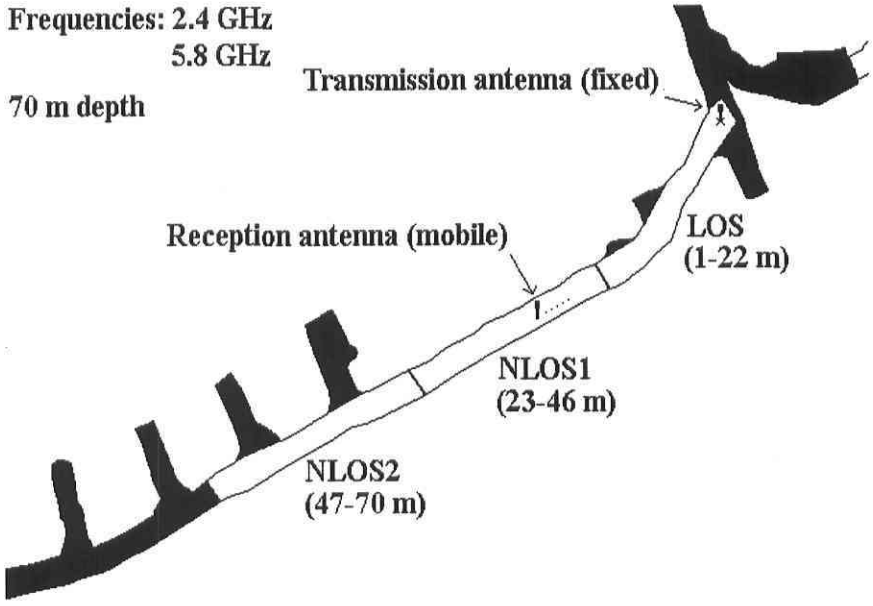

Figure 2. 8: Wideband experiments at 70 m depth (only areas in white are considered).

2.4.2 Wideband mathematical model

The wideband characteristic of the underground mine is described with a particular IR. Under the assumptions of Gaussian scatterers and multiple propagation paths to the receiver, a propagation channel can be completely characterized by the number of multipath components (impulses), amplitudes, arrival times and phases. The vector CIR can be represented by [5]

$$h(t) = \sum_{i=1}^{K} A_i(t) \cdot e^{j\phi_i(t)} \delta(t - \tau_i(t)) \tag{2.3}$$

where, i is the number of multipath components, $A_i(t)$ is the random amplitude (gain) of the i th path, $\tau_i(t)$ is the random time delay of the i th path, and $\phi_i(t)$ is the random phase shift of the i th path.

As per (2.3), the random behavior of radio waves propagation reflects the need to statistically model the channel. As such, many probability distribution functions are used in order to determine the ones which best fit the variables forming the previous equation.

2.4.3 Wideband statistical model for the 70 m depth underground environment

The modeling process considered in [3] includes path arrival modeling and amplitude modeling only. The phase is considered, a priori, to be uniformly distributed over (0, 2π].

2.4.3.1 Path time arrival

The modeling process considers the following distributions for path arrivals, which are the most commonly used in the literature [2]: Poisson, modified Poisson and Weibull. The parameters of each of these distributions were estimated from experimental measurements. The results suggest that in indoor environments, especially in our mining environment where the obstacles are randomly positioned, the *modified Poisson distribution* offers the best fit for all areas and both 2.4 GHz and 5.8 GHz frequency bands [3].

2.4.3.2 Path amplitude

The most popular distributions for path amplitude, especially for indoor environments, are considered as candidate models [2], [3]: Rayleigh, Rician, Nakagami, Weibull and Lognormal. The parameters of each of these distributions were estimated from experimental measurements and results suggest that the Rician and Rayleigh distributions offer the best fit for LOS and NLOS (NLOS1 and NLOS2) areas at both frequency bands [3].

2.5 OFDM system parameters

In OFDM system design, we should consider a number of parameters such as the number of subcarriers, guard time, symbol duration, subcarrier spacing, modulation type, and the type of forward error correction coding. The choice of various OFDM parameters is a tradeoff between various, often conflicting requirements [7]. It is influenced by system requirements such as available bandwidth, required bit rate, tolerable delay spread, and Doppler values. For example, to get a good delay spread tolerance, a large number of subcarriers with a small subcarrier spacing is desirable, but the opposite is true for a good tolerance against Doppler spread and phase noise.

Usually, there are three main requirements which are bandwidth, bit rate and delay spread. The delay spread directly dictates the guard time. Usually, the GI should be about two to four times the root-mean-squared (RMS) delay spread [7]. This value depends on the type of coding and QAM modulation. A higher order QAM, such as 64-QAM, is more sensitive to ISI and ICI than QPSK; while heavier coding obviously reduces the sensitivity to such interferences. After setting the guard time, the symbol duration can be fixed. To minimize the SNR loss caused by the guard time, it is desirable to have the symbol duration much larger than the guard time. However it cannot be arbitrarily large, because a large symbol duration means more subcarriers with a smaller subcarrier spacing, a more complex implementation and more sensitivity to phase noise and frequency offset, as well as an increased peak-to-average power ratio [7]. Hence a practical design choice is to make the symbol duration about five times the guard time.

After the symbol duration and guard time are fixed, the number of subcarriers may be determined by the required bit rate divided by the bit rate per subcarrier. The bit rate per subcarrier is defined by the modulation type, coding rate and symbol rate.

For example, in IEEE802.11a, the OFDM system with punctured convolutional code can provide a variable data transmission rate from 6 Mbps up to 54 Mbps. It loads the information signal into its 52 subcarriers, among which 48 are used for data transmission and 4 are used as pilot subcarriers. The data subcarriers are modulated using BPSK, QPSK, 16-QAM or 64-QAM, depending on the data transmission rate. The pilot signal can be used as a reference to disregard frequency or phase shift of the signal during transmission. Forward error correction (FEC) is used to improve the system performance. The 64-point IFFT and FFT are employed to realize the function of the OFDM modulation and demodulation. Since the required channel bandwidth is 20 MHz, the subcarrier spacing is the inverse of 20/64 = 312.5 kHz and the IFFT/FFT interval is 1/312.5 = 3.2 μs. Then a CP is pre-appended as a GI to avoid ISI and ICI. The GI is chosen as 1/4 of the signal spacing, which is 0.8 μs. So the total interval of an OFDM symbol is 4.0 μs. The key parameters of the IEEE802.11a OFDM system are listed in Table 2.1.

Table 2. 1: IEEE802.11a OFDM parameters.

Data rate	6, 9, 12, 18, 24, 36, 48, 54 Mbps
Modulation	BPSK, QPSK, 16-QAM, 64-QAM
Coding rate	1/2, 3/4, 2/3
Number of data subcarriers	48
Number of pilot subcarriers	4
Number of total subcarriers	52
IFFT/FFT size	64
Subcarrier spacing	312.5 kHz
IFFT/FFT period	3.2 μs
Guard interval	0.8 μs
OFDM symbol duration	4 μs
Channel spacing	20 MHz

2.6 Summary

In this chapter, an OFDM system model was introduced. The principle of OFDM modulation and demodulation was presented. The key components applied in OFDM systems to counteract the multipath fading effect were also discussed, such as parallel transmission, IFFT and GI. In OFDM system design, we should choose parameters carefully to meet the demand of practical wireless communication systems and avoid the conflict among them, such as bandwidth, bit rate and delay spread. IEEE802.11a OFDM system parameters are exemplified to explain the choice of OFDM system parameters.

In OFDM wideband wireless communication systems, the channel is usually frequency selective and time variant and the channel transfer function appears unequal in both frequency and time domain. Therefore dynamic channel estimation is necessary for the demodulation of OFDM signals. As we discussed above, coherent demodulation is preferable for high data rate applications and there are three main algorithms used. Pilot-aided channel estimation is the most often used for OFDM channel estimation and will be introduced in next chapter.

Based on statistical modeling of a wideband wireless propagation channel in our mining environment, it turns out that the number of arrival paths follows a modified Poisson distribution and their amplitudes undergo Rayleigh fading for NLOS areas or Rician fading for LOS areas. This statistical model will be considered as the channel model in our channel estimation systems.

CHAPTER 3
COMB-TYPE PILOT-AIDED OFDM CHANNEL ESTIMATION

3.1 Introduction

To achieve high data rates as well as good performances, coherent detection is commonly used in most existing OFDM systems. Coherent detection relies on knowledge of channel state information. One simple approach to obtain channel state information is to send some pilot symbols at the transmitter. In recent years, many works have been presented on the questions of channel estimation for PSA OFDM systems. To this end, pilot subcarriers are often interlaced with data subcarriers. There are two different pilot arrangements for PSA channel estimation, namely block-type pilot arrangement and comb-type pilot arrangement. Comb-type pilot insertion has been shown to be suitable for channel estimation in fast fading channels.

The channel estimation algorithm based on comb-type pilot is divided into pilot signal estimation and channel interpolation. Pilot signal estimation is based on LS or LMS criteria and interpolation algorithms include Linear Interpolation (LI), Second Order Interpolation (SOI), Cubic Spline Interpolation (CSI) and Low Pass Interpolation (LPI) [12].

In this chapter, comb-type PSA-OFDM channel estimation principle and algorithms are presented. Channel estimation strategies in OFDM systems are also reviewed.

3.2 Basic principle of PSA channel estimation

Channel estimation and equalization method are used to compensate for fading loss. The most powerful and effective method currently used is PSA adaptive equalizer. The basic idea of this approach is that there is a pilot (training sequence) known to both transmitter and receiver. This pilot signal is transmitted and tampered (convoluted) by the channel response, and based on the difference between received signal and known training sequence, the receiver can adjust the parameters (filter coefficients) of the equalizer. These parameters are quite helpful to extract the distorted 'unknown data' transmitted in the same channel or in an adjacent channel.

The typical block diagram of OFDM baseband system with PSA channel estimation is shown in Figure 3.1.

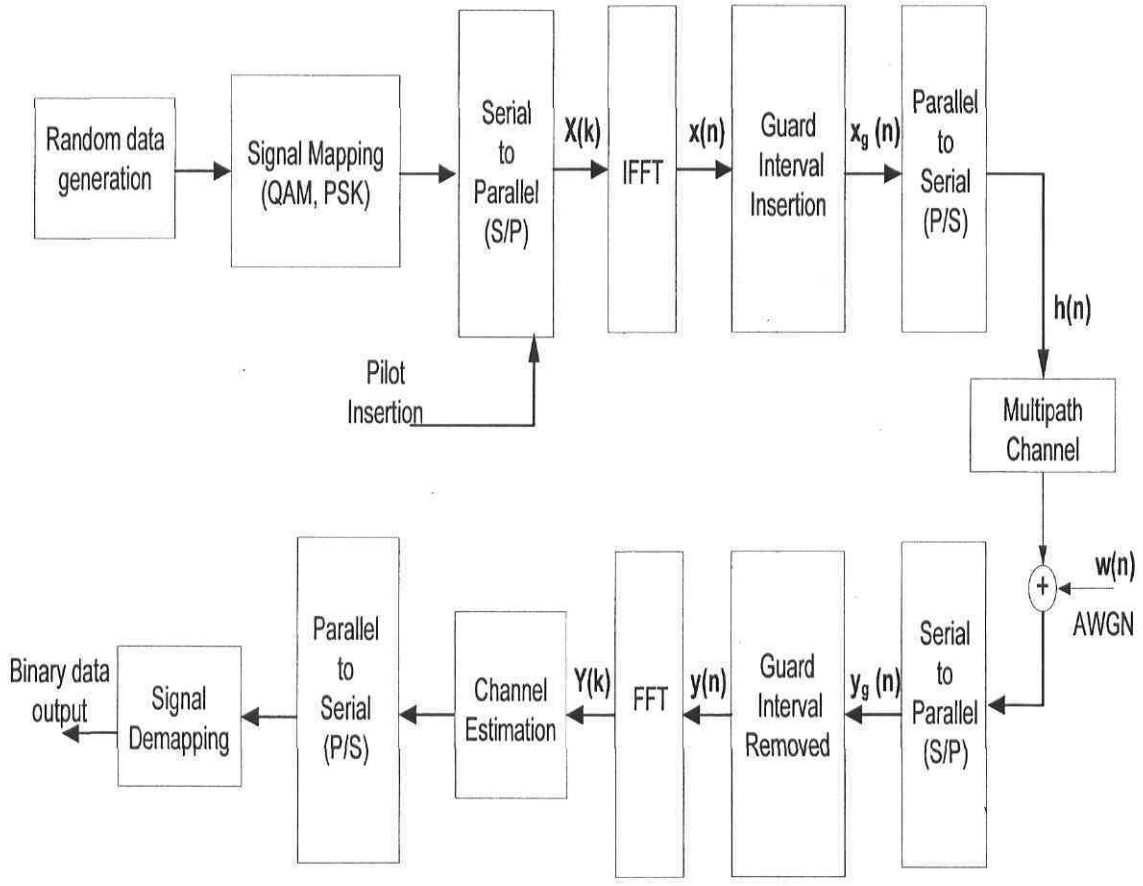

Figure 3. 1: Pilot-aided channel estimation system.

On the transmitter side, binary information is grouped and encoded using M-PSK or QAM modulations. Then pilot tones are multiplexed with data at a pilot rate of $1/R$ (ratio of the number of pilot tones to the total number of subcarriers) and the modulated data $\{X(k)\}$ is converted into a TD signal by taking the N-point IDFT. So the transmitted OFDM signal in the discrete-time domain, excluding GI, can be expressed as:

$$x[n] = IDFT_N\{X(k)\} = \sum_{k=0}^{N-1} X(k) e^{j2\pi kn/N} \qquad n = 0,\ 1,\ \cdots, N-1 \tag{3.1}$$

where k is the subcarrier index ($0,\ 1,\ \cdots, N-1$) with N being the total number of subcarriers.

To prevent possible ISI in OFDM systems, the GI is added, which is chosen to be larger than the expected delay spread. This GI includes the cyclically extended part of OFDM symbols in order to eliminate ICI. The resultant samples $\{x_g(n)\}$ can be expressed as follows:

$$x_g(n) = \begin{cases} x(N+n), & n = -N_g,\ -N_g+1,\ \ldots, -1 \\ x(n), & n = 0,\ 1,\ \ldots, N-1 \end{cases} \tag{3.2}$$

where N_g is the number of samples in the GI.

The transmitted signal $x_g(n)$ is sent to the multipath fading channel and the received signal $y_g(n)$ can be denoted by:

$$y_g(n) = x_g(n) \otimes h(n) + w(n) \tag{3.3}$$

where $h(n)$ is the discrete CIR of the channel and $w(n)$ is the i.i.d. complex zero-mean additive white Gaussian noise (AWGN) whose real and imaginary parts both have variance σ_n^2. The CIR $h(n)$ can be expressed as [6]

$$h(n) = \sum_{i=0}^{r-1} h_i e^{j2\pi f_{D_i} T \frac{n}{N}} \delta(\lambda - \tau_i) \qquad 0 \le n \le N-1 \tag{3.4}$$

where r is the total number of propagation path, h_i is the complex IR of the i^{th} path, f_{D_i} is the i^{th} path Doppler frequency shift which causes ICI of the received signals, λ is the delay spread index, and τ_i is the i th path delay normalized by the sampling time.

At the receiver side, after removing the CP from $y_g(n)$, a DFT is performed on the received samples $y(n)$ to demultiplex the multicarrier signals.

$$Y(k) = DFT\{y(n)\} = \frac{1}{N}\sum_{n=0}^{N-1} y(n) e^{-j(2\pi kn/N)} \qquad k = 0,\ 1,\ 2,\ \ldots, N-1 \tag{3.5}$$

We suppose that the guard interval is longer than the length of channel impulse response, that is, there is no ISI between OFDM symbols. Then the demultiplexed samples $Y(k)$ related to $H(k) = DFT\{h(n)\}$, $I(k)$ which is ICI caused by the Doppler shift, and $W(k) = DFT\{w(n)\}$ can be represented by [20]

$$Y(k) = X(k)H(k) + I(k) + W(k), \qquad k = 0,\ 1,\ \cdots, N-1 \tag{3.6}$$

where

$$H(k) = \sum_{i=0}^{r-1} h_i e^{j\pi f_{D_i} T} \frac{\sin(\pi f_{D_i} T)}{\pi f_{D_i} T} e^{-j\frac{2\pi\tau_i}{N}k},$$

$$I(k) = \frac{1}{N}\sum_{i=0}^{r-1}\sum_{\substack{K=0 \\ K\neq k}}^{N-1} h_i X(k) \frac{1 - e^{j2\pi(f_{D_i}T - k + K)}}{1 - e^{j\frac{2\pi}{N}(f_{D_i}T - k + K)}} e^{-j\frac{2\pi\tau_i}{N}K}$$

Following the DFT block, the received pilot signals $\{Y_P(k)\}$ are extracted from $\{Y(k)\}$ and the channel transfer function $\{\hat{H}_d(k)\}$ for the data subchannel can be obtained from the information carried by $\{\hat{H}_P(k)\}$. With the knowledge of the estimated channel response $\{\hat{H}(k)\}$, the estimated transmitted data sample $\{\hat{X}_d(k)\}$ can be recovered by simply dividing the received signal by the estimated channel response.

$$\hat{X}_d(k) = \frac{Y(k)}{\hat{H}(k)} \qquad k = 0,\ 1,\ \ldots, N-1 \tag{3.7}$$

where $\hat{H}(k)$ is an estimate of $H(k)$.

Finally, the source binary information data are demapped and reconstructed at the receiver output.

3.3 Channel estimation based on pilot assignment

3.3.1 Pilot assignment in OFDM systems

In PSA channel estimation, the pilot symbols can be placed in block-type or comb-type structures. As shown in Figure 3.2 (b), for block-type arrangement, the entire OFDM symbol is dedicated to carrier pilot samples on all the subcarriers for channel estimation and sent periodically in the time-domain. The estimate obtained with the training symbol will be used to detect data symbols within the OFDM packet. This arrangement is most suitable for static or slow varying channel. The estimation of channel response is usually obtained by Least Square (LS) or Minimum Mean Square Error (MMSE) estimation of the training pilots [12], [13], [16], [17]. Because the training block contains all frequencies, channel interpolation in the FD is not required. However, it is relatively insensitive to frequency selectivity.

In a time varying channel, the comb-type structure as depicted in Figure 3.2 (a) is more suitable. In the comb-type arrangement, pilot symbols are spread on selected subcarriers and repeated over multiple symbols. Channel estimation is performed at each symbol and interpolation is required to infer the channel frequency values of the non-pilot subcarriers. The comb-type pilot arrangement is sensitive to frequency selectivity compared with block-type. So the pilot spacing must be much smaller than the coherence bandwidth of the channel. However, assuming that the payload of pilot signals is the same as that of block-type, comp-type pilot assignment has a higher re-transmission rate [17]. The channel estimation based on pilot arrangement in OFDM systems have been investigated in [12]. The choice of pilot arrangement depends on the channel environment.

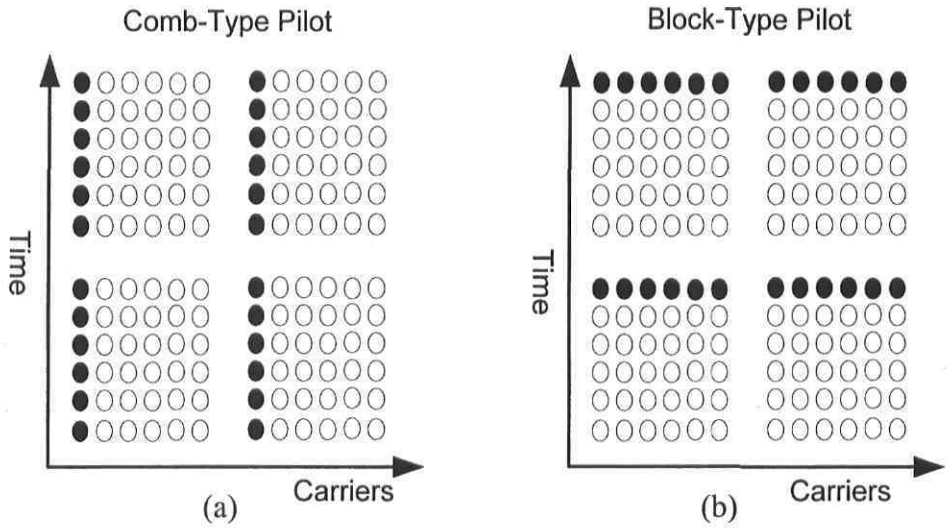

Figure 3. 2: Pilot arrangements for OFDM.

3.3.2 PSA channel estimation review

Based on the principle of PSA OFDM transmission scheme, we can assign pilots both in the TD and in the FD. FD channel estimation can be performed with two main approaches. The first method uses pilot transmitted on every subcarrier [18], [19], [22], [24], where the channel is estimated with the pilots and the channel frequency responses (CFR) in data bearing subcarriers are estimated by an interpolating technique in TD or FD, or both. The second method uses correlation properties of the frequency response (FR) of a multipath channel, and training information that is transmitted on a subset of the subcarriers [33].

Many channel estimations have been done in the FD. [23] derives the two-dimensional time-frequency Wiener filter. The estimator assumes knowledge of the doubly selective channel statistics, a condition which is hard to fulfill in realistic scenarios where the channel is not directly observable. An optimum MMSE channel estimator based on pilots is proposed in [24], which makes full use of the TD and FD correlation of the FR of time-varying dispersive fading channels. Therefore the MMSE estimator can only be found when the channel's statistics are known. A more realistic case is where the channel's statistics mismatch is also considered. It can be shown that the loss in performance is acceptable if the channel correlations match the Doppler spectrum [24]. An optimum MMSE interpolation applied after the CFR estimation at the pilot frequencies is proposed in [18]. This estimator is also dependent on knowledge of the channel

statistics; however, the interpolation can be less sensitive on channel statistics with a properly chosen filtering shape. In [25], a linear MMSE (LMMSE) estimator is proposed, which simplifies the estimator complexity by using a low rank approximation of the channel. The number of pilot symbols used for channel estimation is critical as well as their optimal placements, especially for time-varying channels. In [21], the optimal placement of the pilots is considered when a Kalman filter is used to track the channels in the FD.

The channel estimation methods presented so far process the data in the FD after the DFT at the receiver. The estimate of CFR contains errors, therefore for reliable data detection, one must refine the method. If an IDFT is applied again on the CFR, channel estimation can be performed before DFT processing of the training symbols using the TD approach. In this case, the CIR, instead of the CFR, is estimated. Usually this is an over-estimated channel order since a large number of taps have very little energy. Noise in these channel taps has a higher power than the multipath energy contained in them. Channel estimation can be improved by estimating the channel order and neglecting the low energy taps [14]. After the tap selection operation, the shortest CIR is passed again in the FD and used for equalization. Performance of different strategies for channel tap selection is discussed in [14].

A TD LS channel estimation method is proposed in [13], [16], when entire OFDM training symbols are available. Performance of the estimator is further improved if two consecutive and equal training symbols are available (IEEE 802.11 standard). This reduces the influence of the additive noise. The CFR is computed based on the estimated CIR. In practice, the number of subcarriers is higher than the order of the CIR. The TD channel estimation has been proven to give better results than the CFR estimation [13], [14], [16], since a smaller number of parameters are estimated using the same data. TD channel estimation and tracing method for mobile OFDM communications is proposed in [34]. The algorithm is extended to MIMO systems [26] as well as the estimation of the frequency offsets [27].

However, TD channel estimation approaches have usually higher complexity than that in the FD, because TD methods required additional computations. They also require the knowledge of training data on all subcarriers for a certain time period. However, they do not require any post-processing. Some of the actual standards [11] allow for time-domain channel estimation since special OFDM blocks are allocated for this purpose.

In this thesis, the PSA OFDM channel estimation in FD is studied with the aim of comparing it to conventional channel estimation algorithms for the underground environment channel model, which is significantly different from the normal indoor environment.

3.4 Comb-type PSA-OFDM channel estimation in the frequency domain

3.4.1 Principle of comb-type PSA-OFDM channel estimation

As presented in [17], for comb-type pilot subcarrier arrangement, the N_p pilot signals $X_p(m)$, where $m = 0,\ 1,\ \ldots, N_p - 1$, are uniformly inserted into $X(k)$. That is, all N subcarriers are divided into N_p groups, each with $L = N/N_p$ adjacent subcarriers. In each group, the first subcarrier is used to transmit the pilot signal. The OFDM signal modulated on the k^{th} subacrrier can be expressed as

$$X(k) = X(mL + l) = \begin{cases} x_p(m), & l = 0 \\ x_d(m), & l = 1,\ 2,\ \ldots, L-1 \end{cases} \tag{3.8}$$

Each subchannel transmits either a pilot symbol or a data symbol, and is called a pilot subchannel, H_p or a data subchannel, H_d, correspondingly. In other words, no unused subchannel is considered here. Hence the channel response can be written as

$$H(k) = H(mL + l) = \begin{cases} H_p(m), & l = 0 \\ H_d(mL + l), & l = 1,\ 2,\ \ldots, L-1 \end{cases} \tag{3.9}$$

Subsequently, the received pilot symbols and data symbols can be expressed as

$$Y_p(m) = H_p(m)X_p(m) + I_p(m) + N(m) \tag{3.10}$$

and

$$Y_d(mL + l) = H_d(mL + l)X_d(mL + l) + I_d(mL + l) + U(mL + l) \tag{3.11}$$

where, $N(m)$ and $U(mL+l)$ are the Gaussian noise in the pilot subcarriers and the data subcarriers defined in a similar way as $W(k)$ in (3.6). $I_p(m)$ and $I_d(mL+l)$ are the ICI in the pilot subcarriers and data subcarriers.

For coherent detection of the desired data symbol, the channel state information should be known a priori. In comb-type pilot aided OFDM system, channel state information can be estimated by sending a sequence of pilot symbols. Generally, the process of comb-type pilot aided OFDM channel estimation has two major steps: pilot subchannel identification and data subchannel interpolation, as illustrated in Figure 3.3.

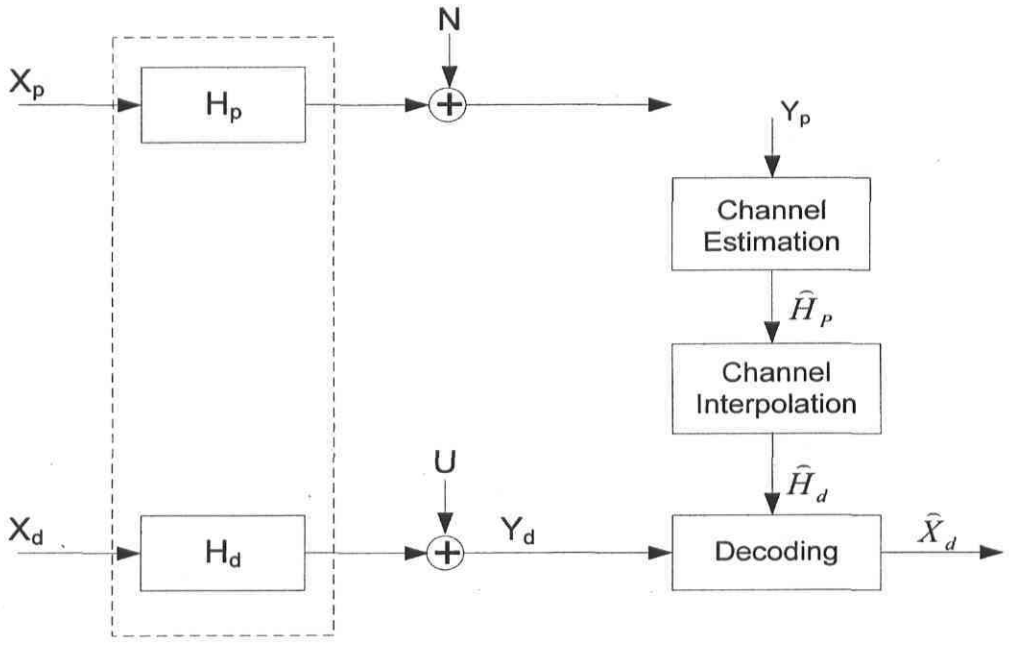

Figure 3. 3: Block diagram of channel estimation based on comb-type pilots.

Here, the pilot signal estimation based on LS or LMS criteria and the interpolation algorithms include linear interpolation (LI), second order interpolation (SOI), cubic spline interpolation (CSI) and low pass interpolation (LPI) algorithms.

3.4.2 Pilot symbols estimation algorithms

3.4.2.1 Least Square estimator

When ICI is eliminated by the GI, the received signal in (3.6) can be modeled with the following equation:

$$Y = XH + W \tag{3.12}$$

where Y is the received signal vector, X is a diagonal matrix of the transmitted signal, H is the CFR vector, and W is the noise vector in the FD.

Equation (3.12) has the structure of the general linear data model described by (C.1). Using the LS estimator developed in Appendix C, the LS estimator for an OFDM system is described as:

$$\hat{H}_{LS} = \left(X^H X\right)^{-1} X^H Y \tag{3.13}$$

Since X is a diagonal matrix, the estimate is reduced to

$$\hat{H}_{LS} = X^{-1} Y \tag{3.14}$$

This indicates that the LS estimate of the frequency response channel is simply the division of the received signal by the transmitted signal.

In the comb-type PSA OFDM channel estimation, the pilot subchannel is first identified by using the transmitted pilot channel X_p and received pilots Y_p. The estimate of the channel at pilot subcarriers based on LS estimation is given by [17]:

$$\hat{H}_p(m) = \frac{Y_p(m)}{X_p(m)} \qquad m = 0,\ 1,\ 2,\ \ldots, N_p - 1 \tag{3.15}$$

where $Y_p(m)$ and $X_p(m)$ are the output and the input at m^{th} pilot subcarrier respectively, and m denotes the index of the pilot subcahnnel. Substituting (3.10) into (3.15), we have

$$\hat{H}_p(m) = H_p(m) + V(m) \tag{3.16}$$

where m is the subcarrier index for pilot tones, and $V(m) = N(m)/X_p(m)$ can be considered as i.i.d. AWGN on the true estimate $H_p(m)$.

3.4.2.2 Least Mean Square estimator

The LMS estimator uses a one-tap LMS adaptive filter at each pilot frequency. The first value is found directly through LS and the following values are calculated based on the previous estimation and the current channel output as shown in Figure 3.4. $e(m)$ is the error signal which is formed by taking the difference between the received pilot symbol $Y_p(m)$ and transmitted pilot symbol $X_p(m)$.

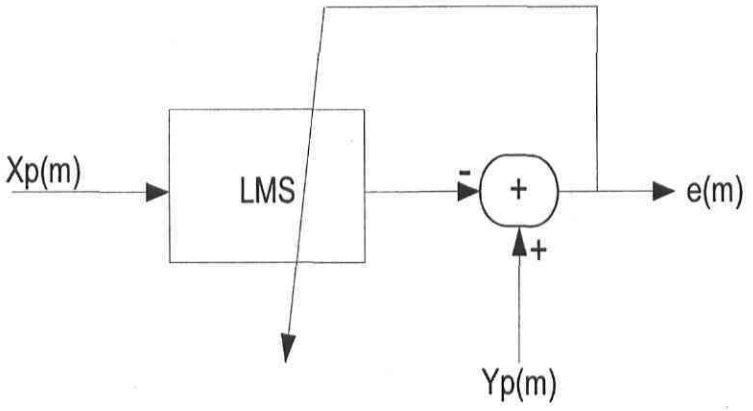

Figure 3. 4: LMS channel estimation scheme.

After pilot-symbol estimation, the data on the other subchannels is estimated by taking interpolation between the pilot subchannel estimates.

3.4.3 Interpolation technique in comb-type PSA-OFDM channel estimation

3.4.3.1 LI (Linear Interpolation)

In the linear interpolation algorithm, two successive pilot subcarriers are used to determine the CIR for data subcarriers which are located between pilots. Using linear interpolation, the channel estimation at the data carrier k , where $mL \le k < (m+1)L$, by is given by

$$\begin{aligned}\hat{H}_d(k) &= \hat{H}_d(mL+l) \\ &= \left(1-\frac{l}{L}\right)\hat{H}_p(m)+\frac{l}{L}\hat{H}_p(m+1) \\ &= \left(\hat{H}_p(m+1)-\hat{H}_p(m)\right)\frac{l}{L}+\hat{H}_p(m) \quad 0 \le l < L\end{aligned} \tag{3.17}$$

3.4.3.2 SOI (Second-Order Interpolation)

Theoretically, using higher-order polynomial interpolation will fit better than LI [12], [17], [30]. However, the computational complexity grows as the order is increased. Here, we consider second-order polynomial interpolation for its acceptable computational complexity. A piecewise second-order polynomial interpolation can be implemented as a linear time-invariant FIR filter. The interpolation algorithm is given by

$$\hat{H}_d(k) = \hat{H}_d(mL+l) = c_1\hat{H}_p(m-1)+c_0\hat{H}_p(m)+c_{-1}\hat{H}_p(m+1) \tag{3.18}$$

where

$$\begin{cases} c_1 = \dfrac{\alpha(\alpha-1)}{2}, \\ c_0 = -(\alpha-1)(\alpha+1), \text{ and } \alpha = \dfrac{l}{N} \\ c_{-1} = \dfrac{\alpha(\alpha+1)}{2}, \end{cases}$$

The channel estimation at the data carrier k is calculated based on three channel estimates of the previous, present, and next pilot symbols. $\hat{H}_p(m-1)$ is the channel estimate of the previous pilot

symbol at position $m-1$, $\hat{H}_p(m)$ is the channel estimate of the present pilot symbol at position m and $\hat{H}_p(m+1)$ is the channel estimate of the next pilot symbol at position $m+1$. So the channel estimation for the first four data symbols of the first OFDM symbol is obtained using two pilot symbols as for the LI method.

3.4.3.3 CSI (Cubic Spline Interpolation)

In the CSI algorithm, the transfer function of each subcarrier is approximated by a third order polynomial with respect to $\frac{l}{L}$. Estimation is done by obtaining polynomial coefficients using four adjacent reference signals and their second order derivatives. In this case, given N_p pilot points in one OFDM symbol, N_p-1 polynomials are obtained. A channel estimate for the data symbols between pilot symbols can then be obtained using these polynomials. The interpolation algorithm is given by [35]

$$\hat{H}_d(k)=A\left(\frac{l}{L}\right)\hat{H}_p(m)+B\left(\frac{l}{L}\right)\hat{H}_p(m+1)+C\left(\frac{l}{L}\right)z(m)+D\left(\frac{l}{L}\right)z(m+1) \tag{3.19}$$

where, $A\left(\frac{l}{L}\right)$, $B\left(\frac{l}{L}\right)$, $C\left(\frac{l}{L}\right)$, and $D\left(\frac{l}{L}\right)$ are constants determined by $\frac{l}{L}$. $z(m)=\hat{H}_p''(m)$ is the second order derivative of the transfer function of the m^{th} reference signal.

For simulations, the CSI algorithm can be implemented using the *spline* function in MATLAB [12] and it produces a smooth and continuous polynomial fitted to given data points.

3.4.3.4 LPI (Low-Pass Interpolation)

Errors caused by interpolation and noise are included in an estimated channel response through the use of an interpolation filter. Therefore these estimators suffer from an error floor caused by these errors. In ordered to reduce this error floor, LPI is performed by inserting zeros into the original sequence and then applying a low-pass FIR filter. This algorithm can be implemented in simulations using the *interp* function in MATLAB [12].

In the LPI algorithm, a low-pass filter plays the role of removing the noise components while preserving the CIR. The maximum channel duration of a CIR can be anticipated from the GI of the OFDM system. A low-pass filter combined with an interpolator for channel estimation has been proposed by [30], where the low-pass filter is implemented using IFFT/FFT modules. After estimating the fading distortion due to the interpolation filter, this estimated channel transfer function is then transformed into the TD by using an IFFT. As a result, this transformed estimate can be regarded as the CIR and separated into two parts. The first part is located within the GI and contains the main energy of the CIR. The second part, which is outside the GI, is regarded as noise components. Therefore zero values instead of noise components are inserted for the IFFT processing. As a result, the original transformed estimate within the GI plus these zero values are then transformed once more in the FD using an FFT to obtain a final CIR estimate without noise components.

The LPI method allows the original data to pass through without changing and the mean-squared error between the interpolated points and their ideal values is minimized.

3.4.3.5 Comparison of the different interpolation algorithms

LI and SOI are simple interpolation methods and LI has the lowest complexity among all of the interpolation methods. Compared with LI and SOI, CSI and LPI can increase the estimation accuracy, yet they are relative complex, with fitted polynomial search, low-pass convolution, and DFT/IDFT computations, respectively. LPI can reduce the noisy component of channel estimates obtained by an interpolation filter. It combines low-pass filtering with interpolation filters to decrease the error and improve the performance. It has the highest estimation accuracy among all the presented interpolation algorithms. The computational complexity of different interpolation algorithms ranking from low to high is summarized in Table 3.1.

Table 3.1: Comparison of complexity of different interpolation algorithms.

Estimation Scheme	Complexity	Comments
LS-LI	Lowest	Simple estimation and interpolation methods.
LS-SOI	Low	
LS-CSI	Moderate	Interpolation methods are relatively complex, with fitted polynomial search and low-pass convolution calculation.
LS-LPI		

3.5 Summary

In OFDM systems, efficient channel estimation is essential for coherent detection of the received signal. PSA modulation is relatively simple to implement. The transmitter just inserts known pilot periodically, so there is no change in pulse shape and peak to average power ratio. There are two basic PSA-OFDM channel estimation based pilot arrangements, which are the block-type pilot channel estimation and the comb-type pilot channel estimation. Compared with block-type channel estimation, comb-type pilot channel estimation is introduced to satisfy the need for equalizing when the channel changes even from one OFDM block to the subsequent one.

The basic idea of the comb-type arrangement is that fewer pilots are used per channel estimation but they are used more frequently. The selected subcarriers are reserved for pilots and channel estimation is calculated at each time interval. Since only a few of the subcarriers contain pilot signals, only the channel response at these frequencies can be determined. Interpolation is required to estimate the channel response of the remaining frequencies. The LS and LMS methods are used for pilot channel estimation. In practice the LS estimator is more commonly used due to its ease of implementation and acceptable performance. There are various methods for performing interpolation, such as LI, SOI, LPI and CSI. As discussed in this chapter, the LS estimator with LPI has the best performance theoretically compared with the other three interpolation algorithms.

CHAPTER 4

OFDM CHANNEL ESTIMATION SIMULATION SYSTEM

4.1 Introduction

In this chapter, channel estimation simulation systems are implemented using Matlab and Simulink (version 7.0). The OFDM transmitter and receiver are set up in Simulink based on the IEEE802.11a standard. The parameters for the channel model are based on the statistics of the wideband channel model for our mining environment [3], where the path amplitudes undergo Rayleigh fading for NLOS cases and Rician fading for the LOS case. According to different choices of parameters for the different cases, six basic simulation channel models are studied.

A brief description of the basic functions of the system model is given in section 4.2. The system parameters and channel model parameters are also listed and explained in sections 4.3 and 4.4.

4.2 Simulink model of the system

To demonstrate the validity of the proposed algorithms and the effect of channel estimation on the system performances, an uncoded OFDM system model is set up in Simulink according to the IEEE802.11a standard. The top-level system model is shown in Figure 4.1.

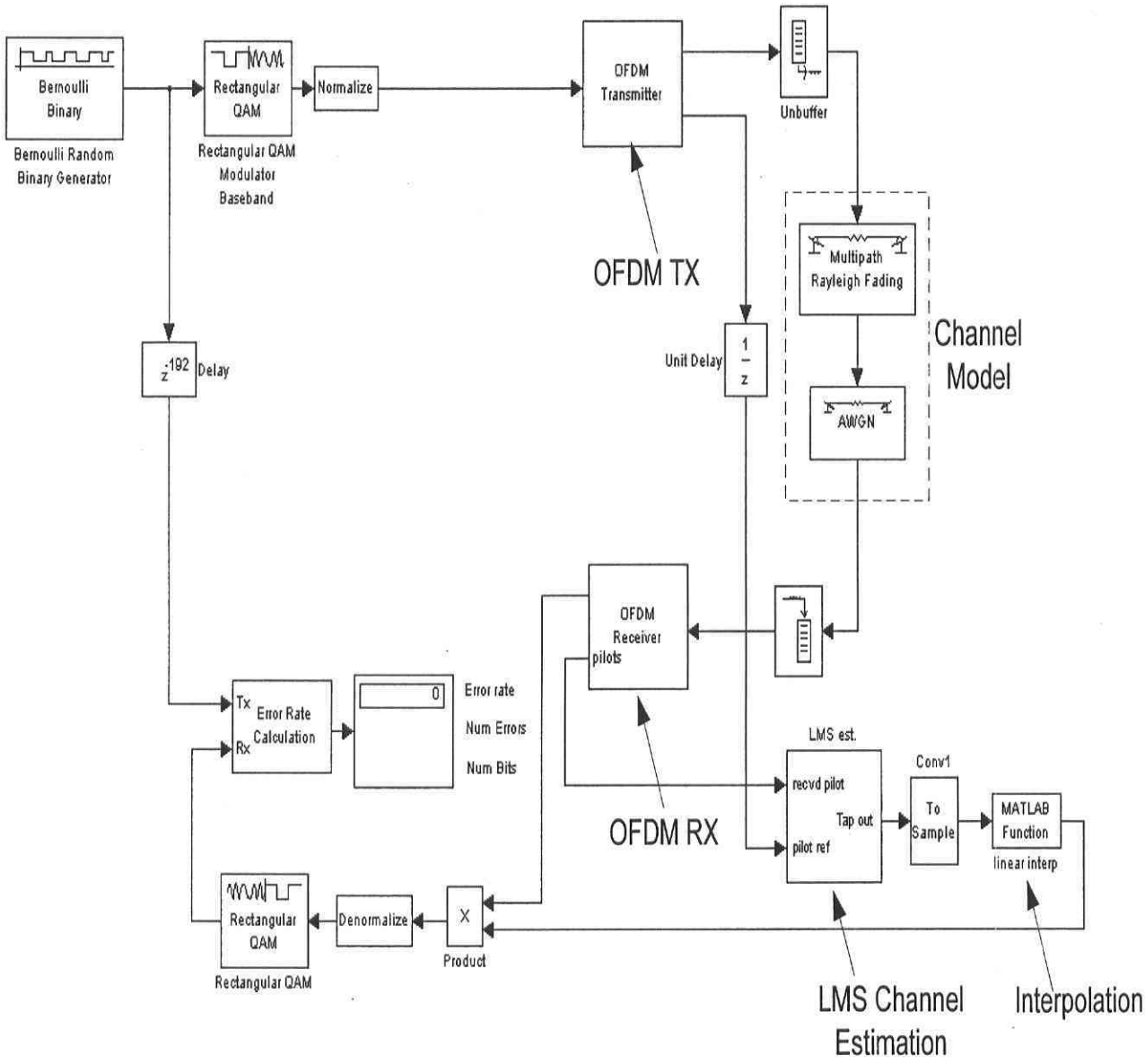

Figure 4. 1: SIMULINK model of the system.

The Simulink model includes four main parts: OFDM transmitter, OFDM receiver, channel model and channel estimation. The OFDM transmitter and receiver models are derived from existing IEEE802.11 OFDM systems. The communication link in this model performs the following tasks:

- Generation of a random bit rate that varies during the simulation. The varying data rate is accomplished by enabling a source block periodically for a duration that depends on the desired data rate. In our simulation system, the data transmission rate is chosen to be 6 Mbps, 12 Mbps or 24 Mbps, which are mandatory in IEEE802.11a/g OFDM systems.

- Modulation using one of BPSK, QPSK, 16QAM modulation schemes specified in the standard of IEEE802.11 standard without coding.

- OFDM symbol transmission using 52 subcarriers (4 pilots and 48 data subcarriers). The 4 pilot subcarriers are modulated with a PN sequence in the FD and are uniformly inserted in each OFDM symbol with a pilot ratio $R = 1/13$. The 64-point IFFT is used and 16 samples are defined as the CP. The Simulink model of the OFDM transmitter is shown in Figure 4.2.

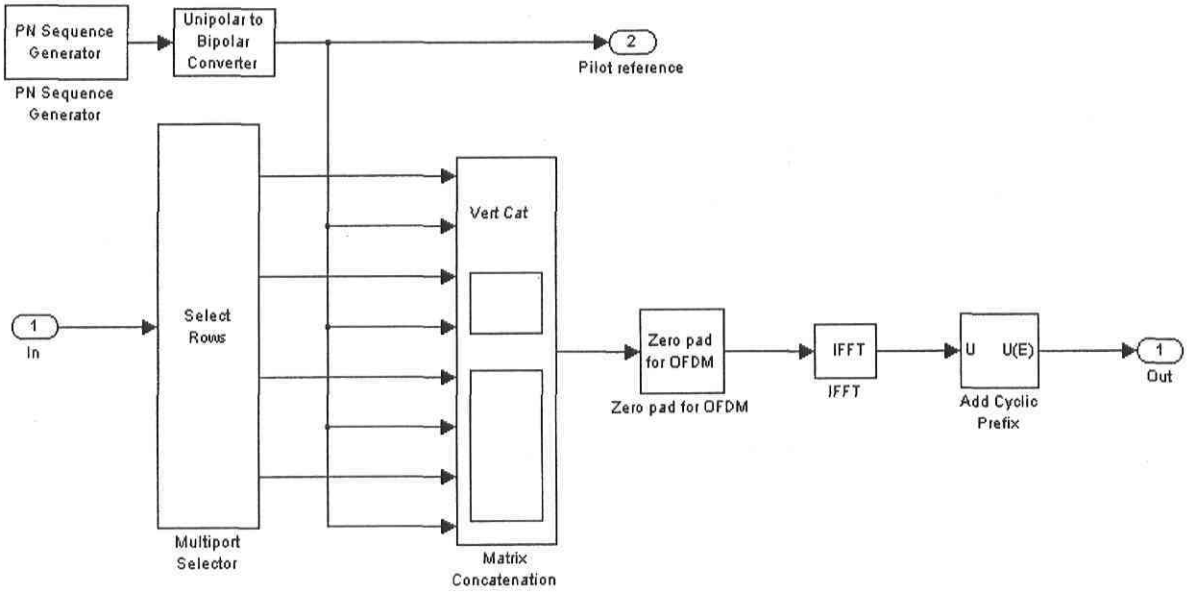

Figure 4. 2: SIMULINK model of the OFDM transmitter.

- The channel model is Rayleigh multipath fading for NLOS (NLOS1 and NLOS2) and Rician multipath fading for LOS based on [3]. The Gain parameters and Delay parameters are specified in Matlab according to the channel model.

- In the receiver, after removing the guard interval and zero-padding, the pilots are separated from the data subcarriers by a "select rows" block. The Simulink model of the OFDM receiver is shown in Figure 4.3.

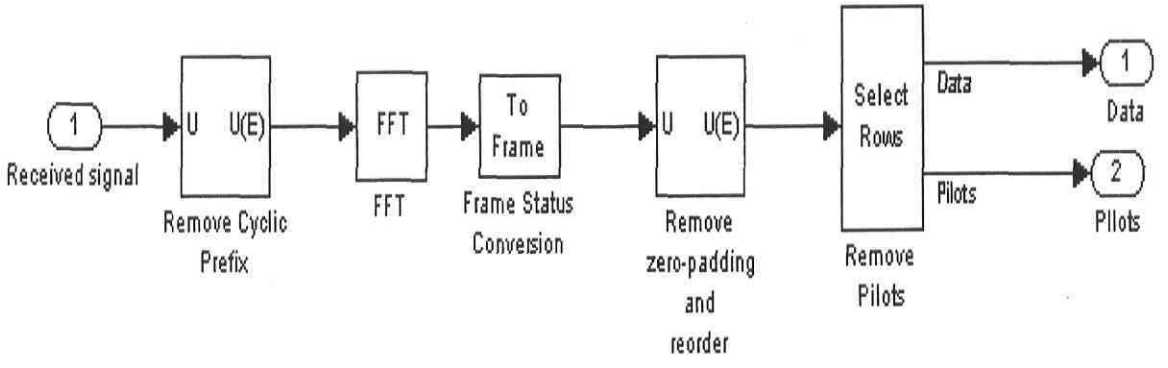

Figure 4. 3: SIMULINK model of OFDM receiver.

- For channel estimation, the received pilot symbol is used for pilot estimation with a reference pilot by an LMS or an LS estimator. The LMS estimator uses a one-tap LMS adaptive filter at each pilot frequency [12]. The Simulink models of the LMS and LS estimators are shown in figures 4.4 and 4.5, respectively.

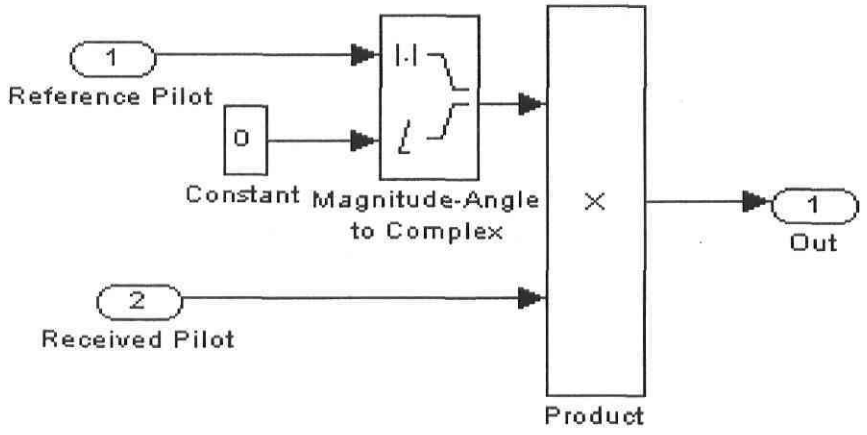

Figure 4. 4: Simulink model of LS channel estimator.

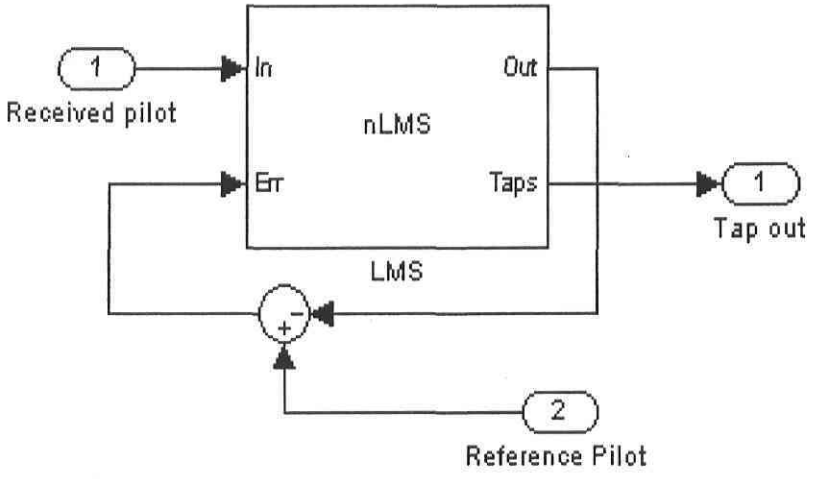

Figure 4. 5: Simulink model of LMS estimator

- Channel estimation is done using one of the following channel interpolation algorithms: LI, SOI, CSI and LPI. The interpolation algorithms are implemented using "Matlab Function" block in Simulink, as shown in Figure 4.6.

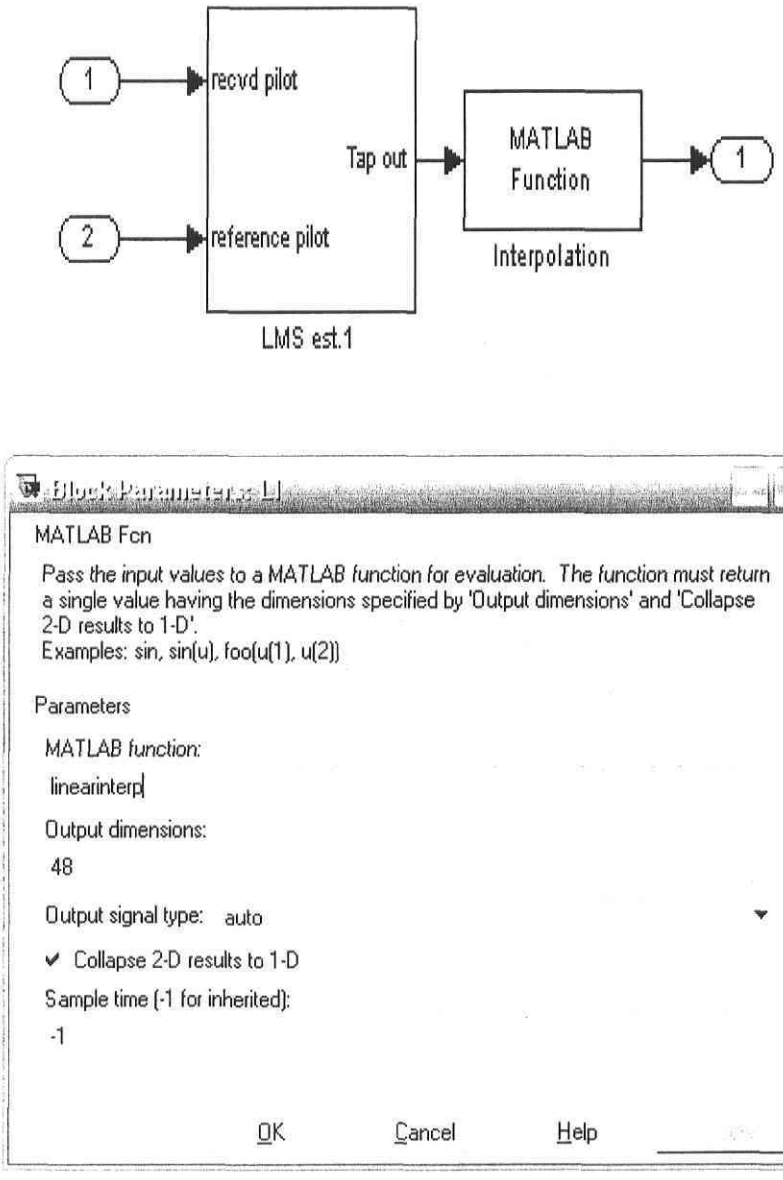

Figure 4. 6: Simulink model of interpolation with Matlab Function block.

- The received symbols after channel estimation are demodulated and the binary data is recovered.

- Error statistics for the entire system are displayed.

4.3 OFDM system parameters

OFDM system parameters used in the simulations are shown in Table 4.1. The aim of our project is to observe channel estimation performances, so perfect synchronization is assumed in the simulation. An uncoded PSA-OFDM system is implemented. OFDM is set up herein similarly to existing WLAN standards, such as IEEE802.11a/g.

The simulations are carried out for different values of SNR with different channel estimation methods and modulation schemes. LS or LMS is used to estimate the channel at pilot frequencies and different interpolation are applied to investigate the interpolation effects. As stated earlier, the estimation of the channel at pilot subcarriers based on LS is given by (3.15). The LMS estimator uses a one tap LMS adaptive filter at each pilot frequency.

The parameters of uncoded OFDM systems are derived from the IEEE802.11a standard, where there are 64 implied subcarriers frequencies with a spacing of 156.25 kHz. It includes 52 nonzero subarriers, 48 carrying data and four used as pilot tones. Each subcarrier transmits at 156.25 k symbols/second. Data is blocked into 6.4 μs frames with an additional 1.6 μs of CP tacked on for mitigation of ISI. A 64-point FFT is performed over 6.4 μs to extract the 48 data symbols on the modulated signals. For BPSK, with 1 bit per symbol, this corresponds to 48 bits in 8 μs, for an aggregate data rate of 6 Mbps. For QPSK, the aggregate data rate is 2 times higher, which is 12 Mbps. For 16QAM, with 4 bits per symbol, the aggregate data rate is 4 times higher, which is 24 Mbps.

Table 4. 1: OFDM system parameters of the simulation system.

Parameters	Specification
Signal constellation	BPSK, QPSK, 16QAM
Data rate	6 Mbps, 12 Mbps, 24 Mbps
Number of subcarriers	52
IFFT and FFT size	64
Number of pilots	4
Pilot ratio	1/13
Length of GI	16 (1/4 of symbol length)
Guard type	Cyclic Extension
Max. Doppler shift	20 Hz, 35 Hz,(55Hz and 80Hz)
Channel model	Wideband statistical channel model [3]
Noise	AWGN
Carrier frequency	2.4 GHz, 5.8 GHz
Channel estimation	LMS with LI and SOI, LS with LI, SOI, CSI and LPI

4.4 Channel simulation model

4.4.1 Channel parameters for the simulations

The statistical characterization of the channel propagation in our mining environment was proposed by Mathieu Boutin [3]. This study revealed that the path arrival time follows a modified Poisson distribution and the multipath number of significant paths varies with 8 nsec resolution (depending on the area and the different carrier frequencies). The time delay for the NLOS1 case at f_0 = 2.4 GHz is shown in Figure 4.7.

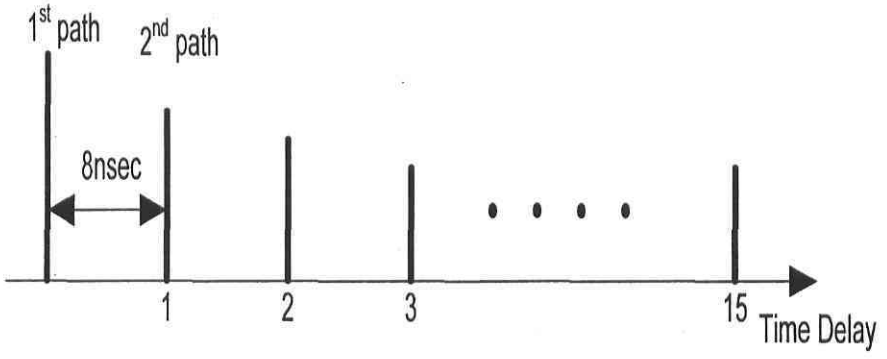

Figure 4. 7: Time delay for NLOS1 at 2.4 GHz.

In [3], the author indicates that the received power can be considered as negligible after the 10th time bin in the measured impulse responses. The Rician K-factor (for LOS case) and the path gain needed for simulation parameters in the Rice and Rayleigh blocksets of Simulink will always consider 10 consecutive paths. For each frequency and each area, the approximated amplitude for each bin is found by curve fitting based on the minimization of the MSE applied to the mean amplitude of each bin. Then the Rician K-factor and the path gains are obtained by considering the values of that curve at each time bin [3]. It shows that the Rician K-factor for the LOS area is 5.5699 for $f_0 = 2.4$ GHz and 5.2366 for $f_0 = 5.8$ GHz. The relative path gains of the 10 consecutive paths (time bin) for LOS, NLOS1 and NLOS2 in both frequencies are presented in Table A.1 and Table A.2 [3].

Table 4. 2: Parameters for the different channel models.

Channel model	Carrier frequency	Area	Maximum number of paths	Path amplitude	Path arrival time
A	$f_0 = 2.4$ GHz	NLOS1	15	Rayleigh	Modified Poisson (see Appendix A.1)
B		NLOS2	16		
C		LOS	11	Rician $K = 5.5699$	
D	$f_0 = 5.8$ GHz	NLOS1	18	Rayleigh	
E		NLOS2	11		
F		LOS	9	Rician $K = 5.2366$	

In our simulation system, six channel models are defined according to the different cases of channel characterization presented in [3]. The parameters for the 6 different channel models are listed in Table 4.2.

The path time arrival for all channels follows a modified Poisson distribution and the phase is considered to be uniformly distributed over [0, 2π], as described in section 2.4.3.

4.4.2 Doppler frequency effect on channel estimation

In this thesis, in order to compare the effect of the Doppler frequency, we used typical vehicle speeds of 10 km/h and 15 km/h for both carrier frequencies according to Table 4.3. In these cases, system operating under the IEEE802.11a/g standards can be treated as time-invariant within one OFDM block. Since the channel is stationary for the duration of one block, the ICI within the OFDM block can be considered negligible. However, over one OFDM frame, which contains a certain number of OFDM blocks, the channel is considered to be time variant. Since the variations become significant at higher velocities over one OFDM frame in the IEEE802.11a/g standards, channel estimation has to be performed throughout the OFDM frame in order to trace the channel variations over the frame. In this thesis, we focus on estimating the channel as it changes over the OFDM frame using a comb-type pilot arrangement. The effect of Doppler frequency is also tested in our simulation.

Table4. 3: Doppler frequencies used in the simulations.

Carrier frequency	Vehicle speed	Doppler frequency
f_0=2.4 GHz	10 km/h	20 Hz
	15 km/h	35 Hz
f_0=5.8 GHz	10 km/h	55 Hz
	15 km/h	80 Hz

4.5 Summary

In this chapter, the simulation system models and parameters are described. The OFDM system is realized with Simulink blocks, combined with Matlab functions to implement channel estimation. The design of the OFDM system and the choice of parameters are derived from the IEEE802.11a/g OFDM standards. The bit error rate is displayed to compare the performance for various scenarios. The channel model is set based on [3], where Rayleigh or Rician models are used for multipath amplitude distributions, and the time of arrival follows a modified Poisson model. The channel parameters are set by Matlab programming in the simulation system.

CHAPTER 5
CHANNEL ESTIMATION RESULTS AND ANALYSIS

5.1 Introduction

In this chapter, the channel estimation algorithms with different modulation schemes for different channel models are simulated and analyzed. BER performances are compared under different conditions, such as modulation schemes, channel estimation schemes, channel model, data rate, etc. The results are displayed in the form of BER vs. SNR curves.

5.2 BER performances for different estimation algorithms

In the figures, the legend "LS-LI, LS-SOI, LS-CSI, LS-LPI" denote all proposed interpolation schemes of channel estimation with the LS estimator at pilot frequencies, "LMS-LI" and "LMS-LPI" are for the linear and low pass interpolation schemes with LMS estimator at pilot frequencies. In this section, BER performances of the channel estimation algorithms used in different channel environments is described. The system parameters and channel parameters for the simulations were summarized in Table 4.1 and 4.2.

5.2.1 Channel estimation for NLOS area at 2.4 GHz

Figures 5.1-5.6 show the BER curves for all proposed channel estimation algorithms for different modulations over channel models A and B for the NLOS area (NLOS1 and NLOS2), where the channel is characterized as Rayleigh fading and the Doppler frequency f_d = 20 Hz at 2.4 GHz.

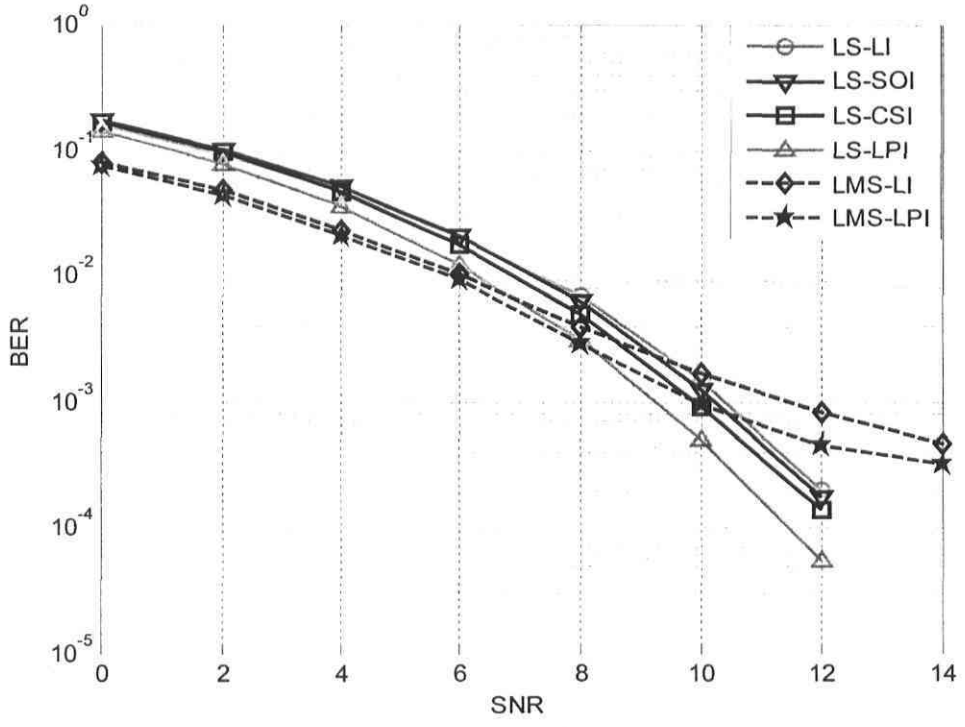

Figure 5. 1: BPSK modulation with Rayleigh fading (Channel A, Doppler freq. = 20 Hz).

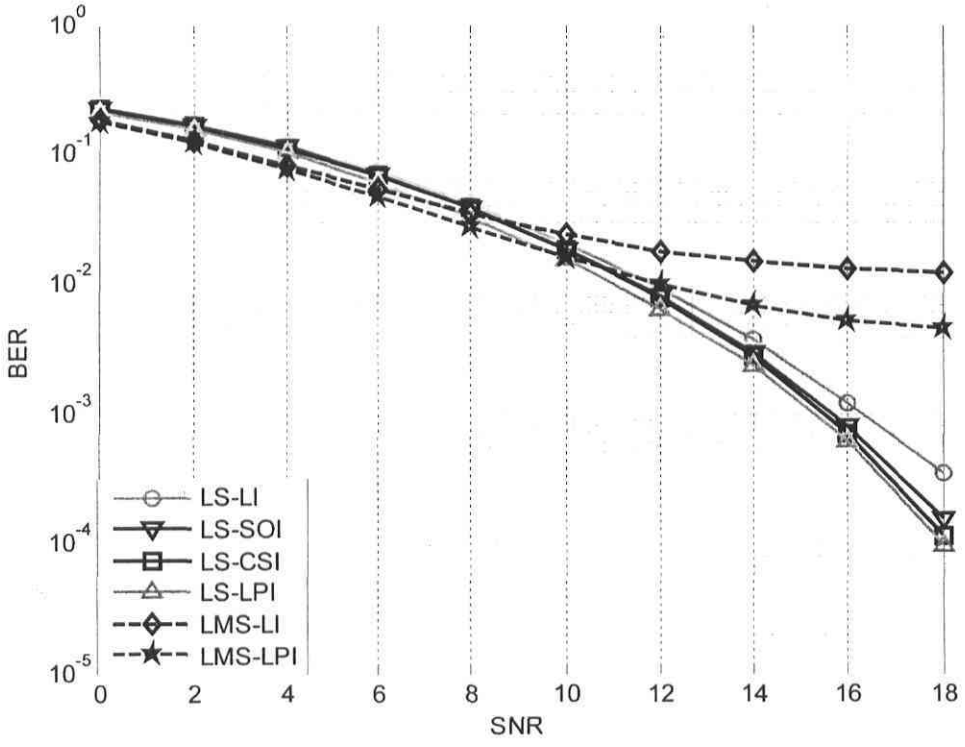

Figure 5. 2: QPSK modulation with Rayleigh fading (Channel A, Doppler freq. = 20 Hz).

As shown in figures 5.1 and 5.2, for channel estimation with BPSK and QPSK modulations over channel A, the LMS estimator has a slightly better performance than LS at low SNRs, which is less than 8 dB for BPSK and less than 10 dB for QPSK with the LMS-LPI method. However, with the increase of SNR, the performance of the LMS estimator deteriorates. Among all of the interpolation schemes using the LS estimator, LPI has the best performance and LI has the worst. These results are expected, because LI uses just two pilot symbols per estimate and the estimation accuracy is slightly decreased.

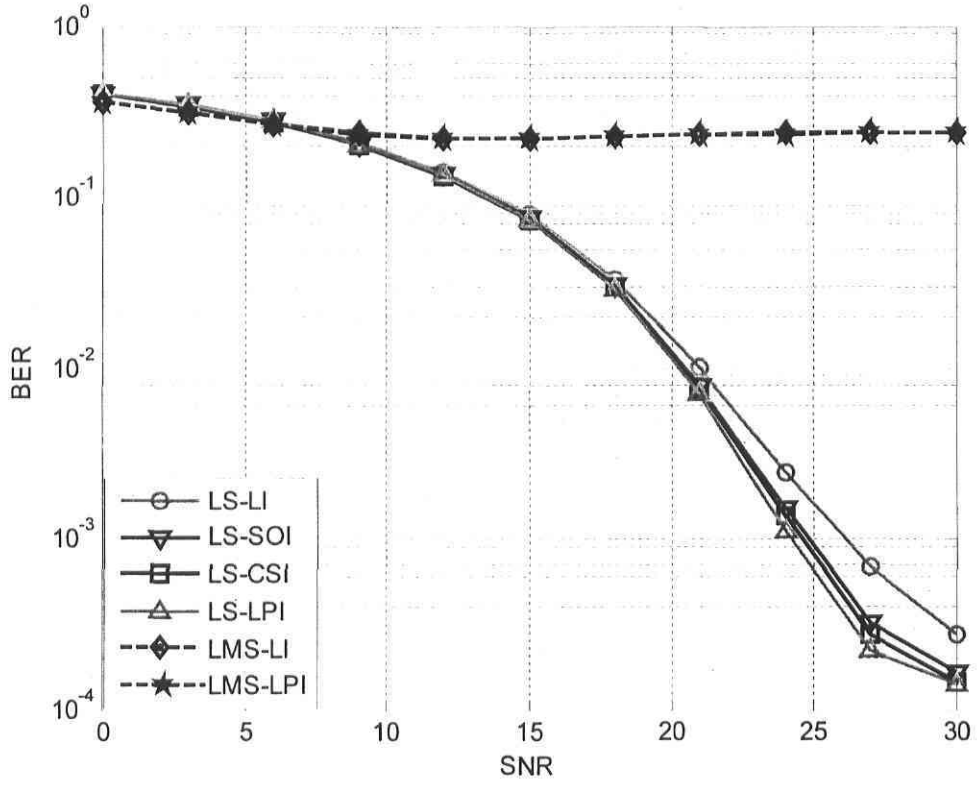

Figure 5. 3: 16QAM modulation with Rayleigh fading channel (Channel A, Doppler freq. = 20 Hz).

For the 16QAM modulation scheme, the data capacity is doubled compared with QPSK at the expense of BER performance. As shown in Figure 5.3, for 16QAM modulation, LS performs much better than LMS estimator at all SNRs and LPI also shows the best performance among all of the interpolation schemes. For high-order modulation schemes, such as 16QAM and 64QAM, LMS is not suitable for channel estimation.

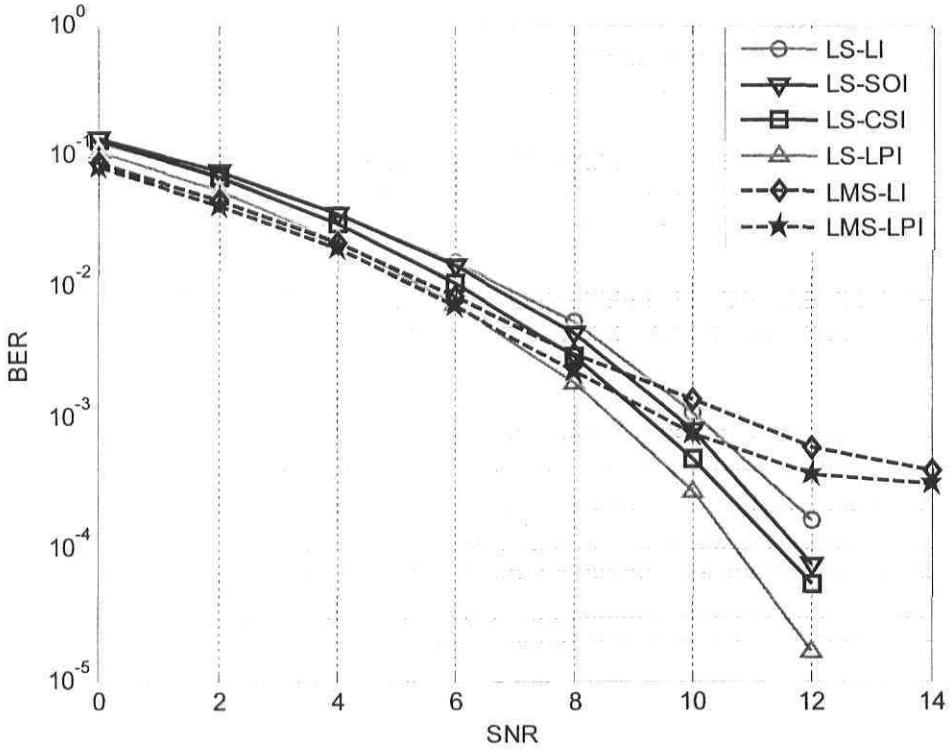

Figure 5. 4: BPSK modulation with Rayleigh fading channel (Channel B, Doppler freq. = 20 Hz).

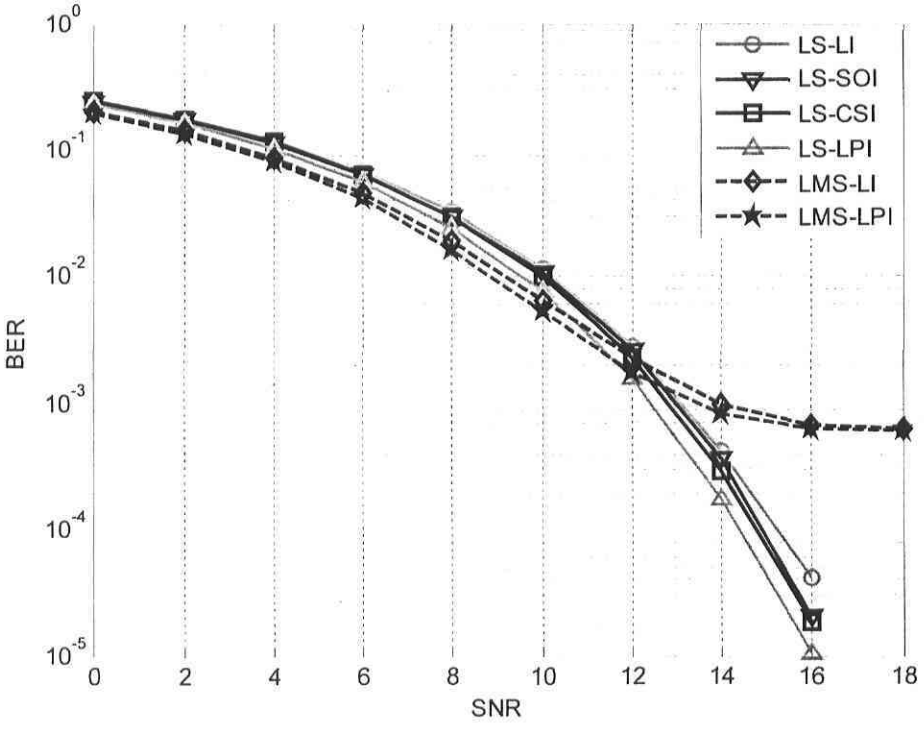

Figure 5. 5: QPSK modulation with Rayleigh fading channel (Channel B, Doppler freq. = 20 Hz).

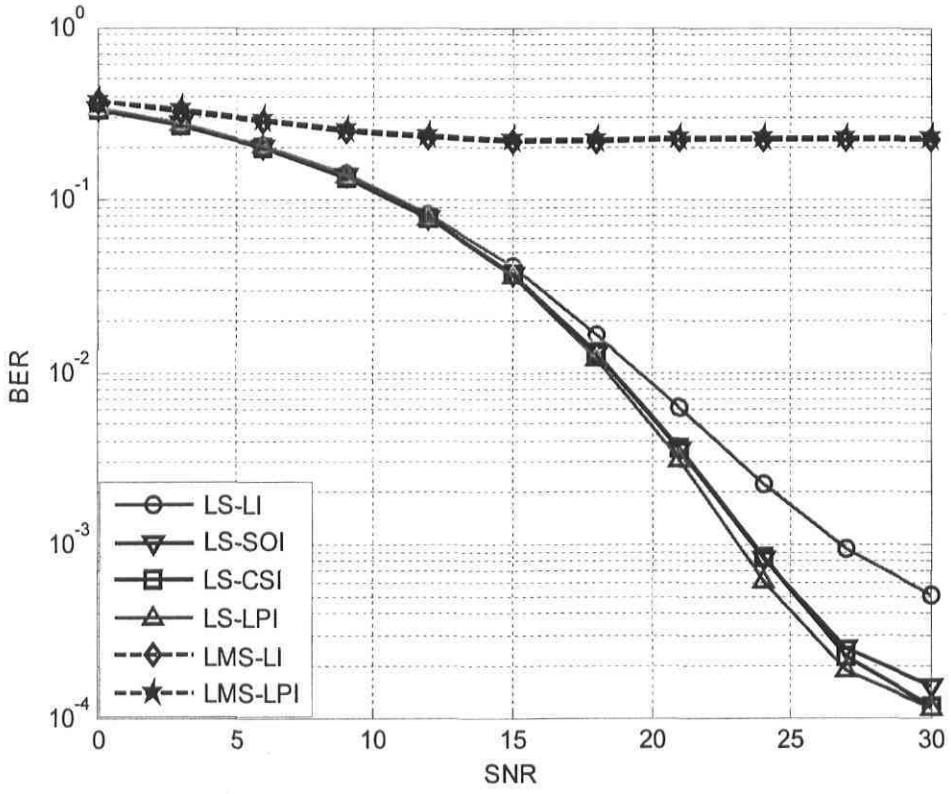

Figure 5. 6: 16QAM modulation with Rayleigh fading channel (Channel B, Doppler freq. = 20 Hz).

Figures 5.4-5.6 give the comparison of BER performances with different modulation schemes for Channel B. Compared with the results for NLOS1, the BER for NLOS2 is slightly lower for all different modulation schemes. For example, using the LS-LPI scheme, the difference is about 0.5 dB. This result is reasonable, because the NLOS2 area presents less attenuation than that of NLOS1 [2], [3].

5.2.2 Channel estimation for NLOS area at 5.8 GHz

Figures 5.7-5.12 give BER performances for the various channel estimation algorithms for different modulation over channel models D and E for the NLOS area (NLOS1 and NLOS2), where the channel is Rayleigh fading at 5.8 GHz. With the same vehicle speeds of 10km/h as in channels A and B, the Doppler frequency is 55 Hz at 5.8 GHz.

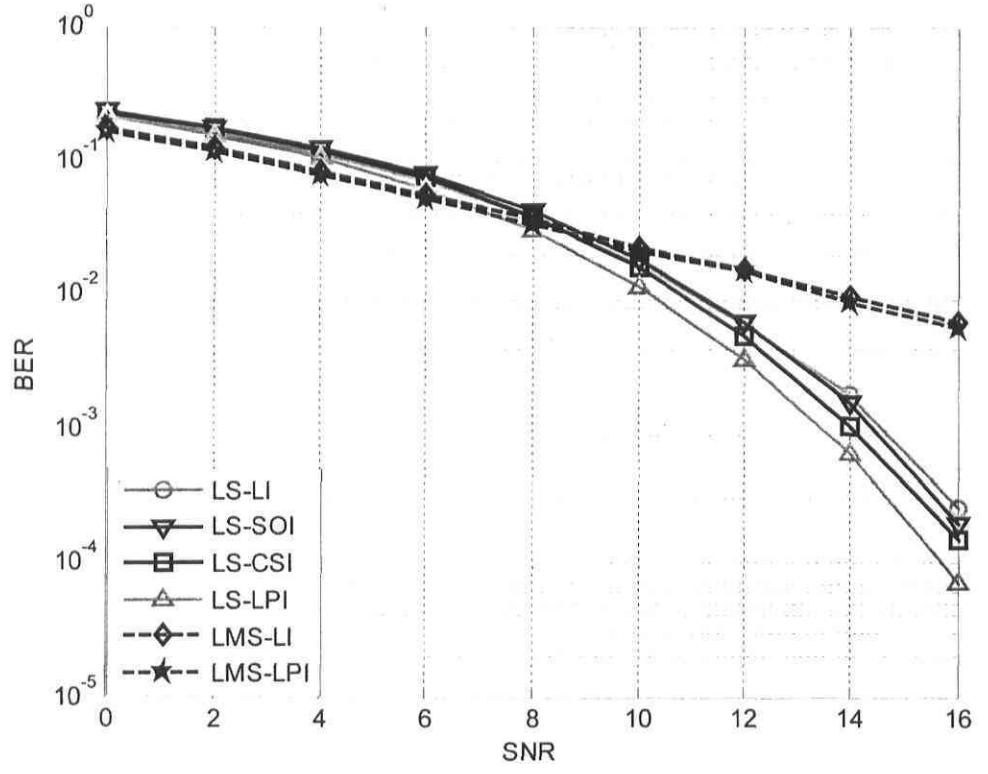

Figure 5. 7: BPSK modulation with Rayleigh fading channel (Channel D, Doppler freq. = 55 Hz).

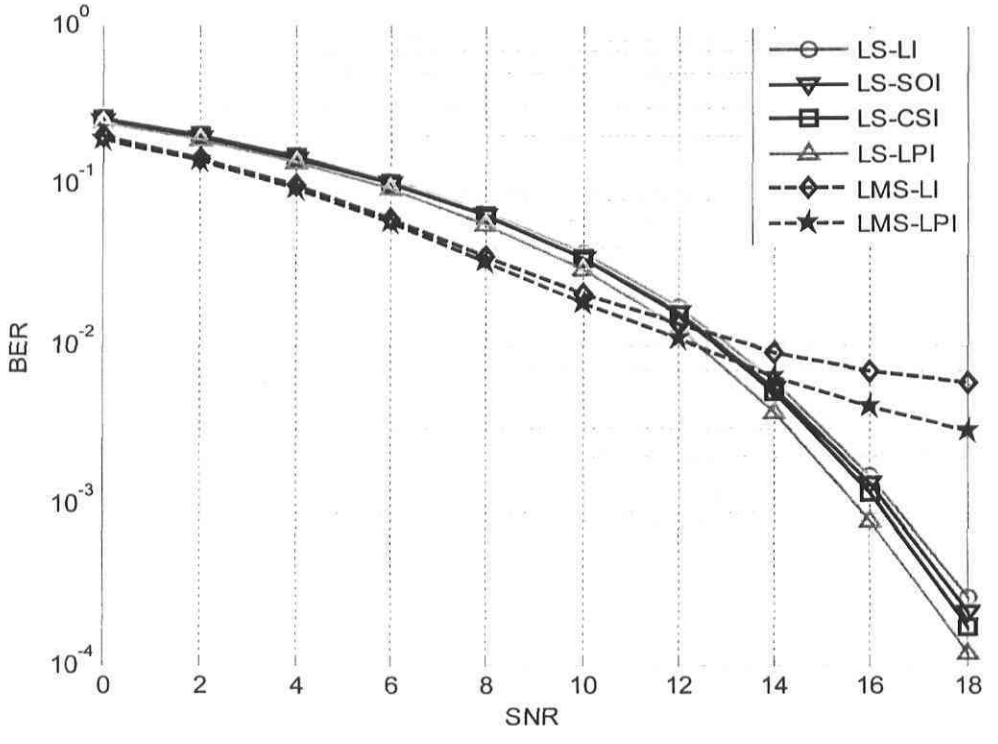

Figure 5. 8: QPSK modulation with Rayleigh fading channel (Channel D, Doppler freq. = 55 Hz).

As shown in figures 5.7 and 5.8, the LS estimator is significant better than the LMS estimator when the SNR is > 8 dB for BPSK. The SNR of the LMS estimator is about 6-8 dB higher than for the LS estimator for a required BER = 0.001. For the QPSK, the LMS outperforms LS when the SNR is < 12 dB. When the SNR is > 12 dB, the estimation based LS is better than LMS and the SNR shows improvement of more than 8 dB for the same BER values. The higher the SNR is, the better is the performance of LS over LMS.

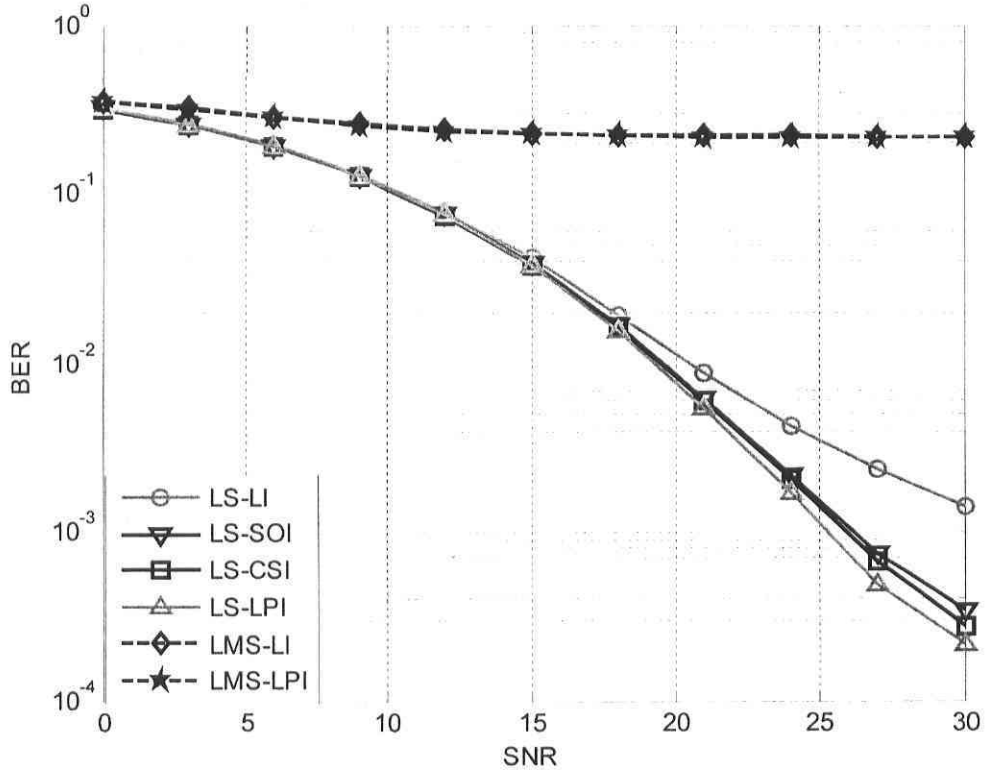

Figure 5. 9: 16QAM modulation with Rayleigh fading channel (Channel D, Doppler freq. = 55 Hz).

For 16QAM, the LS estimator with all interpolation schemes has almost the same performance at low SNRs, while LI becomes rapidly worse with the increase of SNR, as shown in Figure 5.9. Comparing the BER performances with channels A and B at 2.4 GHz, the SNR is a little higher at 5.8 GHz than that at 2.4 GHz for a given BER.

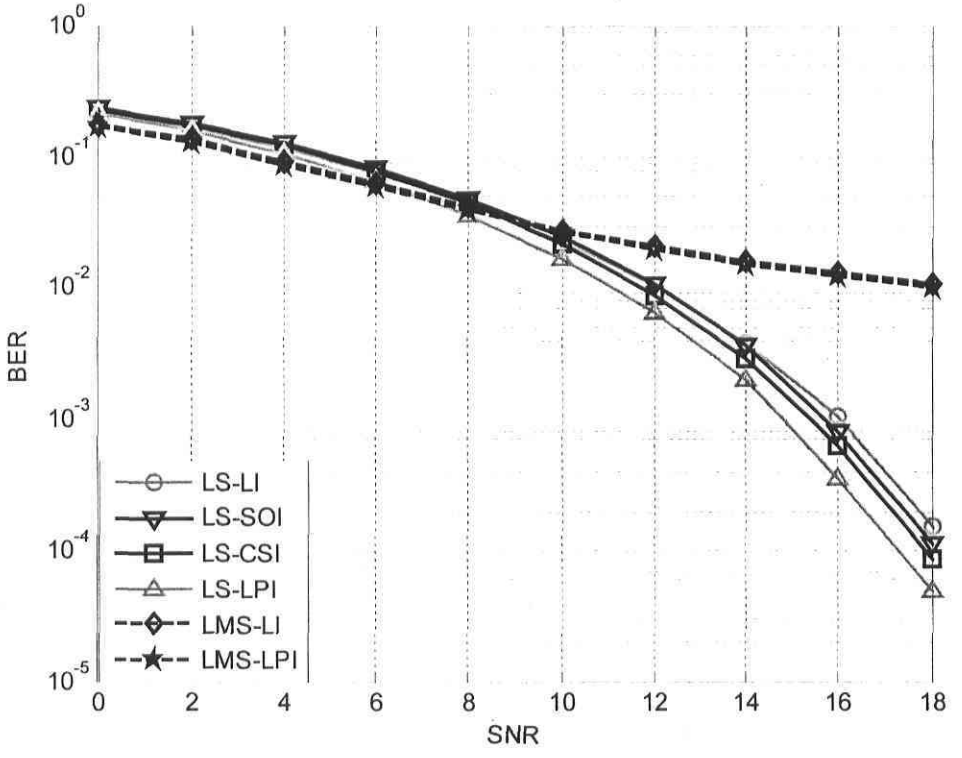

Figure 5. 10: BPSK modulation with Rayleigh fading channel (Channel E, Doppler freq. = 55 Hz).

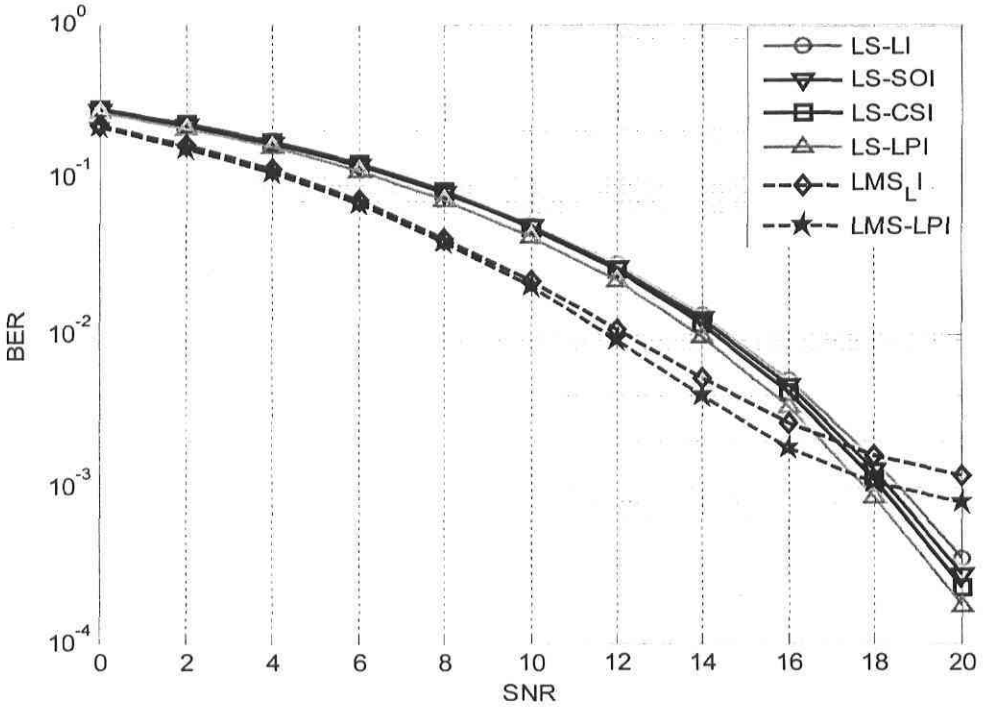

Figure 5. 11: QPSK modulation with Rayleigh fading channel (Channel E, Doppler freq. = 55 Hz).

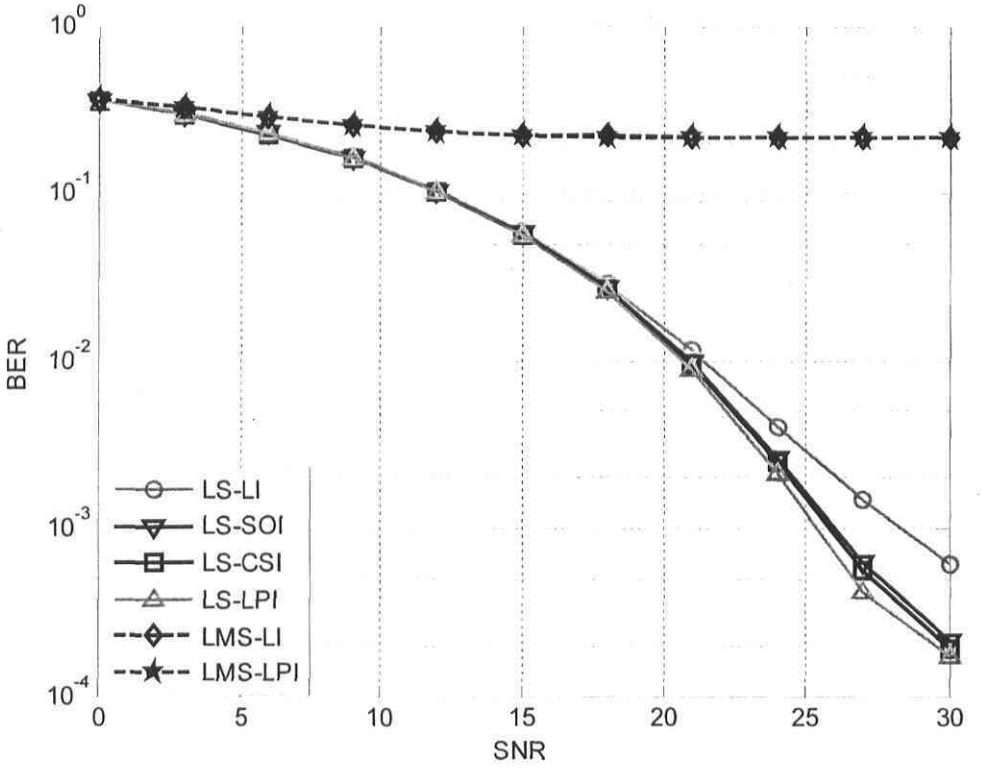

Figure 5. 12: 16QAM modulation with Rayleigh fading channel (Channel E, Doppler freq. = 55 Hz).

Channel D and Channel E have almost the same parameters as channel A and B at different frequencies, so the channel estimation performances show differences caused by differences in the Doppler frequencies, which is higher for channel D and E. Therefore the SNR required for a given BER is higher for channels D and E.

From the simulation results obtained for the Rayleigh fading channel, several conclusions can be drawn regarding the performance of the LS and LMS estimators. First, at low SNRs the LMS outperforms the LS for BPSK and QPSK modulations. However, at high SNRs, the LS shows much better performance and it is more robust against channel noise. When taking complexity into account, the LS estimator is also a good choice under high SNR scenarios. The channel estimation error for LMS is severe in the case of high-order modulations, such as 16QAM. By using the LS channel estimation with interpolation algorithms, the error rate is greatly reduced and the error floor is eliminated.

Our simulation results for Rayleigh fading are consistent with the results in [12].

5.2.3 Channel estimation for LOS area at 2.4 GHz and 5.8 GHz

In this section, the channel estimation performance of the proposed algorithms for different modulations over the Rician fading channel for the LOS area is analyzed. The channels are defined as channels C and F, where the Doppler frequency is 20 Hz with $K = 5.5699$ at 2.4 GHz and 55 Hz with $K = 5.2366$ at 5.8 GHz.

As shown in figures 5.13-5.18, for BPSK and QPSK modulations, the LMS channel estimator performs better when there is a strong component in the signal, such as in a Rician fading channel, at all SNRs. The gain in SNR resulting from the LMS approach as compared to the LS approach is up to 4 dB. However, for 16QAM, the precision of the LMS method is obviously lower than that of the LS method and the LS estimator with LPI still has the best performance among all of the estimation schemes in terms of BER versus SNR. We can notice that the data can be sent with small errors when the SNR is greater than 25 dB for 16QAM.

As in the case of Rayleigh fading, the general shapes of the BER curves for channels C and F for the same modulation scheme at different carrier frequencies are similar.

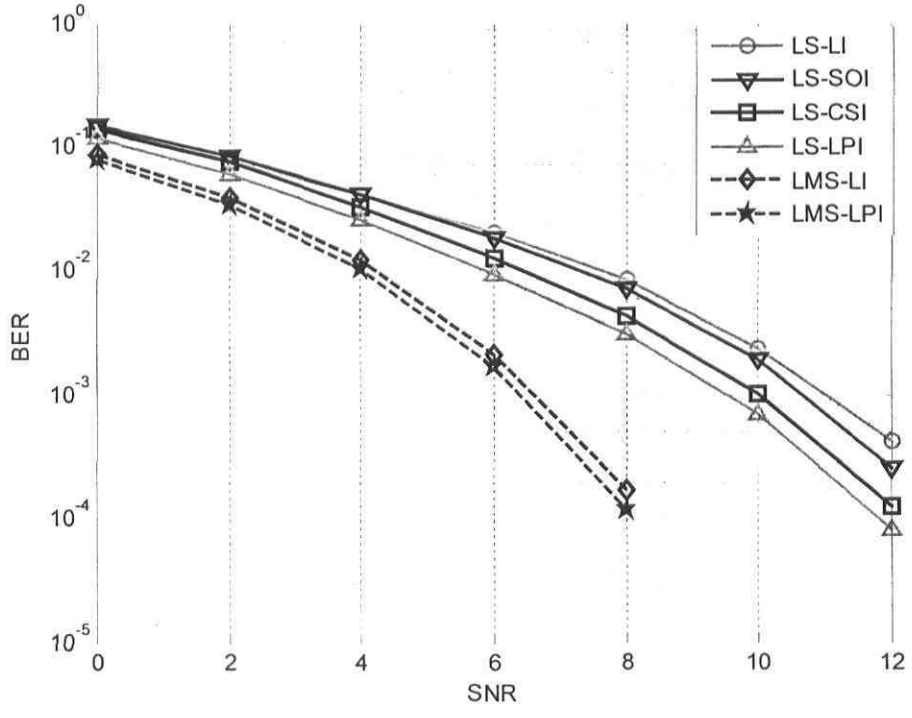

Figure 5. 13: BPSK modulation with Rician fading channel (Channel C, Doppler freq. = 20 Hz, $K = 5.5699$).

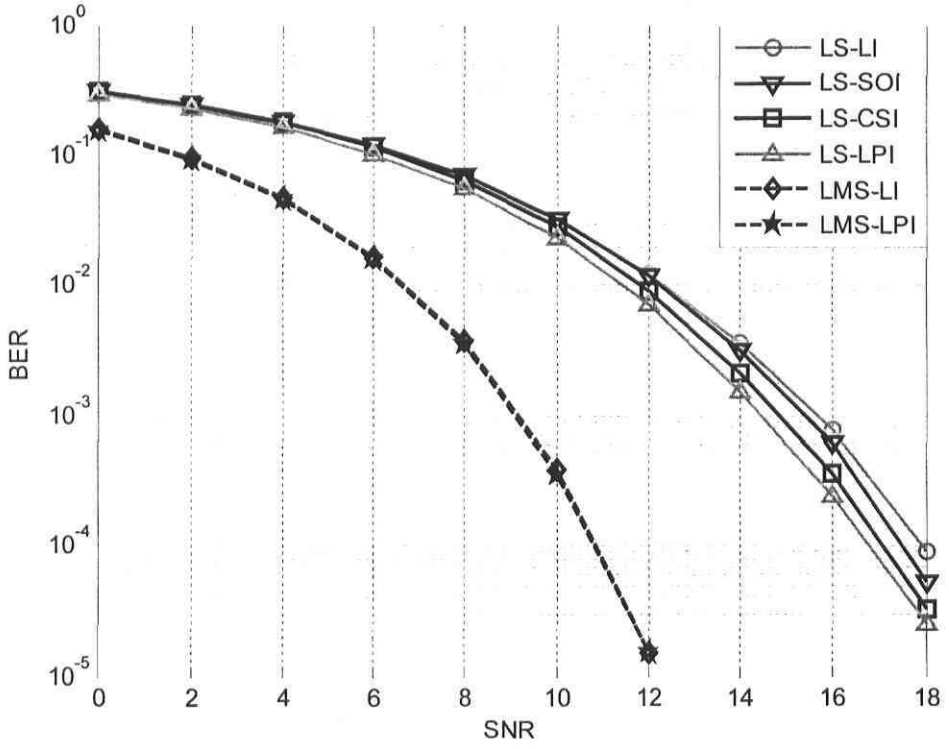

Figure 5. 14: QPSK modulation with Rician fading channel (Channel C, Doppler freq. = 20 Hz, $K = 5.5699$).

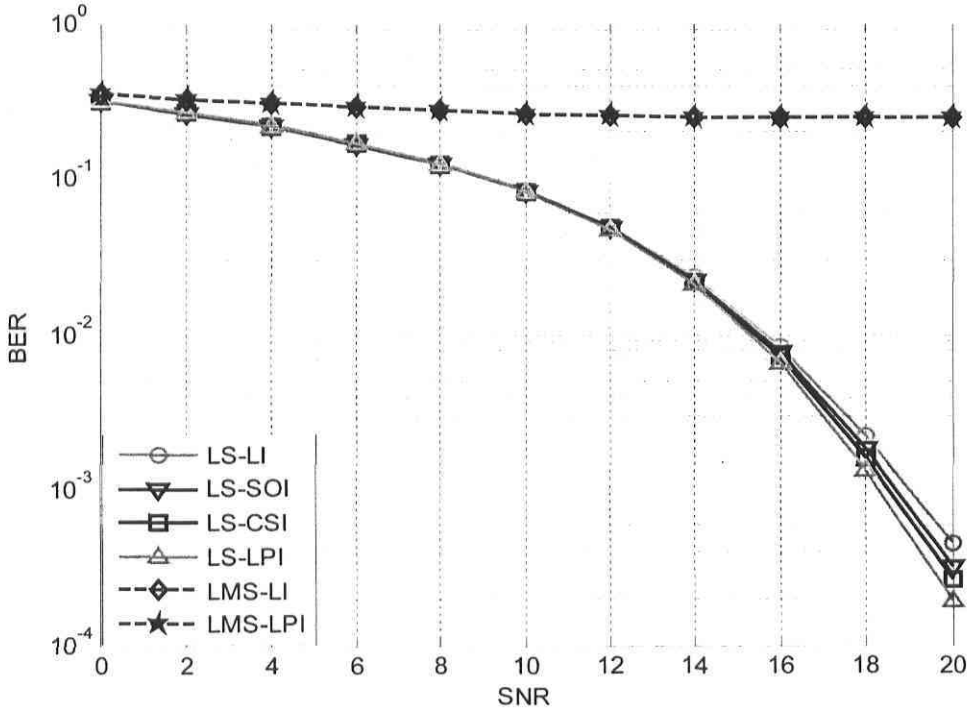

Figure 5. 15: 16QAM modulation with Rician fading channel (Channel C, Doppler freq. = 20 Hz, $K = 5.5699$).

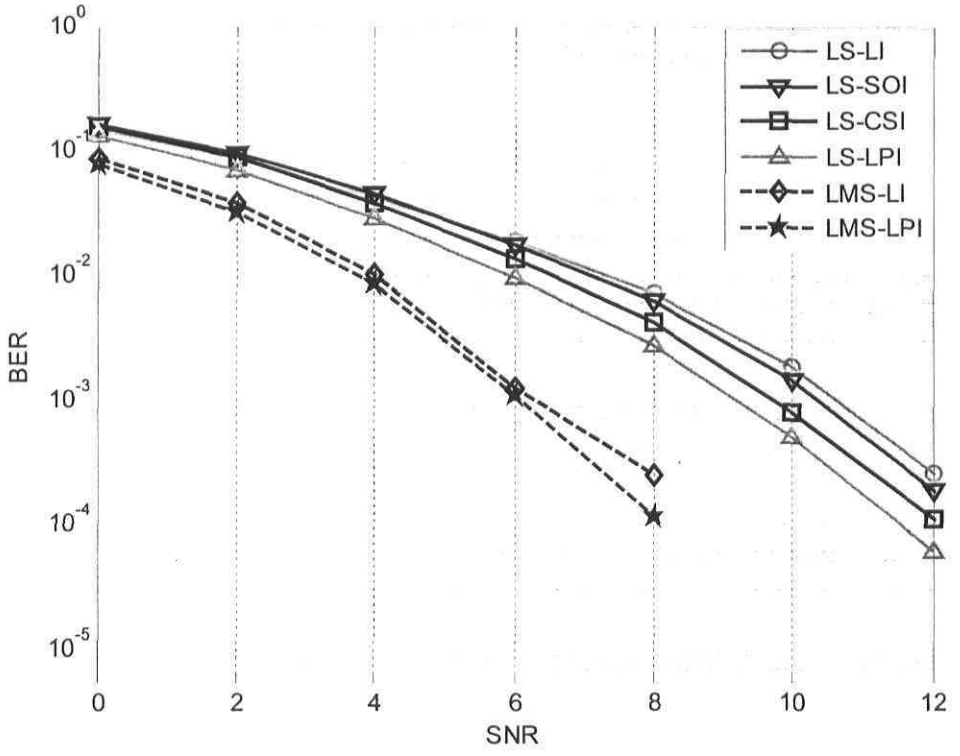

Figure 5. 16: BPSK modulation with Rician fading channel (Channel F, Doppler freq. = 55 Hz, $K = 5.2366$).

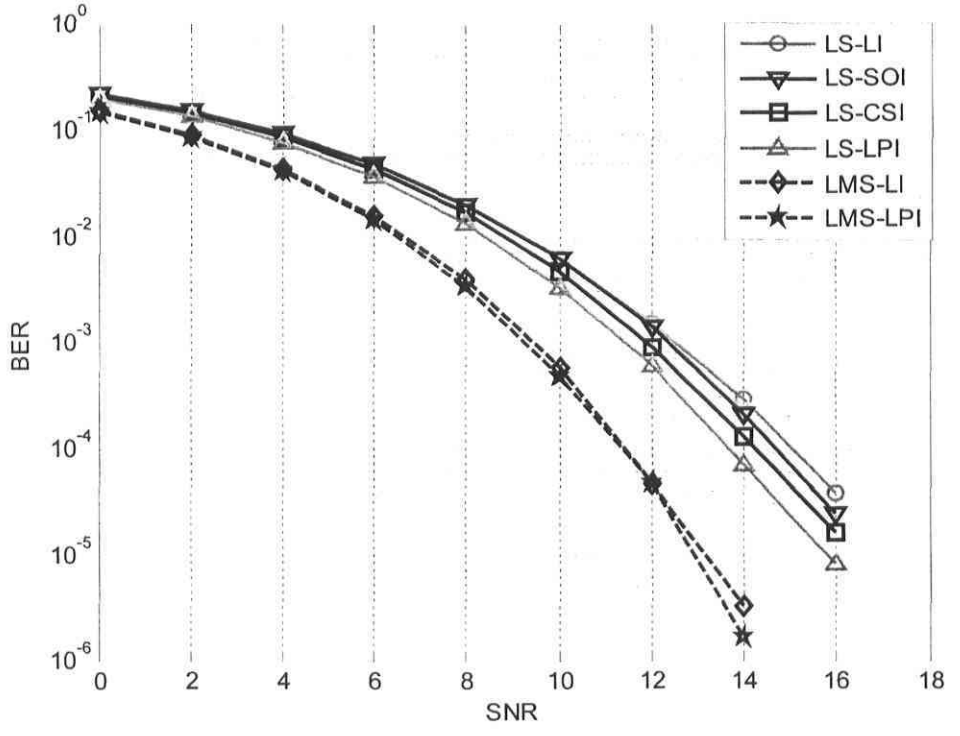

Figure 5. 17: QPSK modulation with Rician fading channel (Channel F, Doppler freq.= 55 Hz, $K = 5.2366$).

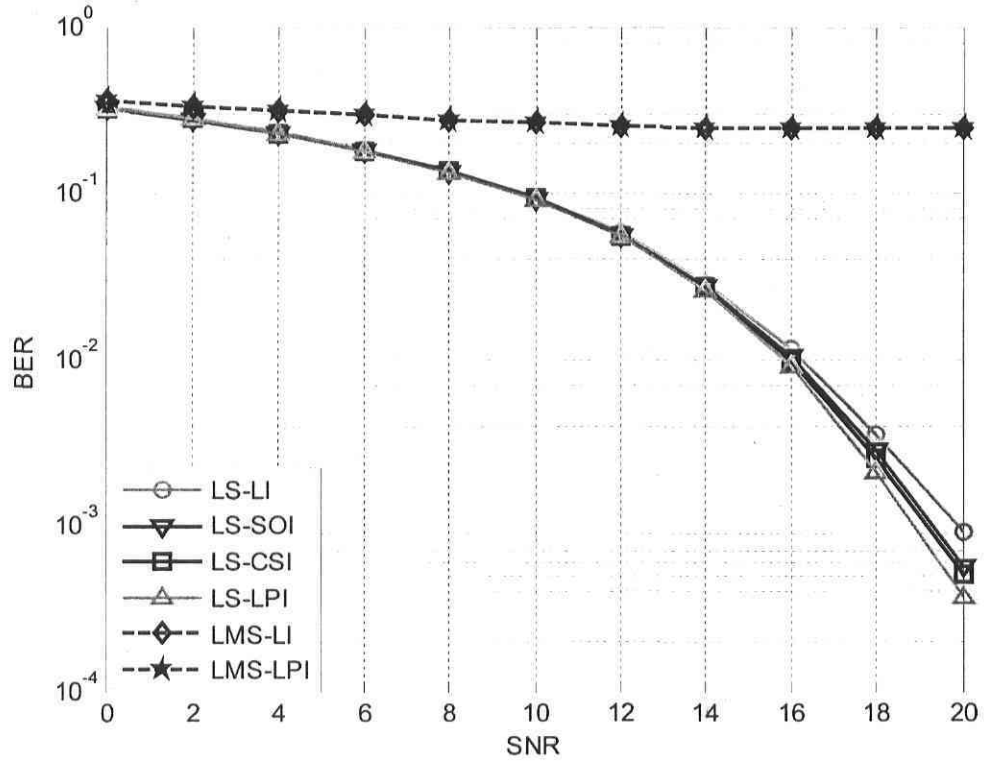

Figure 5. 18: 16QAM modulation with Rician fading channel (Channel F, Doppler freq. = 55 Hz, $K = 5.2366$).

Since there is a strong direct component for the Rician fading channel, the performance of channel estimation is better than for the Rayleigh fading channel under the same conditions. The LS estimator performs better in more random channels, such as the Rayleigh fading channel.

5.3 BER performance for different Doppler frequencies

Figures 5.19–5.21 illustrate the effect of Doppler spread for different modulations with LS-LPI estimation methods in the Rayleigh fading channel. The legends denote the different Doppler frequency for different carrier frequencies. Two vehicle speeds, 10 km/h and 15 km/h, and two carrier frequencies, 2.4 GHz and 5.8 GHz are considered in the simulations. Hence, there are four combinations of the Doppler shift, i.e. 20 Hz, 35 Hz, 55 Hz and 80 Hz, as shown in Table 4.3.

The computer simulation results demonstrate that the improvement in BER performance decreases with higher Doppler frequencies when the time path arrival has a modified Poisson

distribution. It is a general behavior of the plot because of the existence of ICI caused by the Doppler shift.

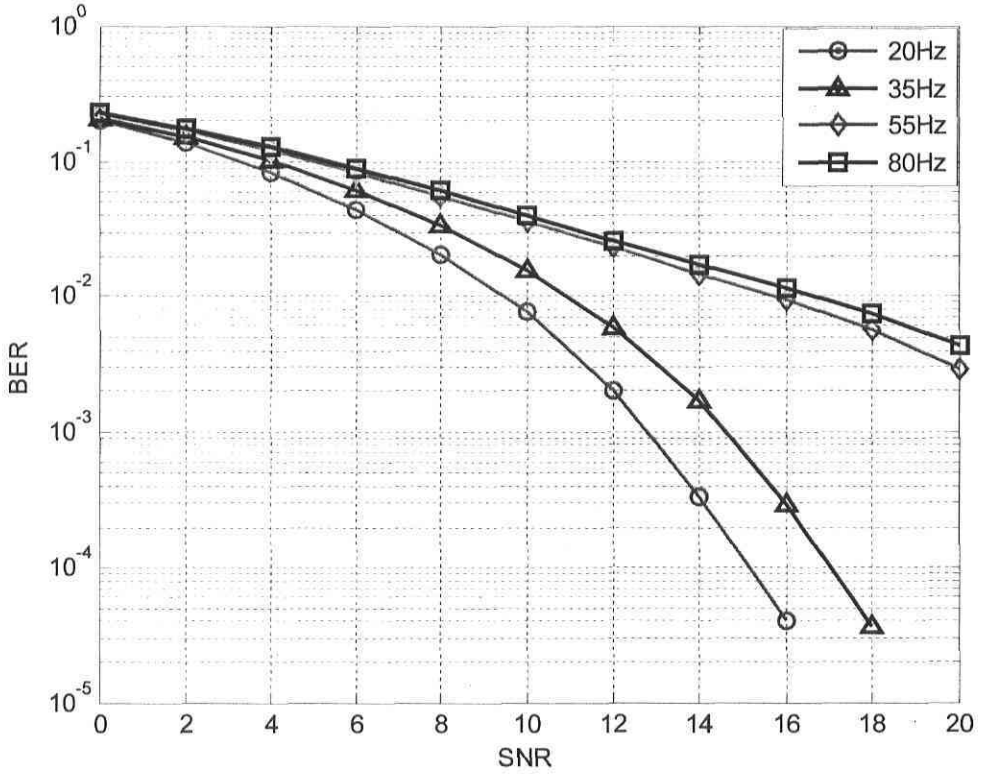

Figure 5. 19: BPSK for different Doppler frequencies, Rayleigh fading, LS estimator with LPI.

Figure 5.19 shows the BER performance of the LS estimator with LPI over the Rayleigh fading channel with BPSK for different Doppler frequencies. Compared with v = 10 km/h at 2.4 GHz, the SNR degradation loss for v = 15 km/h at the same carrier frequency is about 2 dB for a required BER of 0.001. However, at 5.8 GHz, the effect of the Doppler shift is not so obvious; we have almost the same performance for v = 10 km/h and v = 15 km/h.

Figure 5.19 and Figure 5.20 present the BER results for BPSK and QPSK and show similar behaviour. At the lower frequency of 2.4 GHz, the SNR degradation loss for v = 10 km/h is about 3 dB for a required BER of 0.001.

For 16QAM, at the same frequency, the effect of the Doppler shift is not obvious and channel estimation shows almost the same performances for v = 10 km/h and v = 15 km/h, as shown in Figure 5.21.

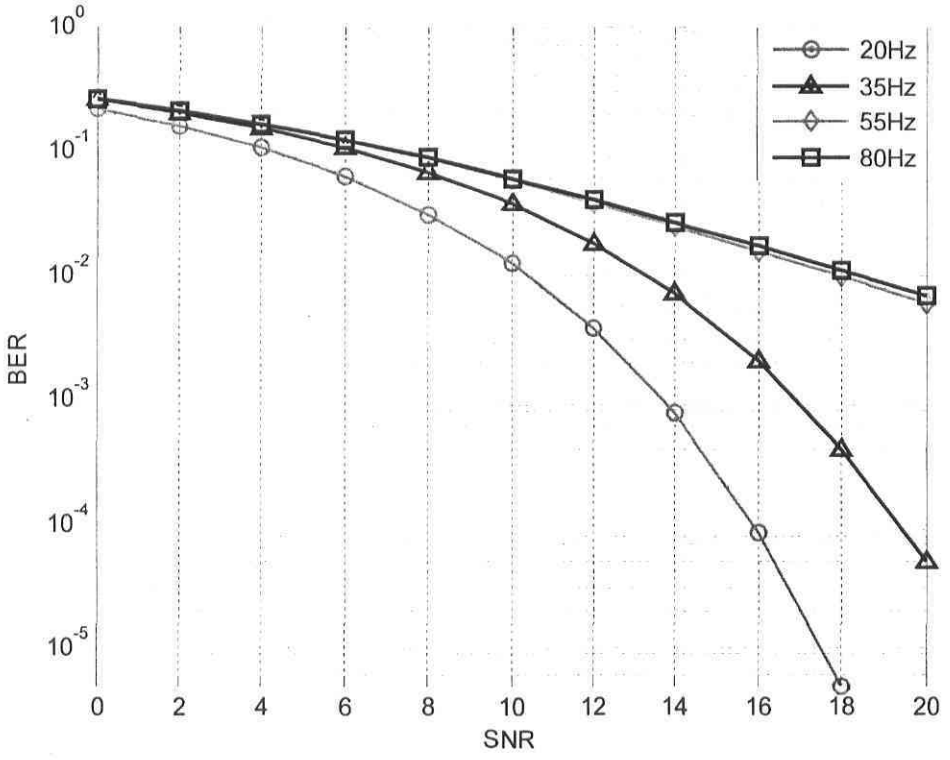

Figure 5. 20: QPSK with different Doppler frequencies, Rayleigh fading, LS estimator with LPI.

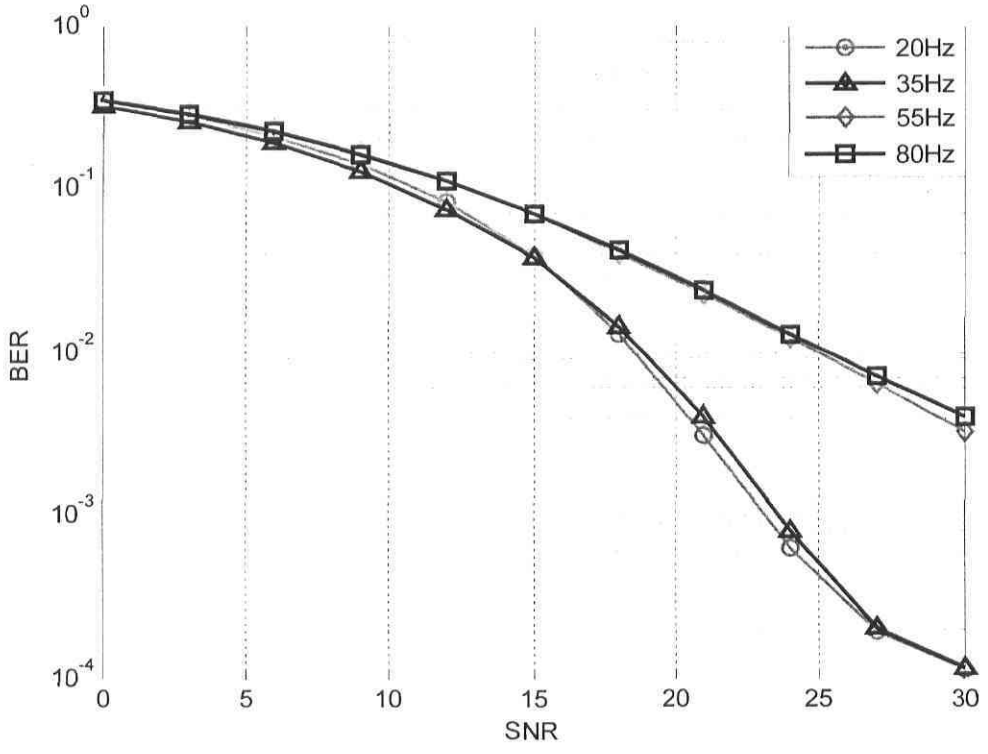

Figure 5. 21: 16QAM with different Doppler frequencies, Rayleigh fading, LS estimator with LPI.

If the received signal has a significant Doppler shift, even when it arrives within the GI, it causes severe ICI. Since in our underground environment the vehicles speeds are lower, the Doppler shift is not significant and the ICI caused by Doppler shift can be compensated using GI with CP in the OFDM systems. Another important observation from the simulation result is that the comb-type pilot estimation is less affected by Doppler shifts compared with the block-type arrangement as discussed in [12]. This is consistent with the theoretical results discussed in previous chapters.

5.4 Summary

In this chapter, the channel estimation schemes based on comb-type pilot arrangement are analyzed through computer simulations under different conditions. The simulation results show that for the Rayleigh fading channel, LS estimation of pilots with interpolation techniques gives better performances at high SNRs with a lower computational complexity than LMS. However, the LMS estimator outperforms the LS estimator for BPSK and QPSK modulation schemes over the Rician fading channel. LPI provides more accurate estimates of the channel transfer function, as compared to the other three interpolation schemes. It works well for both Rayleigh and Rician fading channels, especially for high-order modulation such as 16QAM. The results on the effect of Doppler frequency indicate that performance decreases with an increase of Doppler frequency. PSA channel estimation system works well at low Doppler frequency. For low vehicle speeds, such as would be typical in an underground mine, system performances are less affected by ICI, so ICI can be neglected. In this thesis, the different modulation schemes are also considered to improve tradeoff between spectral efficiency and bit error rate (BER). Generally, when channel conditions are poor, modulation schemes such as BPSK or QPSK are used. As the channel conditions improve, high order schemes such as 16QAM and 64QAM can be used.

CHAPTER 6

CONCLUSIONS AND FUTURE WORKS

6.1 Thesis conclusions

OFDM techniques applications in WLAN communications have attracted a lot of attentions in the last few years, because they make the system robust against frequency selective channels. Using the IEEE802.11a/g OFDM system to construct an underground WLAN and to achieve a high data rate up to 54 Mbps is appealing. To achieve high data rates as well as good performances, coherent channel estimation has to be performed at the receiver. Most of OFDM coherent channel estimation methods are PSA based and in the frequency domain. The transmitter just inserts known symbols periodically, so there is no change in pulse shape or peak to average power ratio. Theses methods have low complexity and implementation should be easy. They require additional processing to estimate the CFR on the subcarriers other than the pilot ones. The channel estimation is performed using either of two channel estimation methods, LS or LMS, at pilot subcarriers and interpolation of the channel at data subcarriers.

In this thesis, some popular PSA channel estimation algorithms for OFDM systems based on comb-type pilot arrangement were studied. The algorithms were tested using Matlab/Simulink to verify their functionalities. The OFDM system model with channel estimation was setup in Simulink based on the IEEE802.11a specification. The system performance was tested under different situations, including different modulation schemes, different channel models, different channel information and different channel estimation algorithms.

In chapter 3, it was established that in PSA OFDM channel estimation based comb-type pilot arrangement is preferable over the frequency–selective channel estimation due to its simplicity. The main estimation schemes are LMS / LS for pilot frequency estimation and LI/SOI/CSI/LPI for channel estimation data frequencies. The simulations have been done over the Raleigh fading channel for the NLOS area and the Rician fading channel for the LOS area at 2.4 GHz and 5.8 GHz. The simulation results gave the following conclusions.

- For channel estimation with BPSK and QPSK modulation over the Rayleigh fading channel, simulation results show that at lower SNRs, the performance of the LMS estimator approaches the performance of the LS estimator. However, with the increase of SNR, the LS estimator outperforms the LMS estimator. So the LS method is preferable for high SNR cases and the LMS is suitable for low SNR cases. Compared with the LMS estimator, the LS algorithm has the advantage of simplicity and robustness against insufficient or inaccurate channel model information.
- For channel estimation with BPSK and QPSK modulation over the Rician fading channel, simulation results showed that the performances of the LMS estimator outperform those of the LS estimator at all SNRs. Therefore, the results demonstrate that the LMS channel estimator performs better when there is a strong component in the received signal.
- For high order modulation schemes, such as 16-QAM, the LS estimator showed superior performances over the LMS estimator. So the LS estimator is suitable for high-order modulation to achieve high data rate transmission.
- Among all of the interpolation schemes, the LS estimator with LPI interpolation achieved the best performances and the LI showed the worst. The results were expected since the low-pass filter used in the simulations does the interpolation such that the MSE between the interpolated points and their ideal values is minimized, while the LI does the interpolation using only two pilot symbols and is therefore less accurate. These results were also consistent with those obtained in [12].
- The effect of Doppler shift was compared at both carrier frequencies. At 5.8 GHz, the effect of Doppler shift was more significant than at 2.4 GHz. The improvement in BER performance decreases with larger Doppler frequencies when the time path arrival has a

modified Poisson distribution. The PSA OFDM channel estimation based comb-type pilot arrangement can efficiently reduce the effect of Doppler shift.

6.2 Future works

Due to the limited time frame of this research, there are still some important issues that have not been dealt with. The following is a list of suggested future works that can be investigated.

- Improve the performance by using channel estimation in the time domain. Channel estimation in FD has low complexity and is easy to implement. However, it is very sensitive to deep fades. If the deep fades occur in the CFR at pilot frequencies, then the channel estimation may be compromised. Its applicability is restricted to fixed wireless scenarios. Moreover, the complexity of channel estimators may significantly increase in high mobility scenarios, where channel tracing may be needed. Although methods in the TD usually have higher complexity than the FD approaches, channel tracing in TD is still preferable.

- Investigate channel estimation in fast–varying channels where the channel changes within an OFDM block. In this thesis, we have limited the time varying channel to change within an OFDM frame, but not within an OFDM block. When the channel changes within an OFDM block, ICI occurs. The effects of ICI on channel estimation should be studied.

- Study the effect of frequency offset on channel estimations. In our analysis, we have assumed perfect frequency synchronization, therefore, the negative effect of ICI has not been analyzed.

REFERENCES

Channel Model

[1] C. Nerguizian, M. Djadel, C. Despins, and S. Affes, "*Narrowband and Wideband Radio Channel Characteristics in Underground Mining Environments at 2.4 GHz,*" Proc. of IEEE PIMRC'03, Beijing, China, Vol. 1, pp. 680-684, September 7-10, 2003.

[2] A. Benzakour, S. Affes, C. Despins, and P.-M. Tardif, "*Wideband Measurements of Channel Characteristics at 2.4 and 5.8 GHz in Underground Mining Environments,*" Proc. of IEEE VTC'04-Fall, Los Angeles, California, USA, Vol. 5, pp. 3595-3599, September 26-29, 2004.

[3] M. Boutin, *Statistical Modeling of a Radio Propagation Channel in an Underground Mine at 2.4 GHz and 5.8 GHz*, Master's Thesis, INRS-EMT, Montreal, Canada, 2004.

[4] T. S. Rappaport, *Wireless Communications Principles and Practice*, IEEE Press, New York, Prentice Hall, pp. 169-177, 1996.

[5] H. Hashemi, D. Lee, and D. Ehman, "*Statistical modeling of the indoor radio propagation channel, part I,*" IEEE 42nd Vehicular Technology Conference, 1992, vol. 1, pp. 338-342, May 10-13, 1992.

[6] R. Steele, *Mobile Radio Communications*, London, England, Pentech Press Limited, 1992.

[7] R. Prasad, *OFDM for Wireless Communications Systems*, Artech House, Boston·London, 2004.

[8] J. Heiskala, J. Terry, *OFDM Wireless LANs: A Theoretical and Practical Guide*, Sams Publishing, 2002.

[9] IEEE Standard 802.16-2004, "*IEEE Standard for Local and Metropolitan Area Networks Part 16: Air Interface for Fixed Broadband Wireless Access Systems,*" 2004.

[10] W. Carney, "*IEEE 802.11g: New Draft Standard Clarifies Future of Wireless Lan,*" White paper by Texas Instrument, 2002.

[11] IEEE 802.11 Standard, *Wireless LAN Medium Access Control (MAC) and Physical Layer (PHY) specifications*, 1999.

[12] S. Coleri, M. Ergen, A. Puri, and A. Bahai, "*Channel Estimation Techniques Based on Pilot Arrangement in OFDM Systems,*" IEEE Trans. on Broadcasting, Vol. 48, No. 3, pp. 223-229, Sept. 2002.

[13] C. H. Yeh and Y. Y. Lin, "*Channel Estimation Using Pilot Tones in OFDM Systems,*" IEEE Transaction on broadcasting, Vol. 45, No. 4, pp. 400–405, Dec. 1999.

[14] H. Minn and V. K. Bhargava, "*An Investigation into Time-Domain Approach for OFDM Channel Estimation,*" IEEE Trans. on Broadcasting, Vol. 46, No. 1, pp. 240-248, Dec. 2000.

[15] M. Morelli and U. Mengali, "*A comparison of Pilot-Aided Channel Estimation Methods for OFDM Systems,*" IEEE Trans. on Signal Processing, Vol. 49, No. 12, pp. 3065-3073, Dec. 2001.

[16] J.-J. van de Beek, O. Edfors, M. Sandell, and S. K. Wilson, "*On Channel Estimation in OFDM Systems,*" Proc. 45th IEEE Vehicular Technology Conf., Chicago, IL, pp. 815-819, July 1995.

[17] M. Hsieh and C. Wei, "*Channel Estimation for OFDM Systems Based on Comb-Type Pilot Arrangement in Frequency Selective Fading Channels,*" IEEE Trans. on Consumer Electronics, Vol. 44, No.1, pp. 217-225, February 1998.

[18] Y. Li, "*Pilot-Symbol Aided Channel Estimation for OFDM in Wireless System,*" IEEE Trans. on Vehicular Technology, Vol. 49, No. 4, pp. 1207-1215, July 2000.

[19] P.-Y. Tsai and T. -D. Chiueh, "*Frequency-Domain Interpolation-Based Channel Estimation in Pilot-Aided OFDM systems,*" IEEE 59th Vehicular Technology Conference (VTC'04), Vol. 1, pp. 420-424, Milan, Italy, May 2004.

[20] Y. Zhao and A. Huang, "*A Novel Channel Estimation Method for OFDM Mobile Communication Systems based on pilot Signals and Transform Domain Processing,*" Proc. of 1997 IEEE 47th Vehicular Technology Conf., Vol. 3, No. 4, pp. 2089-2093, May 1997.

[21] M. Dong, L. Tong and B. M. Sadler, "*Optical pilot placement for channel tracking in OFDM,*" Proc. of IEEE Military Commun Conf., pp. 602-606, 2002.

[22] H. H'mimy, "*Channel Estimation based on coded pilot for OFDM,*" Proc. of IEEE Vehicular Technology Conf., pp. 1375-1379, 1997.

[23] P. Hoeher, S. Kaiser and P. Robertson, "*Two-dimensional pilot-symbol-aided channel estimation by Wiener filtering,*" Proc. of IEEE Intl Conf. Acoust. Speech and Signal Proc., pp. 1845-1848, 1997.

[24] Y. Li, L. J. Cinimi and N. R. Sollenberger, "*Robust channel estimation for OFDM systems with rapid dispersive fading channels,*" IEEE Trans. Commun., pp. 902-915, July 1998.

[25] O. Edfors, M. Sandell, J.-J. van de Beek, S. K. Wilson and P. O. Borjesson, "*OFDM channel estimation by singular value decomposition,*" IEEE Trans. Commun.. 46(7), pp. 931-939, July 1998.

[26] T. Roman, M. Enescu, and V. Koivunen "*Time-domain method for tracking dispersive channels in MIMO OFDM systems,*" Proc. of IEEE Intl. Conf. on Multimedia and Expo, Vol. 2, pp. 609-612, 2003.

[27] T. Roman, M. Enescu, and V. Koivunen, "*Joint time-domain tracking of channel and frequency offset for OFDM systems,*" Proc. of IEEE Signal Proc. Advances in Wireless Commun. Workshop, SPAWC'03, 2003.

[28] L. Deneire, P. Vandenameele, L. v. d. Perre, B. Gyselinckx, and M. Engels, "*A Low-Complexity ML Channel Estimator for OFDM,*" IEEE Trans. on Commun., Vol. 51, pp. 135-140, Feb. 2003.

[29] M.-X. Chang and Y. T. Su, "*Model-based channel estimation for equalizing OFDM signals,*" IEEE Trans. Commun., Vol. 50, pp. 540-544, Apr. 2002.

[30] J. K. Moon and S. I. Chol, "*Performance of Channel Estimation Methods for OFDM Systems in a Multipath Fading Channels*," IEEE Trans. on Consumer Electronics, Vol. 46, No. 1, pp. 161-170, Feb. 2000.

[31] S. Weinstein and P. Ebert, "*Date transmission by frequency-division multiplexing using the discrete Fourier transform,*" IEEE Trans. on Commun., Vol. 19, No. 5, pp. 628-634, Oct. 1971.

[32] A. Peled and A. Ruiz, "*Frequency domain data transmission using reduced computational complexity algorithms,*" Proc. IEEE ICASSP-80, Denver, CO, pp. 964- 967, 1980.

[33] P. Hoher, "*TCM on frequency-selective land-mobile fading channels,*" in *Proc.* Tirrenia Int. Workshop Digital Communications, Tirrenia, Italy, pp. 317-328, Sept. 1991.

[34] T. Roman, M. Enescu, and V. Koivunen, "*Time-domain method for tracking dispersive channels in OFDM systems*," In Proc. of IEEE Veh. Technol. Conf., Vol.2, pp. 1318-1321, 2003.

[35] S. G. Kang, Y. M. Ha, and E. K. Joo, "*A comparative investigation on channel estimation algorithms for OFDM in mobile communications,*" IEEE Trans. on Broadcasting, Vol. 49, No. 2, pp. 142-149, June 2003.

APPENDIX A

CHANNEL MODELING PARAMETERS

Statistical modeling is attractive in that it can quickly and reliably generate simulated impulse responses (IR) for a particular frequency and topography based on accurate models derived from experimental measurements. In [3], prior to IR modeling, the IR has been presented with a discrete time axis divided in time bin of 8 nsec as imposed by the experimental protocol. An example of this discretization is shown in Figure A.1.

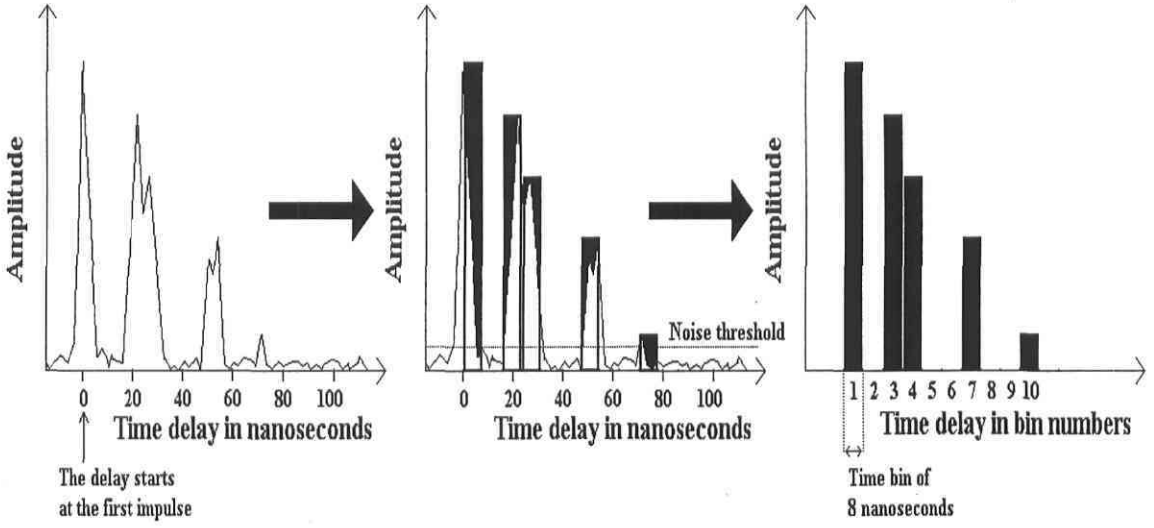

Figure A. 1: Time axis discretization of an impulse response [3].

The modeling process includes path arrival modeling and amplitude modeling only [3] and the phase is considered to be uniformly distributed over $(0, 2\pi]$.

A.1 Path time arrival

[3] shows that the path arrival follows a modified Poisson distribution for all areas and both frequencies.

For each time bin, the experimental occurrence probability of an impulse has been calculated according to experimental measurements, which is called arrival rate r_n. An impulse for the next time bin is obtained as a function of the state and the arrival rate of the present time bin.

The modified Poisson distribution uses possible states associated with each time bin, called state-1 and state-2. When an impulse occurs, it is on the second state, otherwise on the first. The process starts at state-1 with the first time bin for which an impulse response can randomly occur. Therefore, the probability to get an impulse at the first time bin is λ_1. If no impulse has occurred at this time bin, then the probability of having an impulse at the next time bin is λ_2. However, if an impulse occurs at the first time bin, then the occurrence probability of an impulse at the second time bin would be $K_{MP}\lambda_2$. The probabilities λ_n can be found by following equation [3]:

$$\lambda_n = \frac{r_n}{(K_{MP}-1)r_{n-1}+1}, \text{ for } n \neq 1 \text{ and } \lambda_1 = r_1 \qquad (A.1)$$

λ_n can be obtained by repeated use of (A.1). Then the probability distributions are calculated by recursive formulas that calculate the distribution of the impulse number, step by step [3].

The values of the modified Poisson distribution parameters for each area at both frequencies are shown in Table A.1 and Table A.2, for each impulse response time bin.

Table A. 1: Parameters of the modified Poisson distribution for each area at 2.4 GHz [3].

Time bin	LOS		NLOS1		NLOS2	
	K_{MP}	λ	K_{MP}	λ	K_{MP}	λ
1	0	0.34848	0	0.4375	0	0.47917
2	0.7255	0.77907	0.42245	0.8642	0.56046	0.85333
3	0.67529	0.8546	0.3624	0.97989	0.69712	0.62816
4	0.77912	0.58519	0.60556	0.69206	0.67608	0.48891
5	0.88682	0.45772	0.77966	0.48019	0.71542	0.29086
6	1.0313	0.19434	1.0403	0.28677	0.89571	0.10703
7	1.2959	0.18612	1.1992	0.11157	0.98768	0.076487
8	1.3725	0.07058	1.3088	0.073702	0.97531	0.013915
9	1.4325	0.066019	1.4296	0.060514	0.96492	0.027791
10	1.4029	0.014746	1.4167	0.013536	0.95873	0.0069524
11	1.4138	0.037643	1.395	0.013813	0.98483	0.0069452
12	-	-	1.4055	0.013811	0.97592	0.013891
13	-	-	1.4192	0.0069042	0.97592	0
14	-	-	1.4329	0.013847	0.96939	0.00694444
15	-	-	1.4347	0.013806	0.96939	0
16	-	-	-	-	0.96487	0.00694444

Table A. 2: Parameters of the modified Poisson distribution for each area at 5.8 GHz [3].

Time bin	LOS		NLOS1		NLOS2	
	K_{MP}	λ	K_{MP}	λ	K_{MP}	λ
1	0	0.44697	0	0.45833	0	0.41667
2	0.51741	0.75343	0.55297	0.79487	0.42609	0.82143
3	0.76126	0.80262	0.5252	0.86315	0.6276	0.49781
4	0.61211	0.72387	0.71337	0.58792	0.71194	0.17166
5	0.76189	0.47688	0.96524	0.34613	0.84036	0.064062
6	0.66647	0.43992	1.1522	0.2839	0.86928	0.056013
7	0.8108	0.17953	1.3526	0.13822	0.85982	0.013998
8	0.93662	0.09188	1.484	0.12933	0.85982	0
9	0.97371	0.03797	1.6439	0.05737	0.85328	0.0069444
10	-	-	1.6705	0.053321	0.85328	0
11	-	-	1.6833	0.033452	0.84984	0.0069444
12	-	-	1.6837	0.013567	-	-
13	-	-	1.6837	0	-	-
14	-	-	1.7276	0.041667	-	-
15	-	-	1.7407	0.0067365	-	-
16	-	-	1.8551	0.034517	-	-
17	-	-	1.8668	0.033708	-	-
18	-	-	1.9285	0.020183	-	-

A.2 Path amplitude

According to [3], for path amplitude, the Rayleigh and Rician distributions offer the best fit for the NLOS and the LOS areas at both frequencies. The parameters of the Rician and Rayleigh distributions at 2.4 GHz and 5.8 GHz have been presented in [3]. Since the received power can be considered as negligible after the 10^{th} time bin in the measured IR [2], the Rician K-factor and the path gains needed for simulation parameters in the Rician and Rayleigh blocksets of Simulink will always consider 10 consecutive paths. The mean amplitude for each bin, the fitted curve and the Rician K-factor for LOS at 2.4 GHz and 5.8 GHz are shown in Figure A.2 and Figure A.3.

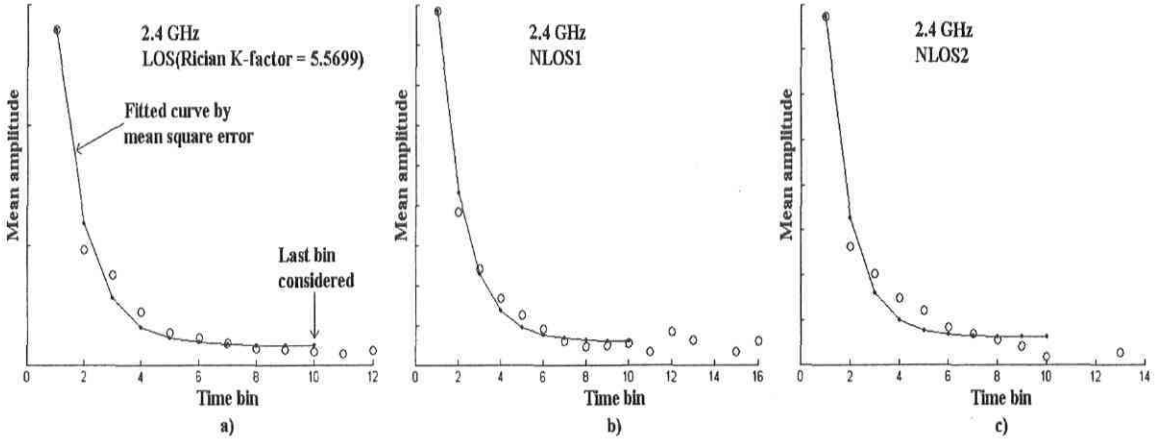

Figure A. 2: Mean amplitude at 2.4 GHz for a): LOS (with Rician K-factor), b): NLOS1 and c): NLOS2 [3].

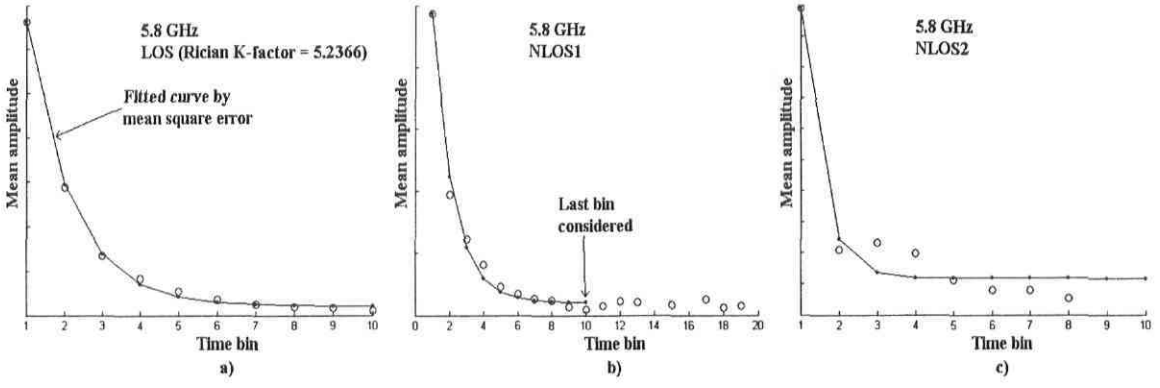

Figure A. 3: Mean amplitude at 5.8 GHz for a): LOS (with Rician K-factor), b): NLOS1 and c): NLOS2.

The mean relative gain of the 10 consecutive paths (time bin) for LOS, NLOS1 and NLOS2 at 2.4 GHz and 5.8 GHz are shown in Table A.1 and Table A.2.

Table A. 3: Relative path gain for LOS, NLOS1 and NLOS2 at 2.4 GHz [3].

Path (time bin)	Gain (dB) for LOS	Gain (dB) for NLOS1	Gain (dB) for NLOS2
1	0	0	0
2	-7.4589	-6.2284	-7.4885
3	-13.9819	-11.8003	-13.6642
4	-18.9334	-16.3267	-17.8911
5	-22.0107	-19.5355	-20.1966
6	-88.6561	-21.4936	-21.2387
7	-89.3449	-22.5468	-21.6605
8	-89.6349	-23.0679	-21.8228
9	-89.7482	-23.3139	-21.8839
10	-89.7925	-23.4273	-21.9067

Table A. 4: Relative path gain for LOS, NLOS1 and NLOS2 at 5.8 GHz [3].

Path (time bin)	Gain (dB) for LOS	Gain (dB) for NLOS1	Gain (dB) for NLOS2
1	0	0	0
2	-7.0373	-6.7742	-12.1758
3	-13.6293	-13.0240	-17.2788
4	-19.3759	-18.3364	-18.3496
5	-23.8066	-22.2986	-18.5165
6	-26.7024	-24.8092	-18.5410
7	-28.3059	-26.1755	-18.5445
8	-29.0906	-26.8431	-18.5451
9	-29.4478	-27.1499	-18.5451
10	-29.6045	-27.2865	-18.5451

APPENDIX B

MATLAB SIMULATION CODE FOR CHANNEL MODEL

The wideband statistical channel model coding [3]

The programming is developed by Mathieu Boutin [3].

```
%%%%%%%%%%%%%%%%%%%%%%%%%%%%%%%%%%%%%%%%%
freq = {'2.4 GHz','5.8 GHz'};           two carrier frequency are considered
topo = {'LOS','NLOS1','NLOS2'};          three part of gallery at 70mth depth are defined

%%%%%%%%%%%%%%%%%%%%%%%%%%%%%%%%%%%%%%%%%
%Choose the different frequency for different area
%%%%%%%%%%%%%%%%%%%%%%%%%%%%%%%%%%%%%%%%%
C_freq = freq{1};              Choose freq{1} for 2.4GHz  or freq{2}for 5.8GHz
C_topo = topo{1};              Choose topo{1} for LOS, topo{2}or topo{3}for NLOS1 or NLOS2

%%%%%%%%%%%%%%%%%%%%%%%%%%%%%%%%%%%%%%%%%%%%%
% Generating the modified Poisson distribution
%%%%%%%%%%%%%%%%%%%%%%%%%%%%%%%%%%%%%%%%%%%%%
load  ('parametres_mpoisson.mat');
switch C_freq
   case '2.4 GHz'
      cell_freq = mpoisson_2400_MHz;
   case '5.8 GHz'
      cell_freq = mpoisson_5800_MHz;
```

```
    otherwise
        error('Error choice of frequency ');
end
switch C_topo
    case 'LOS'
        cell_topo = cell_freq.LOS;
    case 'NLOS1'
        cell_topo = cell_freq.NLOS1;
    case 'NLOS2'
        cell_topo = cell_freq.NLOS2;
    otherwise
        error('Error choice of topo' );
end
T_bin = length(cell_topo);%the normalize time bin of path delay with 8 ns resolution.

%%%%%%%%%%%%%%%%%%%%%%%%%%%%%%%%%%%%%%%%%%%%%%%%%%%%%%%%%%%%%%%%%%%%%%%%%%%%
% The algorithms
%%%%%%%%%%%%%%%%%%%%%%%%%%%%%%%%%%%%%%%%%%%%%%%%%%%%%%%%%%%%%%%%%%%%%%%%%%%%
impulsion_survenu_avant = 0;
vecteur_impulsion = [1];
for index_bin = 2 : T_bin
    k = cell_topo{index_bin - 1}.k;
    lambda = cell_topo{index_bin - 1}.lambda;
    if impulsion_survenu_avant
        prob_mpoisson_cst = k*lambda;
    else
        prob_mpoisson_cst = lambda;
    end
    if (prob_mpoisson_cst > 1)
        prob_mpoisson_cst = 1;
    end
    resultat = binornd(1,prob_mpoisson_cst,1,1);
```

```
    vecteur_impulsion(index_bin) = resultat;
    if (resultat == 1)
      impulsion_survenu_avant = 1;
    else
      impulsion_survenu_avant = 0;
    end
end

%%%%%%%%%%%%%%%%%%%%%%%%%%%%%%%%%%%
%Generate the time delay and path gain for different conditions.
%%%%%%%%%%%%%%%%%%%%%%%%%%%%%%%%%%%
vector_impulse(1) = 0
vector_impulse
V = vector_impulse.*[0:8:64];
V(1) = 1;
G = [0:-3:-24] ;
A = find(V==0);
for k = 2 : length(V)
     i = 1;
    Vs = [V(1:A(1)-1)];
    Vsb = [G(1:A(1)-1)];
    for i = 1 : length(A)
      if i ~= length(A)
         V1 = [Vs, V(A(i)+1:A(i+1)-1)];
         Vb1 = [Vsb, G(A(i)+1:A(i+1)-1)];
         Vs = V1;
         Vsb = Vb1;
     end
      i == length(A);
      V1 = [Vs, V(A(i)+1:length(V))];
      Vb1=[ Vsb, G(A(i)+1:length(G)) ];
    end
```

```
end

V = [vector_impulse' G'];
Vmod = [V1' Vb1'];
GainV = Vmod(:,2);
DelayV = Vmod(:,1)*1e-9
```

APPENDIX C
LEAST SQUARES ALGORITHM

In practice, the LS estimator is more commonly used due to its ease of implementation and acceptable performance. The criteria for a good estimator are that it is unbiased and has minimum variance. The LS estimator uses variance as a measure of performance by choosing an estimate that minimizes the error between the estimate and the true value. Here, the derivation of the LS estimator using the following general linear data model is briefly presented. The general linear data model can be described by the following equation:

$$Y = H\theta + W \tag{C.1}$$

where, H is a known $N \times P$ matrix, θ is a $P \times 1$ vector, and W is an $N \times 1$ vector. The objective is to determine an estimate θ vector. The LS approach tries to solve the estimation problem by minimizing the following cost function:

$$J(\theta) = (Y - H\theta)^H (Y - H\theta) \tag{C.2}$$

The gradient of the above equation is

$$\frac{\partial J(\theta)}{\partial \theta} = -2H^H\theta + 2(H)^H H\theta \tag{C.3}$$

Equating the gradient to zero will yield the LS estimate:

$$\hat{\theta} = (H^H H)^{-1}(H)^H Y \tag{C.4}$$

In LS estimation, the known matrix H must be of full rank to ensure the invertibility of $H^H H$.

Given the estimate, $\hat{\theta}$, the MSE of the estimate is defined as

$$MSE_{\hat{\theta}} = \frac{1}{P} E\left\{\left\|\hat{\theta} - \theta\right\|^2\right\} \tag{C.5}$$

Substituting the LS estimate from (C.4) to (C.5), the MSE of the LS estimator becomes:

$$\begin{aligned} MSE_{LS} &= \frac{1}{P} E\left\{\left\|\left(H^H H\right)^{-1}(H)^H Y - \theta\right\|^2\right\} \\ &= \frac{1}{P} Trace\left\{E\left\{\left(\left(H^H H\right)^{-1}(H)^H W\right)\left(\left(H^H H\right)^{-1}(H)^H W\right)^H\right\}\right\} \\ &= \frac{1}{P} Trace\left\{\left(\left(H^H H\right)^{-1}(H)^H E\left\{WW^H\right\}H\left(H^H H\right)^{-1}\right)\right\} \\ &= \frac{\sigma_W^2}{P} Trace\left\{\left(H^H H\right)^{-1}\right\} \end{aligned} \tag{C.6}$$

APPENDIX D

MATLAB CODE FOR THE INTERPOLATION ALGORITHMS

D.1 Linear Interpolation (LI)

```
function outdata =linearinterp(pilotin)

r = 13;
L = length(pilotin);

for m = 1 : L
   if m == 1
      for i = 1 : (r-1)
         outdata(i) = pilotin(1)-(pilotin(2)-pilotin(1))*(r-i)/r;
      end
   else
      for i = 1 : (r-1),
         outdata((m-1)*(r-1)+i) = (pilotin(m)-pilotin(m-1))*i/r+pilotin(m-1);
      end
   end
end
outdata = conj(outdata);
```

D.2 Second Order Interpolation (SOI)

```
function outdata = interp2order(pilotin)
L = length (pilotin);
r = 13;
N = r * L;
% creat the pilotin(0) according to other pilots by linear for the purpose of the first interpolation
f_pilot = pilotin(1)-(pilotin(2)-pilotin(1));

for m = 1 : L
  if m == 1
    for i = 1 : (r-1)
      a = i/N;
      c1 = a*(a-1)/2;
      c0 = -(a-1)*(a+1);
      c_1 = a*(a+1)/2;
      outdata(i) = c0*f_pilot+c_1*pilotin(1);
    end
  elseif m == 2
    for i = 1 : (r -1)
      a = i/N;
      c1 = a*(a-1)/2;
      c0 = -(a-1)*(a+1);
      c_1 = a*(a+1)/2;
      outdata((m-1)*(r-1)+i) = c1*f_pilot+c0*pilotin(1)+c_1*pilotin(2);
    end
  else
    for i = 1 : (r -1)
      a = i/N;
      c1 = a*(a-1)/2;
      c0 = -(a-1)*(a+1);
```

```
        c_1 = a*(a+1)/2;
        outdata((m-1)*(r -1)+i) = c1*pilotin(m-2)+c0*pilotin(m-1)+c_1*pilotin(m);
      end
   end
end

outdata = conj(outdata);
```

D.3 Cubic Spline Interpolation (CSI)

```
function outdata = splineinterp(pilotin)
pilotin = fliplr(pilotin);
x = 1 : length(pilotin);
y = pilotin;
r = 13;
xx = 1 : 1/r : (length(pilotin)+1-1/r);
outdata = spline(x,y,xx);

outdata = conj(outdata)
```

D.4 Low-Pass Interpolation (LPI)

```
function outdata = lpinterp(pilotin)
pilotin = fliplr(pilotin);
x = pilotin;
r =13;
outdata = interp(x, r,1);
outdata = fliplr(outdata);
outdata = conj(outdata)
```